UNIVERSITY OF CALIFORNIA
RIVERSIDE

Lightweight Impact-Resistant Composite Materials: Lessons from Mantis Shrimp

A Dissertation submitted in partial satisfaction
of the requirements for the degree of

Doctor of Philosophy

in

Chemical and Environmental Engineering

by

Garrett Wayne Milliron

September 2012

Dissertation Committee:

Dr. David Kisailus, Chairperson
Dr. Jianzhong Wu
Dr. Javier Garay

The Dissertation of Garrett Wayne Milliron approved:

_____

_____

_____

Committee Chairperson

University of California, Riverside

Acknowledgements

I want to thank my advisor, Dr. David Kisailus, for his determination in driving these projects to completion. Without his support, guidance, and experience these projects would have taken a very different and far less focused course. Dr. Kisailus managed to tread the very difficult line between authority and friend, appropriately choosing the correct role as the situation required. I have come to know my advisor well through my time at UCR, and I look forward to his guidance for years to come, regarding the professional and personal hurdles my life has yet in store.

I want to thank Dr. James Weaver for suggesting to Dr. David Kisailus that I be admitted to UCR. His help and guidance extends to my undergraduate years where he exposed me to biomaterials. I have learned so much from James, and without him I would likely not have continued in academia.

The number of friends, family, and collaborators whose support have been critical to my success are far too numerous to name individually, but they all know who they are, and I sincerely thank them. Notable mentions include my parents, siblings, Laj Xiong, Ian Marcus, Heather McKenzie, Qianqian Wang, Elaine Ahlers, and Pablo Zavattieri.

Lastly, I would like to thank my wife Hsiao-Yun Milliron. Her love and support go far beyond what are typical for a spouse. Finishing graduate school with 2 children was challenge made possible in large part because of her strength and constant consideration. She has sacrificed so much to see this stage of our lives to completion, and I will spend the rest of my life attempting to grant her my insurmountable gratitude.

ABSTRACT OF THE DISSERTATION

Lightweight Impact-Resistant Composite Materials:
Lessons from Mantis Shrimp

by

Garrett Wayne Milliron

Doctor of Philosophy, Graduate Program in Chemical and Environmental Engineering
University of California, Riverside, September 2012
Dr. David Kisailus, Chairperson

Nature has evolved efficient strategies to synthesize complex mineralized structures that exhibit exceptional damage tolerance. One such example is found in the hyper-mineralized hammer-like dactyl clubs of the stomatopods, a group of highly aggressive marine crustaceans. The dactyl clubs from one such species, Odontodactylus Scyllarus, exhibit an impressive set of characteristics adapted for surviving high velocity impacts with the heavily mineralized prey species on which they feed. Consisting of a multi-phase composite of oriented crystalline hydroxyapatite and amorphous calcium phosphate and carbonate, in conjunction with a highly expanded helicoidal organization of the fibrillar chitinous organic matrix, these structures display several effective lines of defense against catastrophic failure during repetitive high energy loading events. The study of this organism and its relatives has lead to design cues, which were incorporated into prototype composite materials designed for applications in aviation, body armor, and entertainment.

Table of contents

List of Figures

Chapter 1: Introduction

Ideally innovators would have materials that don't fail. A failure proof material would be a fabric that never tears, a rope that never breaks, or a beam that never bends. We can never achieve these targets, but the closer we get the more innovations we enable. The current failure limitations of modern materials have ramifications, which span the product space. Every vehicle has its safety limits. Soldier body armor is highly encumbering. Portable shelters don't protect against much more than rain. Human powered flight, space elevators, and other dreams are currently impractical or impossible. This is why materials define the age. Our species' greatest strength is our ability to create, and our materials play a large role in limiting and enabling those creations.

There are no perfect materials, not just because every material property has its limitations, rather a material can only be perfect for a specific application because each property can take a range of desired values. When multiple properties are desired there are often tradeoffs and optimizations that are required when selecting or engineering materials. While current technology is limited by the capabilities of existing materials there is good reason to consider that vast improvements have yet to be made in the area of composites, which allow for the addition of properties across different classes of materials (Schram, 2007), and in some occasions synergistic mechanisms can result in properties far exceeding the sum of the parts (Cronin, 1989).

Ashby plots allow us to compare a range of materials across 2 material properties per plot. By comparing specific stiffness against specific toughness you would find materials far from the origin, which would be very suitable for aircraft because they

would be lightweight, resistant to deformation, and able to take large amounts of energy. However, if ones objective was to make a craft that utilized wing warping then high stiffness is no longer desirable and an optimal stiffness would be sought. Body armor also desires materials that can be stiff, tough, and lightweight with the addition of shock resistance. This is a very difficult demand because the first two properties are both proportional to weight and inversely proportional to each other; additionally, shock resistance can be a very complex consideration. It is for these reasons that designers must find a balance between weight and survival rate. If armor were lighter, more people would wear it, which could save lives. If it were more impact and shock resistant, it would prevent more deaths.

When discussing current technology there are often intellectual property issues involved. This can constrain ones knowledge about the design, mechanisms, and synthesis processes, in order of decreasing availability. Furthermore, when the target product has defense application this issue is heavily compounded. Finally, body armor technology has an additional form of facts obfuscation concerning issues of implied corruption and controversy regarding its military testing over the past decade. In spite of this some details are known. Protection against handguns is achievable with pure fabric based armor systems, but the ubiquitous presence of rifles in combat situations requires additional protection in the form of rigid components. This is achievable with either small overlapping scales notably used in Dragonskin armor or large plates (e.g., the SAPI and ESAPI plates, Fig. 1.1). The hard components of Dragon Skin are silicon carbide

laminated composites.

Figure 1.1 A comparison of the scale armor of Dragonskin (left) to the SAPI plate of the Interceptor Armor (right). Note the warning on the SAPI plate suggesting a material specialized for projectile impact (it cannot be dropped).

A hard material like silicon carbide has the disadvantage of being susceptible to catastrophic failure from a propagating fracture. A laminated design scheme is an effective method to induce a periodic modulus with interfaces, which can arrest potentially catastrophic fractures. An alternative design scheme employed by the makers of the US Army's currently issued body armor system is a larger SAPI (Small Arms Protective Insert) plate which utilizes a hard exterior composed of silicon carbine and boron carbide mixtures. As the plate is loaded fractures could form on the backside, but this side is toughened with the presence of a fiber reinforced resin composite. This layer also catches any spalling from the back of the ceramic, protecting the individual from any potentially dangerous particles which may separate from the ceramic at high speeds. A

similar design is used in vehicular armor systems as well. There are many choices of fibers and resins, which are commonly employed based on the particular considerations of the armor. The main classes of fibers include carbon, basalt, glass, polyester, Aramid, and polyethylene. Nylon was once used in flak jackets, but has been phased out with advent of Aramid fibers, and is now only seen in experimental designs. The architecture of the fibers currently under use is not known, but leading weaves have been a "ballistic weave" such as a 2x2 or 2x3 basketweave.

On the horizon there are a handful of mechanisms and materials, which have shown promise. There is now a company selling CNT fabrics and tapes, which are likely to see their way into the next generation of armor systems. There has been continued interest in shear thickening materials such as materials derived from PDMS, along with granular solids which display "shear jamming" for their ability to rigidify in response to dynamic loads, but no know armor system has incorporated these materials into their designs. Inorganic fullerenes have also shown experimental results, which show promising impact resistance, but also have yet to leave the laboratory.

Before venturing into the space of impact resistant materials research it is important to do our best at understanding what has already been done and why, but true due diligence does not end at the patent office. Humans are not the only ones optimizing material properties for impact resistance. The kingdoms of life have been modifying multi-scale arrangements of materials for over a billion years. Life has solved the same problems in the same environments many ways over and over again, each time employing mechanisms that span from the obvious to the confounding. Designers across

all human history have likely taken inspiration from the designs of life, and the examples across history are numerous. This ancient field has been named “biomimicry” or “bioinspiration” and continues to provide insights to many areas of engineering today. The process of evolution has many advantages and disadvantages when compared with human engineering practices, and therefor has produced designs, which are both superior and inferior to our own. This has led to revolutions in our understanding of flight, energy conversion, recycling, and most relevant to this thesis: mechanically robust materials.

There are many examples of mechanically interesting insights gleaned from biomaterials, but only a few chosen to illustrate the common themes within biomaterials will be discussed here. First, it is a seashell from the marine snail: abalone, which to first approximation, uses the same design scheme as a SAPI plate, with a hard exterior of prismatic calcite and a tough posterior of a material called Nacre (Arzt, 2003; Tang, 2003; Viani, 1999). The search term “Nacre” produces 1246 results on isi web of knowledge making it one of the most well studied of all biominerals, next to bone. This same design scheme is seen in many load bearing biominerals such as the hard enamel,

and tough dentine in mammalian teeth with analogues in teeth from other phyla as well.

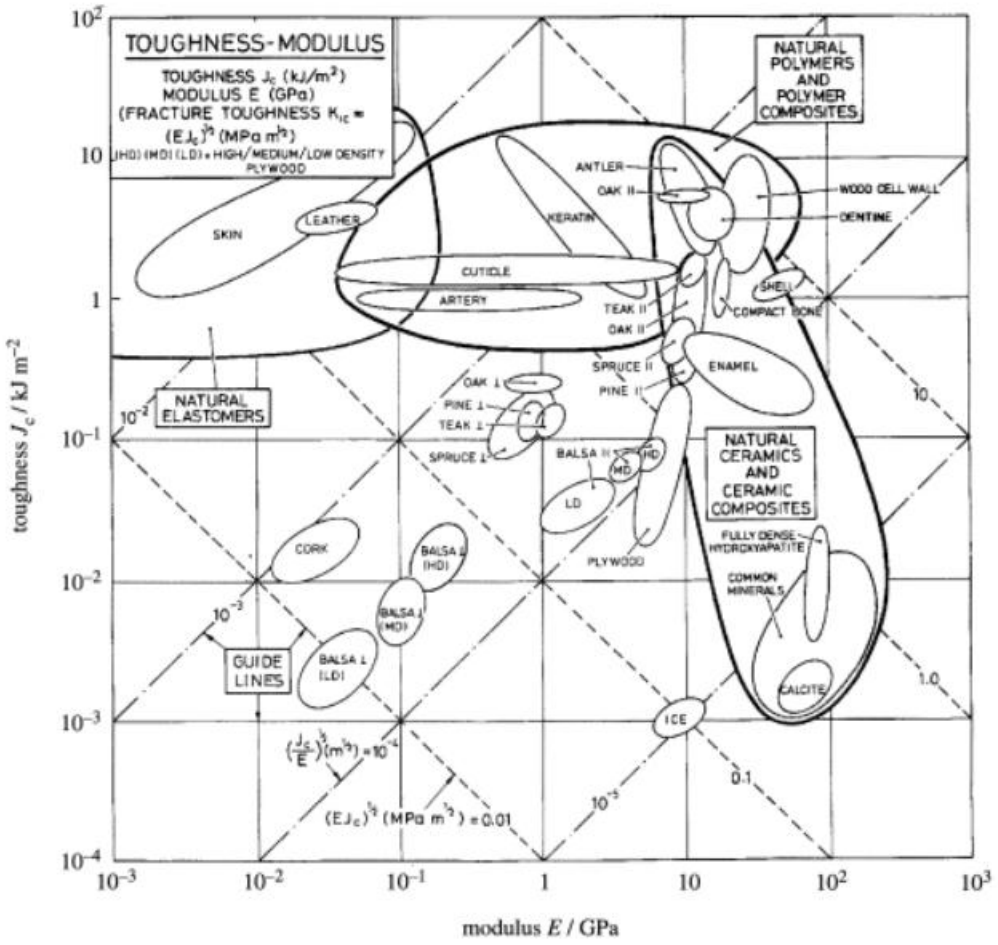

Figure 1.2 An Ashby plot comparing toughness and elastic modulus for numerous natural and synthetic materials. Note the 3 orders of magnitude difference in toughness between calcite and shell. From (Ashby, 1995)

The nacre, or backside material, of seashells is 3000 times tougher than its primary constituent: aragonite (Fig. 1.2) (Ashby, 1995). Whether a multiplier of this magnitude is achievable with synthetic composites is not yet known, but the pursuit of understanding the mechanisms responsible for the impressive bulk properties of biomaterials has yielded some very unintuitive and scalable design principles. The structure of nacre is composed of aragonite tablets with less than 1 percent organic

material separating tablets, in the form of β-chitin and various proteins (Lowenstam, 1989). As a fracture forms it must either break tablets and be subjecting to the arresting nature of the graded modulus, or take a tortuous path around the tablets through the organic. The material properties appear to favor the latter fracture regime, which results in the interlocking of many tablets across a fracture. The consequence is that the tablets must then slide past one another in order for the crack to open and separation to occur.

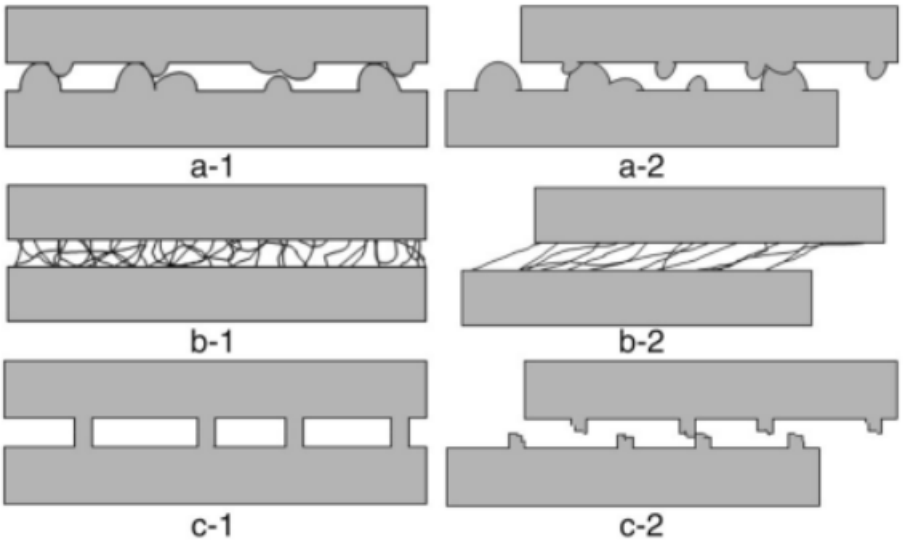

Figure 1.3 Schematic of 3 toughening mechanisms that dissipate energy as tablets slide past one another: (A) nanoasperities, (B) sacrificially bonded organic, (C) mineral bridges. From (Meyers, 2008)

Four features have been identified which contribute to the ultra-toughening effect resulting in large amounts of energy dissipated during the fracture of nacre. The first is mineral bridges, which connect each tablet to the tablets in neighboring layers (Fig. 1.3) (Meyers, 2008). These act as columns, which must be sheared before the tablets can begin sliding past each other. The second structural feature is the presence of nano-asperities or little bumps on the surface of each tablet. Once the tablets start sliding these asperities greatly increase the kinetic friction between layers resulting in further energy

dissipation. The tablet geometry itself is also responsible for enhancing these two mechanisms due to is subtle “bow-tie” cross-section. Because the tablets are thickest at the edges as they slide apart the laminate expands resulting in a slightly auxetic material. This puts more tensile strain on the mineral bridges, which allows them to dissipate more energy at a higher stress before failure. Additionally the auxetic effect causes the tablets to be pressed harder together which enhances the normal force experienced by the nano-asperities and therefor the frictional energy dissipation when they slide past each other (Barthelat, 2007).

The final feature responsible for toughening in nacre is the presence of organic material between the tablets, which acts as glue filled with numerous self-conforming bonds. As the glue is strained bonds break, reform, and break again as the proteins are elongated. This has been described akin to the process of pulling apart a bundle of double-sided tape. The advantage is that the bundle is stiff until a bond breaks, but instead of catastrophic failure, load is transferred to a new bond, and stiffness is restored. This process is repeated until the tape is fully elongated, dissipating energy all along the way. The presence of organic glues, which bind stiff materials together in an ultra-tough matrix has been seen in many other materials, bone being the most notable and well-studied (Fantner, 2005).

The common theme within all of the mechanisms mentioned is the breaking of bonds to dissipate energy. The material accepts excess energy by inducing a controlled failure. The danger of a fracture in a monolithic material is that the fracture concentrates stresses breaking bonds within a plane of the material. If this plane fracture is allowed to

propagate through the material it will reach the edges and result in the catastrophic failure of the material as it is broken into two of more pieces. The energy dissipated by such a fracture is negligible compared to the energy dissipating capacity of a bulk volume. A particularly salient quality of biomaterials is their ability to prevent this catastrophe, while still breaking bonds and dissipating large amounts of energy.

Biomaterials are often multifunctional, hierarchically ordered, self-healing, self-assembled at benign conditions, biodegradable, and containing unintuitive mechanisms, but their study is far from trivial (Bosia, 2012; Shan, 2008). Nature doesn't give up her secrets easily, and not every secret is worth mimicry, for a number of reasons. This is why the study of biomimetics has benefited greatly from advancing technology, and why it requires knowledge from many disciplines including geology, materials science, biology, physics, engineering, computer science, etc. To understand the process of biomimicry, as applied to materials, it has been simplified into a basic funnel: 1. Research behavior and evolutionary history. 2. Characterize the material's structure and properties. 3. Use theory and simulation to support structure-property-function relationships. 4. Synthesize new materials to verify the relationships. 5. Apply insights and inspired synthesis methods to enable innovation.

The first step in the funnel is to understand the organism of interest. If the organism is an animal thorough background work must be performed on its behaviors, environments, evolutionary history, interspecies and intraspecies interactions, and the biomechanics regarding the material of interest. This will provide details of how the material is loaded, what is required of it, and how it came to be. An example of a bad

project, which might disregard this step would be to study a human spine to make a biomimetic column. When the evolutionary history of humans is considered the flaw in this research plan becomes apparent. Humans have been walking upright for less than 5 million years. In evolutionary time scales this is not nearly enough time to have arrived at an optimized design. The ubiquity of individuals suffering from back pain (80%) is a testament to the inadequate design. Conversely, "living fossils" are ideal systems of study. These organisms have been called "primitive" due to their fossil record showing little evidence of change, but in reality it is only their body plan, which is evidenced as being superficially similar to its ancestors. These organisms' body plans rest in local optimums across the fitness landscape given the range of genetic pressures experienced over that time. However, "primitive" does not appear to be an appropriate word. Their microscale and nanoscale structures could easily have been undergoing further optimization during this extended period of time. This means a living fossil's materials have a prerequisite for optimization: time, and a hint of its existence: macro scale morphological equilibrium.

Next one must one must consider which materials could be improving within the organism's body based on environmental constraints. In the case of the cuttlefish there exists a porous composite of primarily aragonite called a cuttlebone, which functions as a buoyancy controller and skeletal structure. Unlike the swim bladder of a fish, which is a flexible membrane, this structure must withstand an air/water pressure differential across a rigid structure. Its channeled shape must both allow the passage of fluids and support the loads from the water pressure. Deeper water produces stronger pressure. This means

that cuttlebones from cuttlefish must favor strength the deeper the cuttlefish inhabit. Depending on species they can handle depths of 200-600 meters before imploding. This is a spacial gradient, which can cause a genetic drift in a predictable fashion. Conversely, birds found at higher elevations must compensate their flight mechanisms for the thinner air. Slightly more abstract is a temporal gradient caused by a genetic pressure changing over time.

Catastrophic events, whereby changes occur faster than an organism can evolve are detrimental to a species and have been the cause of extinctions, but slow changes can steer an organism in a predictable path along the fitness landscape. When two organisms influence each other's environments they each respond in turn, continually changing the environment for their symbiont. This is why coevolution is an ideal driving force for a biomimetic scientist. By finding a biological association that favors the sought trait the scientist has found two organisms worth investigation. Cheetahs and antelope are prime examples, where favoring speed has determined their survival strategies. In the case of trigger-hair response-time the trapjaw ant and many species of flea are among the fastest do to their co-driven need. However, even in an unchanging natural environment, with no co-evolution, there are still genetic pressures, which can lead to optimums in the fitness landscape. This is because a gene pool can affect itself. In lieu of all other competition each member of a species must compete for what are often limited resources with the other members of the species. Sometimes this competition can lead to ritualistic fighting in which the victor has a greater chance of reproducing. In the case of desert bighorn sheep, battles are won by repeatedly smashing skulls. This is why their horns have

developed into impressive impact resistant materials (Tombolato, 2010).

Figure 1.4: (left) A land crustacean. (right) A millipede. Distantly related arthropods that have convergently evolved a near identical body plan. An example of an independently verified design.

The last example of an established biological concept, which can greatly aid in motivating a biomimetic research project is convergent evolution. To an engineer this translates to independent verification. Because biomaterials are hierarchical, multi-functional, and loaded with all sorts of confounding structure, which could be vestigial or independent of the properties of interest, confirming structure function-relationships can be very difficult. Convergent evolution provides a useful aid by potentially supporting hypotheses when the same independently evolved structures are found in organisms that share the same function (Fig. 1.4). In fact merely identifying the existence of morphological conversion could motivate a new project, which attempts to find the associated function for the convergent structures. Even if their designs are not optimized, the question of why they independently arrived at the same region of the fitness landscape could yield interesting answers.

Once a structure has been found, and there has been sufficient support to justify its study, it must be characterized. This, like all steps in the biomimetic funnel, is an

ongoing process that continually benefits from modern advancements in the field, and the amount of time spent. Each species of interest will have natural variability within and across gender, population, environment, and more. For this reason multiple samples must be studied, and environments must be controlled. Samples can be taken from the wild or captivity, but their preparation is highly dependent on the measurement to be made. Each measurement gives a new piece of information that can be used to start making hypotheses, and these hypotheses can be tested with further characterization, using different techniques, or corroborating with evidence from another part of the funnel. One may find what they are after immediately, move on, and the material's further investigation is picked up by others decades later.

Characterization methods can be dived into 2 main groups: wave interactions and chromatography. Wave interactions can be further divided into 3 groups spectroscopy, microscopy, and force measurements. Spectroscopy involves the analysis of spectra, which encode information about a material sample. A spectrum of interest is typically acquired by probing a precise location with some form of wave most commonly photons, neutrons, or electrons. Electrons and neutrons require high energies to transmit and diffract through even very thin materials (less than 100 nm). However, photons have various uses across a large range of frequencies including X-rays which can diffract through much thicker sections encoding a spectrum, which contains information regarding concentration, orientation, and the geometry of crystal structures contained within a diffracting volume. Electrons can also interact with each other in atomic shells emitting x-rays, which have a spectral variance depending on the elements present. This

technique is known as energy dispersive spectroscopy or EDS, and is an effective first step in understanding the elemental composition of a material. It can conveniently be performed in an SEM or TEM, both of which are also capable of focusing electrons into an image, making them microscopic techniques as well.

In the range of the visible spectrum, microscopy with controlled polarization has been and continues to be a powerful and readily available technique, but is limited in magnification. FTiR and RAMAN spectroscopy also use light in frequency ranges neighboring the visible, but manage to probe the vibrational modes of molecules and their lattice structures. This provides a means of identifying materials independent of a diffraction technique, with the advantage of being able to identify the molecules present in amorphous phases, a common occurrence in biomaterials.

Finally, force measurements include techniques in which a probe directly interacts with a material and measures the effect of "contact". These techniques may only approach a sample in the case of a scanning tunneling microscope, or touch the sample, which is sometimes the case in an AFM. This technique can be used in its most basic application to map the topography of a surface, but it is also capable of tapping a surface at high frequency and mapping the force of contact. This is useful for acquiring high resolution maps of regional variance in mechanical properties, but more information about the mechanical properties can be deduced by measuring a force displacement curve under controlled loading conditions. This process is achieved macroscopically for many loading arrangements in a mechanical loading device such as those made by the company

Instron. However, to probe the microstructural variance a nanoindenter, forcing a diamond tip into a sample, provides a compressive curve from a micron sized area.

Once the microscopy techniques have been chosen and data has been collected hypotheses regarding structure-function relationships begin to form. From there models are developed, which are simplified embodiments of the structures and properties measured. These models can be theoretical, seeking to model the proposed mechanisms at work, or they can be computational, providing the basis for visualization and simulation. Fracture mechanics, elastic/plastic theory, acoustical mechanics, and all the case specific considerations that have been developed for composite materials must be considered when trying to model or simulate an impact event on a biomaterial, which can easily produce unsolvable equations, and simulations that would take the largest supercomputers decades. This is why simplifications must be made, but always at the risk of neglecting a crucial component to the workings of the whole. Just as a single characterization technique does not detail the entire structure, a simulation or model will also be inherently limited. However, despite their limitations, models can provide powerful insights. If the modeled mechanisms do not yield results of the right magnitude then evidence for additional mechanisms has been found, and the search continues.

Nearing the bottom of the funnel is where the creation begins. Synthesis techniques are developed to verify the hypotheses formed or supported by the modeling. This is where biomimetic materials scientists can take large departures from their peers. The choice of method for creating mimetic materials depends on what features are desired. If the material is desirable for its organics ability to template mineral growth,

then demineralizing the mineral from the organic template of the biomaterial and a subsequently remineralizing onto the organic template with a mineral precursor may be worth attempting. However, in the case of impact resistant materials most biological examples are formed from constituents mechanically inferior to synthetic materials. Nacre is composed predominately of calcium carbonate in the form of aragonite tablets. If these tablets and their mineral bridges were replaced with a robust engineering ceramic even better mechanical performance could be expected from the composite. However, replicating this microstructure has proved a challenge for many decades. While some groups are focused on the synthesis of aragonite, others are more interested in drawing inspiration from the geometry that it exhibits within the shell. This latter approach is less involved in the mineralization chemistry, instead focusing on synthesizing mimetic structures, which exemplify the mechanisms present in biomaterials.

Synthesis techniques can take advantage of existing self-assembling or self-organizing systems, arise solely for their mimetic purposes, or utilize more conventional methods while testing biomimetic architectures. Regardless of the scale and methods, the first step is to create structures, which demonstrate the mechanisms that were observed, modeled, and/or simulated. Once the mechanism is replicated in a physical mimic the project is nearing completion. In the case of impact resistant materials the discovered design cues could then be inserted into engineered materials that demand impact tolerance.

The last step in the biomimetic materials funnel is application. At this stage, the insights are collected from what is known and what has been learned, into the

manufacture of new materials suitable for a myriad of products. New generations of SAPI plates could be made along with materials for vehicles, aviation, sports, shelters and more. With each product, the materials and their properties are tuned using synthesis parameters, which alter the mechanisms to suit the specific needs of the application.

Each stage of the funnel provides insights to the others, so the same groups can easily take many passes through the funnel with the same organisms for the same application, and learn new insights each time. This speaks to the richness of the process and complexity of the numerous insights to be gleaned. Beginning at the top of the funnel we have selected a group of organisms known as stomatopods.

The stomatopod known as the peacock mantis shrimp, or *Odontodactylus scyllarus*, is a nearly ideal organism of study. The peacock mantis shrimp produces a hammer capable of extreme speeds used to smash open shells, exoskeletons, skulls, and other previously studied biomaterials (Patek, 2005). Mantis shrimp are considered living fossils, because they have been using the same body plans for hundreds of millions of years, as evidenced by their fossil record (Ahyong, 2000). This means they have had many generations to refine the microstructure of their dactyl clubs. In addition to their weapon of choice against prey, the dactyl club is also used in interspecies battles over prime coral real estate (Taylor, 2010). This self-selecting behavior acts as an additional genetic pressure, which continuously drives the species to produce the most impact tolerant weapons possible, even if the need dictated by the armor of their prey has been

surpassed.

Figure 1.5: The peacock mantis shrimp, a feisty crustacean.

Peacock Mantis shrimp (Fig. 1.5) can deliver impact forces exceeding hundreds of pounds by swinging a club with speeds sufficient to cavitate the surrounding seawater (Patek, 2005). The induced cavitation produces an additional pulse of forces also in excess of hundreds of pounds. Cavitation is the mechanism behind decomposition via ultra-sonication and destructive enough to dictate the lifetime of marine propellers (Komfeld, 1944). A biomineral capable of withstanding subjugation to such extreme forces 1000's of times, before being molted and replaced, requires that the club ultrastructure have exceptionally high strength, stiffness, and toughness.

Optimization for high stiffness is inferred from the recognition that deliverable impact forces for a fixed shape, mass, and velocity are proportional to stiffness, so the ultrastructure must have been optimized for stiffness in order to make improvements in deliverable impact forces. In order to withstand the increases in forces over generations, club strength would need to be improved in parallel. Lastly, using the same selection criterion of optimizing impact force, the club biomechanics must have evolved improvements in impact velocity, and therefore, kinetic energy. The club material thus, has responded with increases in toughness. These properties typically suffer a tradeoff in engineered materials, but the dactyl club has genetic pressures, which have been optimizing for all three.

The stomatopod dactyl club provides two additional advantages over other biomaterials from the perspective of biomimetics. Unlike armor, such as shells, which employ translationally symmetric ultrastructures for resisting impact anywhere along the surface, the dactyl club's point of impact is constrained to a minute area with a known center. This means the club's substructure had the freedom and requirement to optimize for a consistent impact location and orientation; additionally, this information allows for a simulation of a realistic impact event. Furthermore, because the club is a modification of the crustacean's cuticle there are numerous other segments of the cuticle, which serve as control materials. Comparisons between the dactyl club and other cuticle segments allow a method of prioritization amidst otherwise overwhelming hierarchical complexity. Any structural difference unique to the club over other cuticle segments is a deviation

which presumably relates to the difference in function of the dactyl club, and is likely important for enhancing impact tolerance.

With the evolutionary arguments presented and a wealth of supporting data, we expected to provide convincing motivation for the biomineralization community to direct more attention to the clubs of the hundreds of stomatopod species alive today. Mollusk nacre has been extensively studied by many groups for decades, each adding insight into the complexities of the material. The dactyl clubs of stomatopods are ripe for a thorough investigation, which will inevitably prove a fruitful endeavor for years to come. To date there has only been one publication regarding the substructure of a stomatopod dactyl club published in 1982 by Currey and Nash (Currey, 1982). Hydroxyl apatite was speculated to be a potentially present phase after measuring significant concentrations of calcium and phosphorus. Proportionality was found between the phosphorus / calcium ratio and microhardness values, which both ranged through multiple orders of magnitude, when taken at various points of a dactyl club cross-section. Fracture surfaces were analyzed and homology between other crustaceans was noted, specifically the helicoidally stacked fiber reinforcement ubiquitous in biological materials (Weiner, 1997;

Giraud-Guille, 2004; Giraud-Guille, 1998).

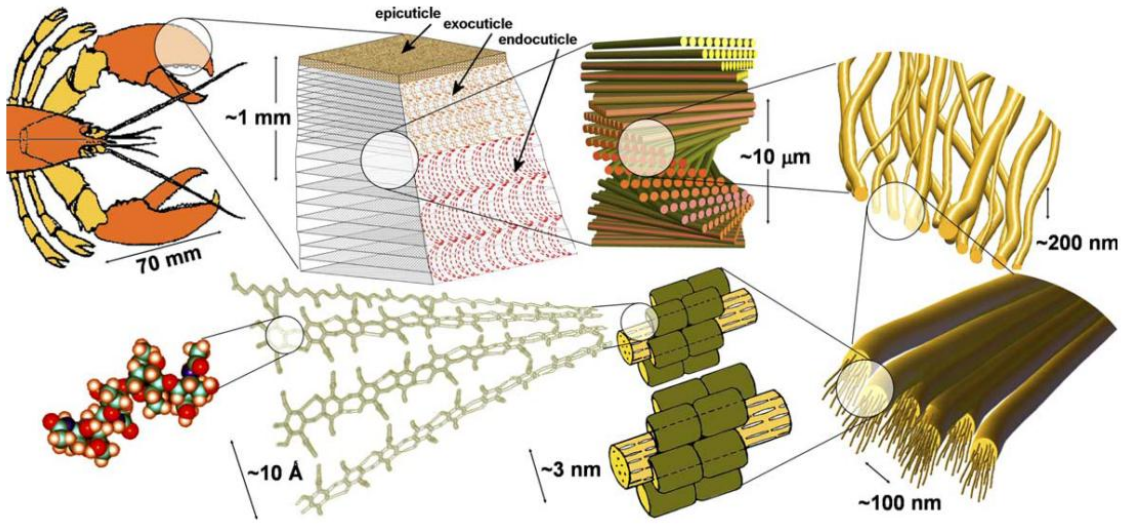

Figure 1.6: The hierarchies of the organic matrix within lobster cuticle, reminiscent of all known crustacean cuticle.

A model for crustacean cuticle has been refined to the point where a near complete hierarchical picture has been established (Roer, 1984). Crustacean cuticle, like most hierarchical biomaterials displays half dozen hierarchies (Fratzl, 2007), until the smallest scale of molecules is reached. From the bottom up, the first hierarchy is sugar residues (acetylglucosamine), which bond to form antiparallel chains of α-chitin (Fig. 1.6). Multiple chains form a crystalline nanofibril, which surrounded by proteins. Chitin-protein nanofibrils assemble into aligned sheets, with each fiber forming around a vertically aligned pore structure (waviness at the 200 nm scale). Each sheet is aligned with an offset with respect to adjacent sheets, until a helicoidal architecture is formed. The entire structure is finally encased in a mineral-protein matrix, with the pore structure remaining intact.

While helicoidally aligned fiber reinforcement has been observed as an evolutionarily convergent structure for many years, a surprisingly small amount of research has been performed to compare the effectiveness of the structure to modern fiber reinforced designs. In 2006, Apichattrabrut and Ravi-Chandar modeled and tested helicoidal composites with unidirectional layers offset by 10 degrees per layer (Apichattrabrut, 2006), not attempting to make a biomimetic composite, but motivated by a theoretical investigation into the reduction of interlaminar sheer stress. Continuing the work of Rugg et al. (Rugg, 1998), who also used through-laminate reinforcement to resist such forces, Apichattrabrut and Ravi-Chandar demonstrated considerably large improvements over conventional layup patterns in many material properties, including impact tolerance, by combining these two design principles. Later in 2006, Chen et al. measured the fracture toughness of a biomimetic helicoidal composite to have a fracture toughness of 23.7 MPa*m^0.5 vs. 14.6 MPa*m^0.5 in a unidirectional control (Chen, 2006). In 2011, Cheng et al. tested beams of helicoidal composites with promising results especially in the area of residual strength under static load (Cheng, Thomas, 2011).

With the small amount of research that has been devoted to realizing the full potential of a helicoidal architecture in a fiber reinforced composite, and the promising results attained thus far, it is clear that this avenue of research is worth pursuing. As insights are gleaned from the club regarding the helicoidal architecture, and the surrounding variations, which support its impact tolerant function, biomimetic improvements will be incorporated into synthetic helicoidal composite designs for use in impact tolerant materials.

Objectives:

1. **Uncover compositional and structural details of the stomatopod dactyl club ultrastructure sufficient to guide a focused investigation of its toughening components.**
2. **Measure the mechanical properties of the dactyl club to provide qualitative and quantitative targets for simulated and synthetic materials.**
3. **Utilize FEM, or other modeling techniques to validate the properties of the observed structures responsible for toughening.**
4. **Confirm the utility of the uncovered mechanisms via synthesis of biomimetic composite materials.**

Chapter 2: The Stomatopod Dactyl Club: A Formidable Damage-Tolerant Biological Hammer

Abstract

Nature has evolved efficient strategies to synthesize complex mineralized structures that exhibit exceptional damage tolerance. One such example is found in the hyper-mineralized hammer-like dactyl clubs of the stomatopods, a group of highly aggressive marine crustaceans. The dactyl clubs from one species, *Odontodactylus scyllarus*, exhibit an impressive set of characteristics adapted for surviving high velocity impacts on the heavily mineralized prey on which they feed. Consisting of a multi-phase composite of oriented crystalline hydroxyapatite and amorphous calcium phosphate and carbonate, in conjunction with a highly expanded helicoidal organization of the fibrillar chitinous organic matrix, these structures display several effective lines of defense against catastrophic failure during repetitive high energy loading events.

Introduction

The stomatopods are an ancient group of marine tropical and subtropical crustaceans with a fossil record that dates back more than 300 million years (Schram, 2007). Modern representatives can reach lengths of nearly 40 cm, although most species are significantly smaller (e.g., 15 cm). To the casual observer, stomatopods superficially resemble heavily armored caterpillars and the group is best known for their complex visual systems (Cronin, 1989), their solitary nature, and aggressive hunting strategies (Caldwell, 1975). Stomatopods second pair of thoracic appendages are highly modified and specifically adapted for powerful close-range combat. The dactyl modifications (the terminal segment) of these appendages divide the group into those that either hunt by impaling their prey with spear-like structures or those that smash them with a powerful blow from a heavily mineralized club (Taylor, 2010). This robust hammer-like composite structure is capable of inflicting significant damage following impact with a wide variety of heavily mineralized biological structures (e.g., mollusk shells, crab exoskeletons, the skulls of small fish, and the occasional weary fisherman) (Claverie, 2011). Significantly, many of these prey items represent model systems for the study of tough and damage tolerant biological materials (Lukis, 1835; Dunlop, 2010) and investigation into their micro- and nano-architectural features have provided critical insight into the design of robust synthetic analogs (Deville, 2006; Heuer, 1992). This observation highlights the unique structure and impressive performance of the stomatopod dactyl club, and the important lessons that can be learned from its investigation. The complexity of stomatopod behavior and their aggressive hunting activities were best described by Lukis in 1835 (Lukis, 1835), while observing them in captivity. He writes, “It sported about,

and after a first approach, exhibited boldness rather unexpected. When first alarmed, it sprang backwards with great velocity, after which it placed itself in a menacing attitude... The prominent appearance of the eyes, their brilliancy and attentive watching, the feeling power of the long antennae, evinced quick apprehension and instinct. I brought a silver teaspoon near them, which was struck out of my hand with a suddenness and force comparable to an electric shock: this blow was affected by the large arms, which were closed and projected in an instant with the quickness of lightning."

We report a comprehensive study of the structural complexity and mechanical properties of the dactyl clubs of *Odontodactylus scyllarus*, a common reef-associated stomatopod from the tropical Indo-Pacific (Ahyong, 2000). As described by Patek, *et al*. (Patek, 2005), these formidable structures are capable of accelerations to 10,400g and speeds of 23m/s from a stationary position. Their rapid strike can generate cavitation bubbles between the appendage and their prey, with the collapse of these bubbles producing significant stresses near the contact point, in addition to the instantaneous forces upwards of 700N resulting from the direct impact (Patek, 2005). Despite these significant loads, the dactyl clubs are extremely damage tolerant and are able to withstand thousands of highly energetic blows (Peaka, 1975).

Structural and Micromechanical Characterization

At the macroscale, the club comprises the two terminal segments (the propodus and the dactyl) of the second thoracic appendage (Fig. 2.1A-C). For deployment during a striking event, the dactyl is folded back into a groove in the propodus to form the functional club. Whole body micro-computed tomographic analysis (Fig. 2.1D) of *O. scyllarus* reveals that the dactyl club is the most electron dense region of the stomatopod exoskeleton, being up to five times thicker than its adjacent appendages. When viewed in a transverse cross-section, the club can be divided up into three distinct regions (Fig. 2.1E); the impact region, the periodic region, and the striated region.

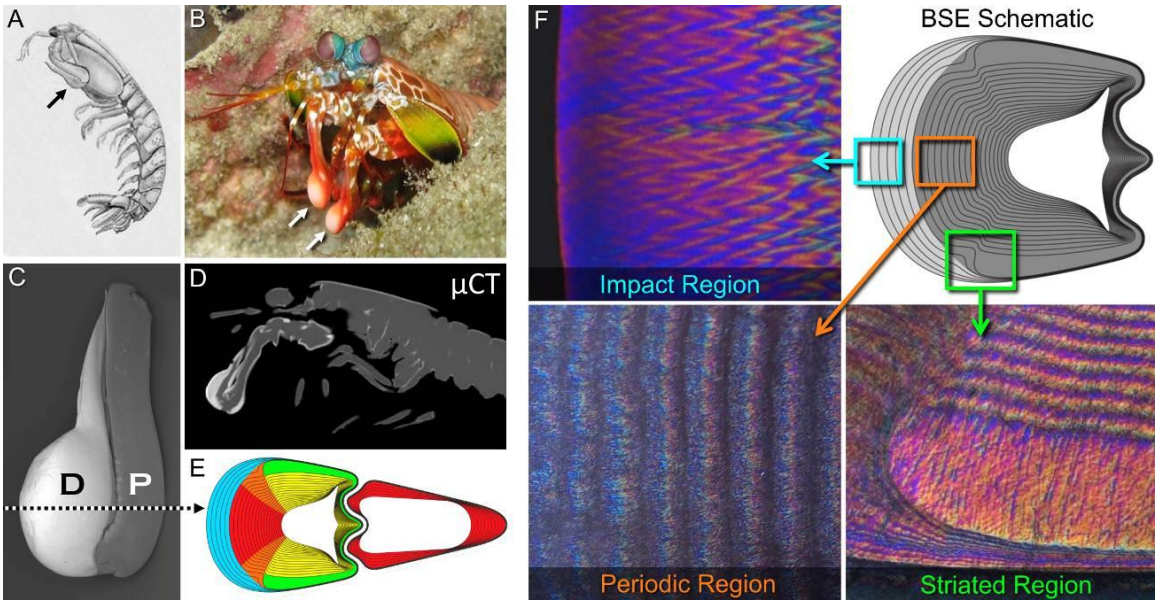

Figure 2.1: Morphological features of the stomatopod dactyl club. (A) A generalized stomatopod body plan and (B) a close up of the anterior end of *Odontodactylus scylarus*. The arrows denote the location of the dactyl club's impact surface. (C) Backscattered scanning electron micrograph of the club's external morphology and (D) a microCT longitudinal section though the anterior half of a complete specimen showing the constituent dactyl, D and propodus, P segments, revealing their differences in electron density (the second thoracic appendage with its terminal dactyl club modification is highlighted in red). (E) Cross-sectional analysis of the club illustrates the three distinct structural domains: *(i)* The impact region (blue),

***(ii)* the periodic region [further subdivided into two discrete zones: medial (red) and lateral (yellow)], and *(iii)* the striated region (green). The periodic region of the propodus is also shown in red. (F) Optical micrographs, revealing the buckled rotated plywood structural motif of the impact region, the pseudo-laminations of the periodic region, and the thickened circumferential band with parallel chitin fibers in the striated region (A adapted from (Brooks, 1886), B courtesy of Silke Baron, and D courtesy of DigiMorph.org)**

Nanoindentation and Energy Dispersive Spectroscopy (EDS) measurements (Fig. 2.2A-C) of sectioned clubs reveal a distinct correlation between the extent of mineralization and their corresponding mechanical properties. EDS measurements tracking regiospecific elemental distributions reveal decreasing phosphorus and calcium concentrations from the impact surface to the interior of the dactyl club and a concomitant increase in carbon and magnesium throughout the same region. While there is an abrupt step-like decrease in calcium concentration through the transition from the impact region to the periodic region, the phosphorous concentration decreases in a gradient-like fashion (Fig. 2.2C). These results indicate a biphasic mineral system, with the impact region dominated by calcium phosphate and the remainder of the club likely consisting of a mixture of calcium phosphate and calcium carbonate. Large area nanoindentation maps and high resolution line scans through the midline of the dactyl club reveal that the highest phosphorus content region also exhibits the highest hardness and modulus, which is consistent with previous single point measurements made on a related species (Currey, 1982). Based on these measurements, the club can be divided into three mechanically distinct domains: *(i)* The outermost region of the club (the impact surface), measuring ca. 50-70 μm thick, and exhibiting modulus and hardness values of 65-70 GPa and 3-3.5 GPa, respectively, *(ii)* a sharp transitional zone with an abrupt

decrease in modulus and hardness within the bulk of the impact region, and *(iii)* a periodic region with oscillating minima and maxima modulus values of 10 and 25 GPa.

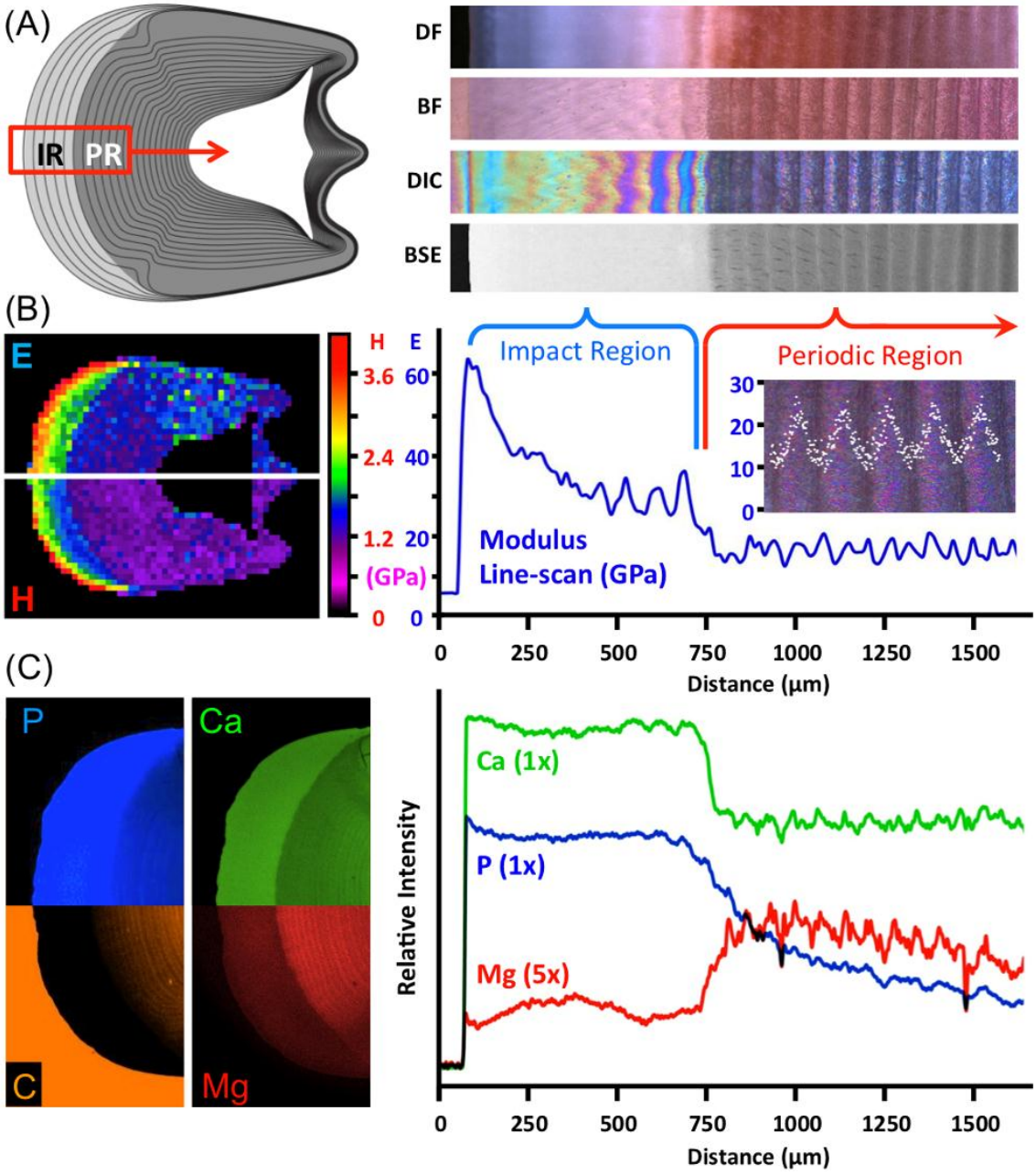

Figure 2.2: Micromechanical and compositional variability in the stomatopod dactyl club. All of the images and plots in the right hand column of the figure correspond to parallel analyses through the same region, facilitating direct comparisons between ultrastructure, micromechanics, and elemental composition. (A)

Diagrammatic backscattered electron micrograph through the dactyl club indicating the locations of the impact region (IR) and the periodic region (PR) and the corresponding optical [darkfield *(DF)*, brightfield *(BF)* and differential interference contrast *(DIC)*], and backscattered scanning electron (BSE) micrographs of the area boxed in red. (B) Large area nanoindentation [Elastic Modulus *(E)* and Hardness *(H)*] map of the dactyl club and a corresponding linescan, including a high resolution plot through five super-layers; periodicity: ca. 75μm overlayed on a corresponding DIC micrograph. (C) Energy dispersive spectroscopy maps and line scans showing the non-uniform elemental distributions in the periodic and impact regions (the Mg concentration EDS data has been expanded by 5-fold relative to the Ca and P concentrations).

Cross-sectional synchrotron micro-diffraction mapping (Fig. 2.3) reveals hydroxyapatite as the dominant mineral phase within the impact region. X-ray diffraction patterns acquired from this region reveal, that compared to the apatitic mineral phase found in bovine bone (Ooi, 2007), the dactyl club hydroxyapatite exhibits a higher degree of crystallinity as evidenced by the distinct separation of the (211), (112), and (300) reflections (Fig. 2.3B). In stark contrast, the periodic region lacks any defined crystallinity and is instead dominated by an amorphous mineral phase, a feature common for other groups of crustaceans (Luquet, 2004; Giraud-Guille, 1984). This observation is also consistent with the elevated magnesium concentrations of the periodic region, which has been shown to aid in the stabilization of amorphous calcium carbonates in other biological systems (Aizenberg, 1996; Loste, 2003; Politi, 2010; Tan, 2008). Further analysis of the synchrotron mapping data reveals that the hydroxyapatite crystallites exhibit a preferred orientation with the (002) lattice planes oriented parallel to the impact surface, a theme observed throughout the impact region.

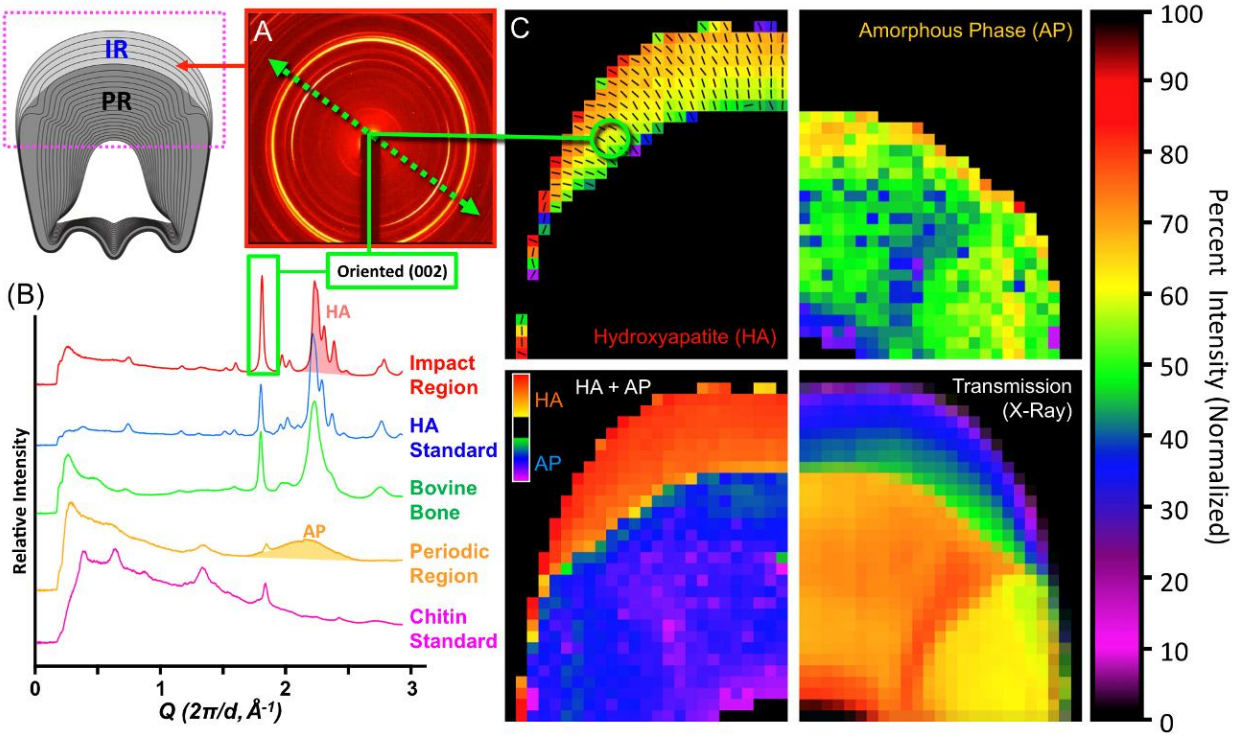

Figure 2.3: Synchrotron X-ray diffraction (XRD) analysis and distribution of various mineral phases in the dactyl club. (A) A single diffractogram taken from the impact region of a transverse cross section. The preferred orientation of the hydroxyapatite (HA) crystal's c-axis (green arrows) is placed at the peak intensity of the HA (002) reflection. (B) Representative XRD patterns from the impact and periodic regions compared against standards. The colored areas were used to estimate the mineral concentrations shown in (C). (C) Mineral concentration maps for the HA and the amorphous phases (each of the 4 maps measures ca. 2.5 mm across). The sloped black lines denote the preferred orientation of the HA c-axis (002). A composite mineral concentration map (lower left) confirms that both maps measured the same boundary between phases. An X-ray transmission map (lower right) correlates inversely with mineral concentration.

Underlying the mineral phases is the chitinous organic matrix, which exhibits a characteristic helicoidal organization (Fig. 2.4). The sheets of locally parallel chitin fibrils are stacked upon each other with each sheet skewed by an angle from the sheet below it. This constant difference in angle between neighboring sheets ultimately produces a rotation of 180°, defining a characteristic wavelength and a super-layer. These super-

layers are easily identified using SEM or optical microscopy (Figs. 2.1F, 2.2A) and decrease in thickness from the club exterior to the interior in a linear fashion. Each super-layer follows the club's contours (Fig. 2.1E), defining *(i)* the medial zone beneath the impact region and *(ii)* the lateral zone along the sides of the club. Compared to other helicoidal biocomposites (Cheng, 2011; Weiner, 1997; Roer, 2011) the highly expanded helicoidal periodicity of the stomatopod dactyl club makes it an ideally suited system for synchrotron fiber diffraction studies that have been previously resolution limited in other crustacean species by the x-ray beam spot size (Al-Sawalmih et al, 2008). Texture analysis of the helicoidal ultrastructure using a micro-diffraction beam line with a spot size of 5x5 μm is shown in Figure 2.4D,E using the d-spacing of the (110) peaks of α-chitin (Minke, 1978; Lichtenegger, 1999; Paris, 2003).

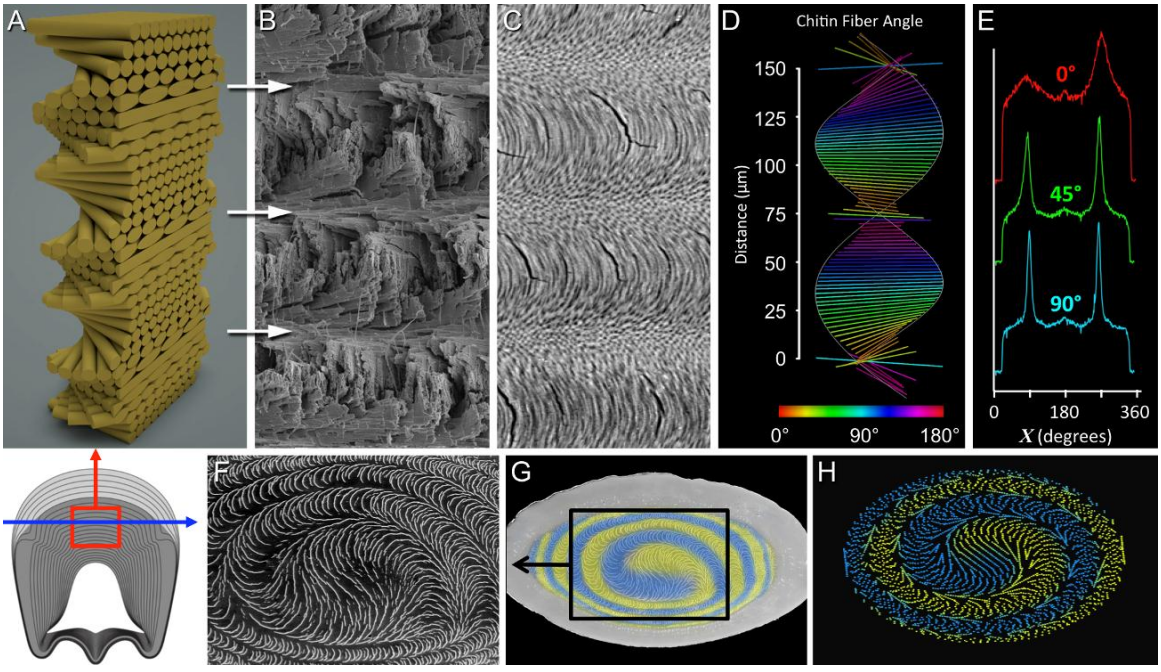

Figure 2.4: Chitin fibril helicoidal structural motif within the periodic region (with periodicity: ca. 75 □m). Comparisons between a generalized 3D model of a helicoid (A) with an SEM fractograph (B) and a polished surface from a transverse cross-

section (C). (D) A visualization of the chitin fiber orientations from the SAXS analysis of 92 separate diffractograms obtained through two super-layers. (E) Three representative χ plots of the α-chitin (110) reflection used to calculate fiber angles. The plots show changes in χ across the range of angles between each chitin fiber bundle and the X-ray beam. A charge contrast scanning electron micrograph from a damaged coronal cross-section (F) with false color (G) and a model of a helicoidal slice (H) which accurately reproduces the fracture patterns.

Dynamic Finite Element Analysis

In order to gain insights into the damage tolerance of the club, we performed Dynamic Finite Element Modeling (DFEM) of a striking event against a solid target (Fig. 2.5A-C), with the mesh following the complex macroscale geometry of the dactyl and propodus (Fig. 2.5A). To accurately compare the obtained results with previous data from Patek et al. (Patek, 2005), the target was modeled as a steel cylinder (E= 200 GPa) with 1mm thickness and 5mm radius, and the impact velocity (20m/s) was based on their measured final velocity. The simulations were validated by comparing the computed strike force with the measured one, which gave a comparable value of 600-700 N (*vs.* 693+/-174 N in the experiments). Additional simulations were performed in order to assess the influence of isotropic damage (cracking) or softening (plasticity) on the stress distribution, with the tensile load to initiate cracking or plasticity ranging from 10 to 50 Mpa. While the impact energy absorbed by micro-cracking or micro-plasticity reduced the strike force by ca. 15%, the critical stress values and overall distribution in the impact region did not change significantly.

The dynamic evolution of the maximum principal stress (σ_{max}) following contact (Fig. 2.5B) reveals that the impact wave travels through the entire club and reaches the end of the dactyl ca. 2.5 μs after contact, before being transmitted through the propodus. Since these simulations predict that the maximum values of σ_{max} are achieved 2 μs after impact, they imply that the propodus has no significant effect on the distribution of these critical stress values. Analysis of the maximum stress components at 2 μs after impact (Fig. 2.5C) include: *(i)* the hydrostatic pressure σ^H (blue tones), *(ii)* the in-plane

maximum principal stress $\sigma_{\max}^{IP}$ (green tones), and *(iii)* the out-of-plane maximum principal stress, $\sigma_{\max}^{OP}$ (red tones). These computations imply that the club is subjected to extremely high hydrostatic compressive stresses, with σ^{H} up to 6 GPa reached within a 0.2 mm radius from the contact point. For comparison, the compressive strength of engineering ceramics such as zirconia or silicon carbide is on the order of 2–3.5 GPa (Dowling, 2006). Since the dactyl club does not fail catastrophically during impact, this highlights its ability to sustain extremely high levels of localized impact pressure.

Internal damage can follow the direction of conical stresses (in the plane of the club's long axis) or radial stresses (orthogonal to the computational plane), with crack initiation governed by $\sigma_{\max}^{IP}$ or $\sigma_{\max}^{OP}$, respectively. The maximum values of $\sigma_{\max}^{IP}$ are located beneath the impact surface and close to the interface with the periodic region, reaching values well over 100 MPa, which correspond to the tensile strengths of monolithic ceramics. Conical cracks would hence be expected to nucleate near the impact/periodic region interface. The periodic region, which in contrast, has a lower mineral content, is subjected to lower in-plane stresses. The highest values of $\sigma_{\max}^{OP}$ are highly localized beneath the initial point of impact, reaching values that can exceed 100 MPa, suggesting that radial cracks are likely to also nucleate near the impact/periodic region interface. Most of the club is subjected to moderate $\sigma_{\max}^{OP}$ values (10–50 MPa), implying that radial cracks are less likely to occur in these regions. We also performed DFEM to directly investigate the potential contribution of the striated region (described in Fig. 2.1F) during an impact event, by imposing a stiffer modulus in this location. These simulations (Fig. 2.8) revealed that this circumferential band-like structure

prevents lateral deformation of the club, hence restricting the maximum principal strain within the periodic region and locally reducing the crack opening displacement of a potential propagating crack, and consequently limiting its driving force (Shih, 1981). Furthermore, these simulations indicate that the highly aligned chitin fiber bundles of the striated region, which are oriented perpendicular to the transverse cross section (Fig. 2.1F) may provide additional compressive stiffness during compression of the club.

Mechanistic Origins of Toughness and Damage Tolerance

While DFEM simulations provide important insight into the stress distribution, macroscopic structural integrity, and potential sites of microcrack nucleation, they do not take into account the complex microstructural features of the dactyl club. In order to correlate these features with the observed damage tolerance and the high toughness of the club, a micromechanical analysis must also be considered. Intuitively, it is not surprising to find a hard outermost layer in a structure employed for high-energy impacts as this design is widely used for mechanically active (Habelitz, 2002; Weaver et al, 2010) or protective (Bruet, 2008) hard tissues. In the dactyl club, this enhanced surface hardness is achieved by a higher degree of crystallinity, combined with a preferred orientation of the hydroxyapatite crystallites near the impact surface (Fig. 2.3C, upper left) which imparts additional rigidity due to the greater hardness and stiffness of the hydroxyapatite basal vs. prismatic faces (Viswanath, 2007). In addition to this first line of defense, its microstructural complexity imparts the club with several mechanisms against catastrophic failure that are detailed in Figure 2.5D.

Although DFEM suggests that internal cracks are likely to nucleate beneath the impact region, the helicoidal architecture provides several toughening mechanisms that hinder catastrophic propagation of such cracks (Fig. 2.5D). Charge contrast secondary electron micrographs of coronal cross-sections (Fig. 2.4F) illustrate the tendency of cracks to nest volumetrically within the periodic region between the chitin fibers. In three dimensions, this can be represented as a helicoidal fracture pattern propagating between layers, with a rotating crack front that remains parallel to the fibers without severing them. This hypothesis was confirmed by modeling a coronal cross-section of a helicoidal

stack of fibers curved around a spherical core (Fig. 2.4H), which results in the distinctive double spiral-like motif shown in Figure 2.4G and H. This model precisely reproduces the charge contrast fractographs, providing strong evidence that cracks predominantly propagate helicoidally between the chitin fibers. One key implication is that this pattern creates a much larger surface area per unit crack length in the main direction of propagation, hence amplifying the total energy dissipated during impact and crack propagation, a behavior which has also been observed in engineered helicoidal composites (Apichattrabrut, 2006).

When a crack deviates from its helicoidal path and propogates straight into neighboring layers, it encounters an elastic modulus oscillation due to their anisotropic stiffness. This oscillation period is on the order of 75 μm, and the relative thickness of stiff (E_{max}) and compliant (E_{min}) layers depends on the angle of the crack front relative to the helicoid axis (Fig. 2.2B). As shown by Fratzl *et al.* (Fratzl, 2007), this oscillation provides an additional protection against damage. Indeed, the *J*-integral crack driving force, J_{far}, surrounding the crack is shielded at the tip, $J_{tip} = J_{far} \cdot f_{inh}$, where f_{inh} is the shielding factor, which directly depends on the relative thickness and modulus ratios $\rho = E_{max}/E_{min}$. We used our nanoindentation linescan profiles to fit the oscillation wavelength and modulus ratio ρ, and applied this analysis to the club (Fig. 2.9). These results suggest that crack propagation across layers is hampered by the modulus oscillation, which improves the damage tolerance with an efficiency that depends on the crack propagation direction relative to the chitin fiber orientation. This prediction was supported by the observed presence of micro-cracks crossing the helicoid and arresting

within a few layers in scanning electron micrographs of transverse polished cross-sections (Fig. 2.4C).

A final protective mechanism against catastrophic fracture is provided by the sharp transition between the impact surface and the bulk of the impact region. If a crack approaches the impact surface, it encounters an elastic modulus mismatch. A crack propagating from a more compliant region (E_2) can either be deflected at the interface, or propagated through the stiffer region (E_1). This tendency depends on the Dundurs' parameter $\alpha=(E_1-E_2)/(E_1+E_2)$ (modulus mismatch) and on the fracture toughness of the interface, $G_{IF,}$ and of the stiff material, G_{C1}. The propensity for a crack to exhibit either of these regimes can be expressed as a critical (G_{IF}/G_{C1} *vs.* α) curve (He, 1989). The □ value at this interface beneath the impact surface is 0.37 (significantly smaller than 0.52 of dentin/enamel junction in mammalian teeth (Imbeni et al, 2005)), corresponding to a critical G_{IF}/G_{C1} of ca. 0.4 (He, 1989). Hence if G_{IF} is less than 40% of G_{C1}, crack deflection occurs at the interface. Such a mechanism has important implications, because the crack-tip stress amplification is greatly reduced when debonding occurs (Chan, 1993). If on the other hand, $G_{IF}>0.4G_{C1}$, the impinging crack is likely to penetrate through the hard impact surface, which would significantly affect the club's structural integrity. Charge contrast scanning electron micrographs indicate that cracks remain mostly contained within the periodic region, with evidence of deflection within the impact region, implying that the G_{IF}/G_{C1} ratio successfully prevents cracks from reaching the club's outer surface. Given the complexity of the club's microstructure, other dissipative mechanisms at the micro- and nano-scale must also contribute to its toughening. As in

other mineralized biocomposites, these could include micro-cracking at the crack-tip process zone, crack bridging from mineralized chitin fibers, or crack deflection at interfaces (ABAQUS, Version 6.10), as well as time-dependent mechanisms, which will all be amplified by the helicoidal crack pattern.

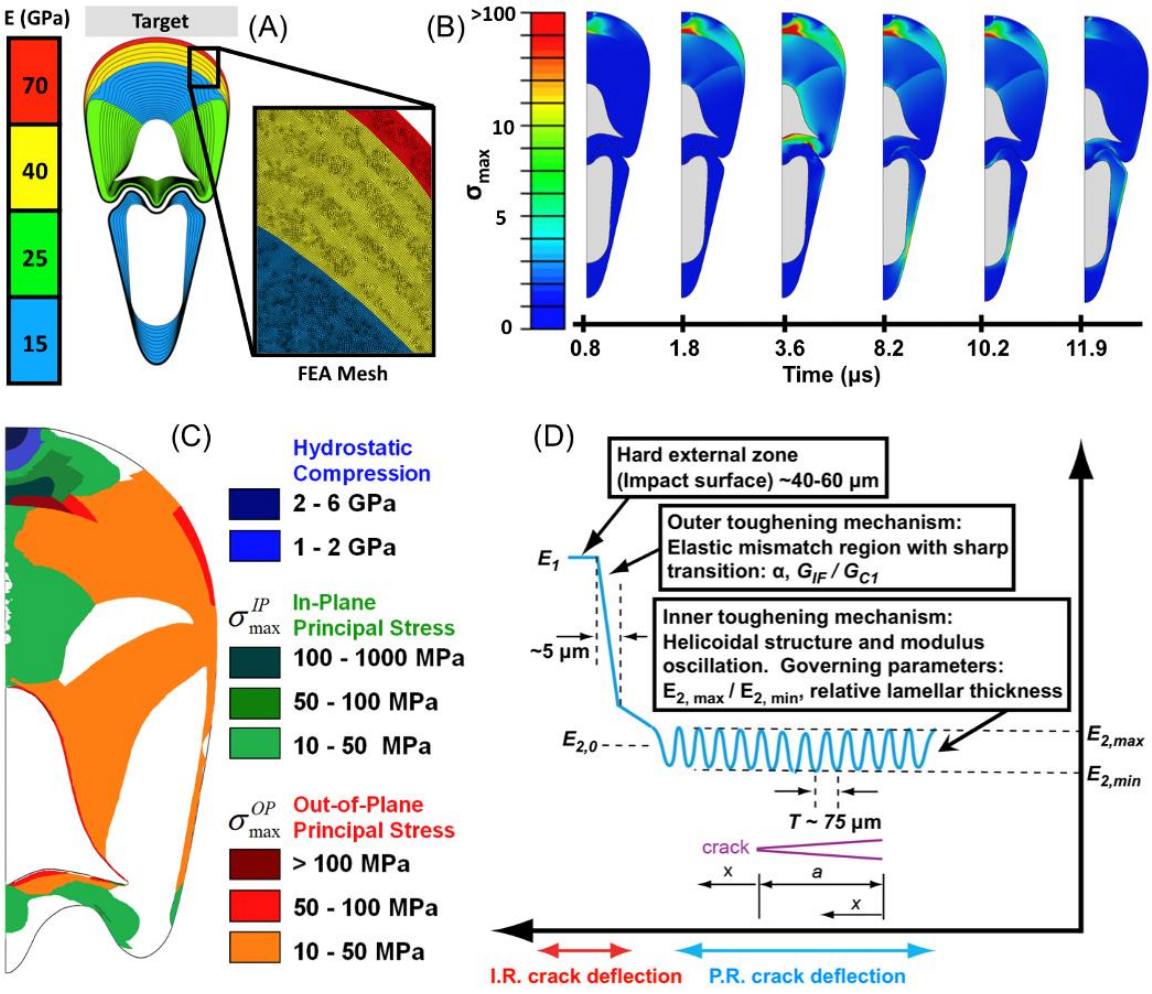

Figure 2.5: Dynamic Finite Element Analysis (DFEA) and micromechanical modeling. (A) Geometry of the dactyl club/propodus system impacting a target at 20m/s. Color coding corresponds to the different elastic properties and mass densities used for DFEA simulations. (B) Evolution of the maximum principal stress σ_{max} during the impact event until the propagating pressure wave reaches the end of the propodus. (C) Maximal principal stresses within the dactyl club at ca. 2μs after impact. (D) Toughening strategies of the dactyl club: (*i*) hard outer layer for maximum impact force; (*ii*) modulus transitional domain for crack deflection

between the impact surface and the bulk of the impact region; (*iii*) periodic region with helicoidal pattern and modulus oscillation for crack shielding. (*a*: crack length, *x*: coordinate perpendicular to the crack front propagation, ξ: relative coordinate ahead of the crack tip in the periodic region (ξ = x-a), *E*(x): elastic modulus oscillation).

Influence of modulus oscillation on the crack-driving force

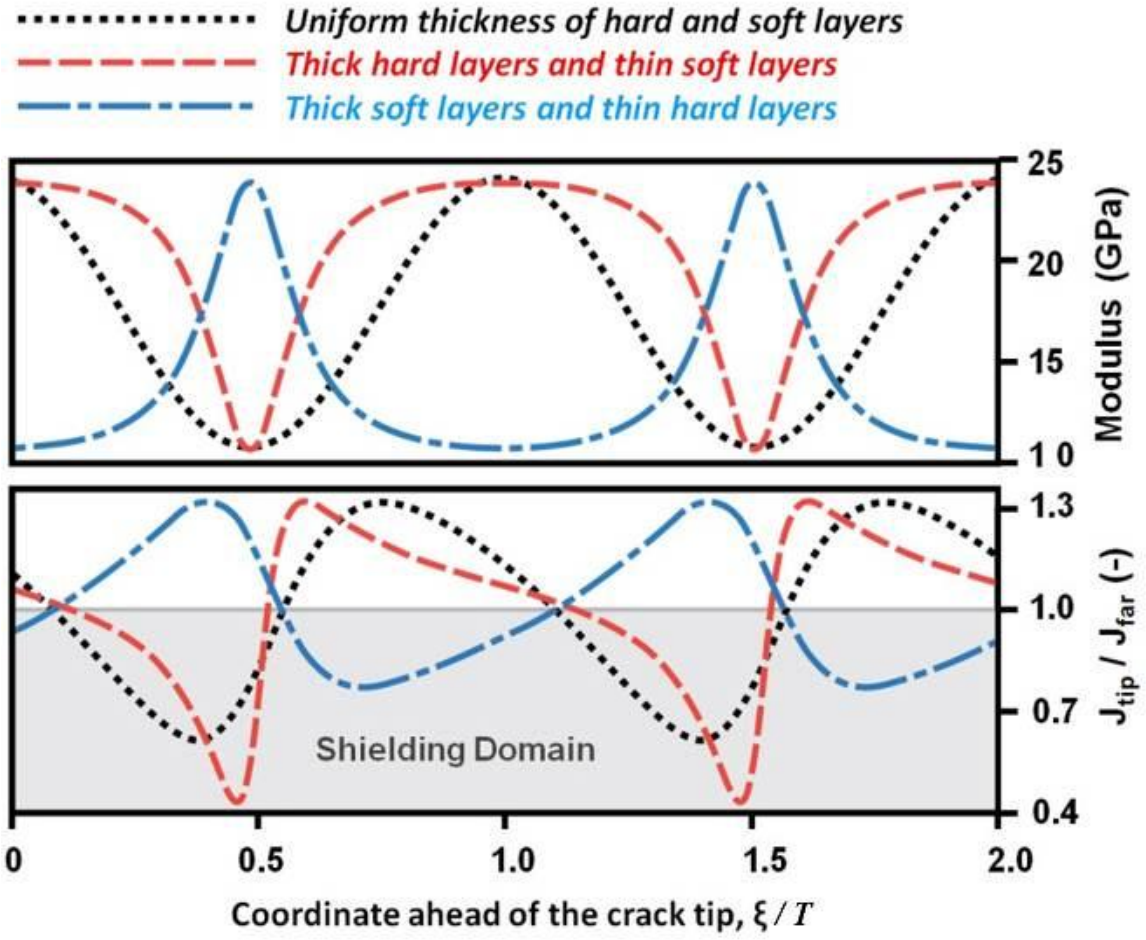

Figure 2.6: Elastic modulus (upper) oscillation and crack-shielding J_{tip}/J_{far} (lower) *vs.* the normalized coordinate ahead of the crack-tip, ξ/T (where *T* is the oscillation wavelength), in the periodic region of the dactyl club for three limiting cases of crack propagation/fiber orientation relative direction. The crack-driving force ahead of the crack tip for the three cases was computed according to Eq. S2. J_{far} corresponds to the far-field crack-driving force for a homogenous material with modulus E_0 and J_{tip} is the crack-driving force at the crack tip for materials with periodic moduli (He, 1989).

When an impinging crack deviates from its helicoidal pattern and crosses helicoidal super layers in the periodic region, it encounters a modulus oscillation. Depending on the direction of crack propagation relative to chitin fiber's orientation within the layers, the relative thickness of soft and hard layers vary, and three limiting cases can be considered. In the first case, the thickness of soft and hard layers is equivalent, and the modulus features a sinusoidal profile of period $T \sim 75$ μm (Fig. 2.4B), with maxima and minima values of 25 and 10 GPa (Fig. 2.2B, inset). In the second case, the modulus profile will feature hard, thicker layers separated by thin, softer layers. The third case is the opposite, with soft thicker layers separated by thin harder ones. We analyzed the effect of this modulus oscillation on the crack propagation using the formalism developed by Fratzl *et al*. (He, 1989), which show that the crack tip propagation driving force, J_{tip}, in a non-linear elastic material with periodic modulus can be expressed as :

$$J_{tip} = J_{far} \times (1 + f_{inh}) \quad \text{(Eq. S1)}$$

where J_{far} is the far-field J-integral surrounding the crack tip as defined by standard fracture mechanics (40), and f_{inh} is a factor related to shielding or anti-shielding due to modulus oscillation. With a far field modulus taken as the average modulus E_0, and the condition that the layer wavelength T be much smaller than the singularity-dominated

zone *R*, which is obeyed here (*R* is on the order of a few mm whereas *T* is in the μm range), they derived the following expression for f_{inh}:

$$f_{inh} = p_0 \int_0^T \left(\frac{E_0}{E(a+x)} - \frac{E_0}{E(a-x)} \right) dx - p_0' \left(\frac{E_0}{E(a)} - \frac{1}{T} \int_0^T \frac{E_0}{E(x)} dx \right) \quad \text{(Eq. S2)}$$

where *a* is the crack length, *x* is the coordinate perpendicular to the crack front propagation, ξ is the relative coordinate ahead of the crack tip in the periodic region (ξ = x-a), and *E*(x) is the elastic modulus oscillation. We used the periodic function suggested in (He, 1989) to describe *E*(x), which was fitted to our nanoindentation data to obtain values of the oscillation wavelength, thin layer thickness, and modulus ratio $\rho = E_{max}/E_{min}$. The three cases mentioned above are depicted in Figure 2.6 (upper), and the effect of modulus oscillation on the crack tip driving force is shown in Figure 2.6 (lower), here expressed in terms of the normalized crack-driving force (J_{tip}/J_{far}) as a function of the coordinate ahead of the crack tip ξ. As discussed in (He, 1989) shielding regions exist whereby the crack driving force is significantly reduced, with the actual amount of shielding depending on the relative thickness of soft and hard layers. A value ρ = 2.5 was measured in the stomatopod club, which is most likely a lower bound value: indeed in our measurements, the variation in modulus at the length scale of indents is related to anisotropy changes of mineralized chitin fibers. At a finer scale which is not captured by the nanoindentation measurements, much more dramatic modulus differences are expected between chitin bundles and the mineral phase. Nevertheless, in order to

obtain conservative values of toughening by the observed modulus oscillation, we used ρ = 2.5 in the calculations, and we see that case 2 (thin soft layers between thick hard layers) is the most efficient in reducing the crack tip driving force, with minima J_{tip}/J_{fa} ratio of 0.4. A regular sinusoidal oscillation (case 1) yields to minima of J_{tip}/J_{fa} of 0.6. Although case 3 (thin hard layers between thick soft layers) provides some shielding, it remains limited in comparison to the other cases. With larger differences in modulus oscillation (as discussed above), more dramatic crack shielding is predicted. Hence in the periodic region, had a crack deviated from its helicoidal trajectory, the analysis suggests that subsequent propagation is hampered by the modulus oscillation, with an efficiency that depends on the direction of crack propagation relative to the fiber orientation in the helicoid.

Conclusion

Our studies show that the stomatopod dactyl club represents a significant departure from previously-studied damage tolerant biological composites, in that it is specifically employed for high velocity offensive strikes. Our structural investigations coupled with nano-mechanical characterization and finite element simulations have shown that the club consists of several microstructural features that permit the infliction of crippling impacts while simultaneously minimizing internal damage within the club. These characteristics include a graded helicoidal architecture constructed from mineralized chitin fibers that can dissipate the energy released by propagating microcracks, an oscillating elastic modulus that provides further shielding against catastrophic crack propagation, a modulus mismatch in the impact region that acts as a crack deflector near the impact surface, and an ultra-hard outer layer correlated with a high level of mineralization and a radial organization of apatitic crystallites. The structural lessons gained from the study of this multi-phase biological composite could thus provide important design insights into the fabrication of tough ceramic/organic hybrid materials in structural applications, where components are subjected to intense repetitive loading.

Materials and Methods:

Specimen Handling and Sample Preparation

Live specimens of *Odontodactylus scyllarus* from the tropical Indo-Pacific were obtained through commercial sources and maintained live in a recirculating seawater system until ready for use. The dactyl clubs were dissected from these specimens and rinsed in fresh seawater to remove any loose organic debris. The samples were then rinsed briefly in deionized water to remove any residual salt and then air dried at 30 ºC. The resulting samples were either imaged in their entirety for whole-club scanning electron microscopy (SEM) or imbedded in Epofix resin for the preparation of cross-sections. The obtained resin blocks were manually trimmed down to the desired imaging plane with a diamond saw and polished to P1200 with progressively finer grades of silicon carbide paper and then with polycrystalline diamond suspensions down to 100 nm to obtain a smooth finish. The resulting samples were imaged either by optical microscopy, backscattered scanning electron microscopy, Energy Dispersive Spectroscopy (EDS), or subjected to nanomechanical testing. In total, the dactyl clubs from more than 15 different individuals were investigated and the results reported here are representative of the trends observed.

Scanning Electron Microscopy (SEM) and Energy Dispersive Spectroscopy (EDS)

Whole or polished dactyl club samples were gold or carbon coated and examined with an FEI XL-40, a Tescan VEGA TS-5130MM, or a Tescan VEGA XMU scanning electron microscope equipped with an Oxford Instruments (X-Max) energy dispersive

spectrometer. EDS line scans and compositional maps were acquired at a 20 kV accelerator voltage.

Nano-Mechanical Testing

Nanoindentation studies were performed on transverse cross-sections through the center of the dactyl club in ambient air using a Triboindenter nanomechanical testing system (Hysitron, Minneapolis, MN, USA) equipped with a berkovich tip at a peak force of 5 mN. The load function consisted of a 5-second loading to 5 mN, followed by a 5-second hold at that force, and then a 5-second unloading. The hardness and reduced modulus were calculated from the unloading curve of each, using the Oliver-Pharr method (38).

For the area maps presented in Figure 2.2B (left), the indentations were performed in a grid-array with ca. 100 µm spacings. For the higher resolution line scan measurements through the center of the transverse dactyl club section shown in Figure 2.2B (right), the indents were spaced ca. 15µm apart. For the very high resolution line scan plot through five super-layers (with periodicity: ca. 75µm) of the periodic region (Fig. 2B, inset) a grid array of indents (with 10 µm spacings) was performed at an angle of ca. 5 degrees from the vertically oriented super layers (Fig 2.7). These data were then collapsed to form an averaged linear plot of modulus through the layers. This method was chosen to obtain a high resolution line scan through the structure to observe variations in modulus as a function of chitin fiber orientation, while simultaneously maintaining adequate indent spacing to prevent problems associated with indent overlap

and subsequent damage-induced changes in the local mechanical properties of the sample.

Similar indentation measurements were also performed on the same samples that had been hydrated with seawater using rows of intents that crossed from the outer impact surface into the periodic region. These measurements were performed to investigate the possible influence that sample dehydration might have on the measured mechanical properties. These results revealed that due to the highly mineralized nature of the dactyl club, there was on average only a ca. 15% reduction in both modulus and hardness within the clubs in the hydrated vs. the dry state. In addition, the measured hydrated vs. dehydrated differences in modulus and hardness were within the measurement variability observed between different individuals. For this reason, and to standardize measurements from sample to sample, all subsequent measurements were performed with dry samples.

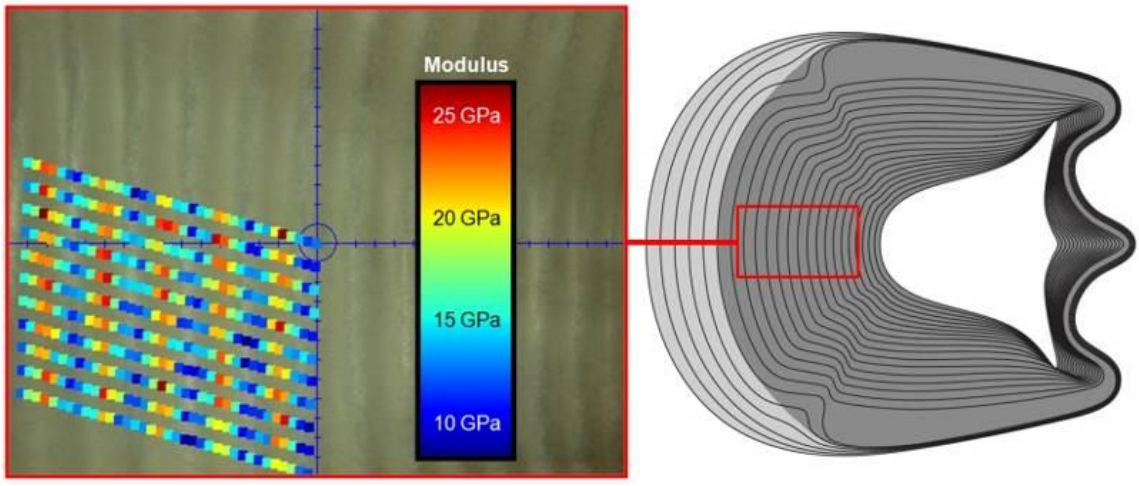

Figure 2.7: Indentation grid array used to generate the high resolution line scan data depicted in Figure 2.2B, inset. The indents (each denoted by a colored square)

have been overlaid on an optical micrograph of the club's periodic region to show the relative X-location of each indent. In this figure, the Y-distance between the indents has been exaggerated to reveal the underlying banding pattern.

Synchrotron X-Ray Diffraction Studies

Synchrotron X-ray data was collected at Beamline X13B at the National Synchrotron Light Source, Brookhaven National Laboratory, using 19 keV X-rays (λ = 0.65 Å) and a beam spot focused to ca. 5 μm × 5 μm. Specimens consisting of dactyl clubs embedded in Epofix resin were sliced with a diamond saw to create 0.5 mm thick slices which were then mounted onto the beamline sample holder in transmission geometry. Transmitted X-ray intensity was recorded using a photodiode detector fixed beyond the sample at the beam stop and normalized by incident intensity measured with an upstream ion chamber. Diffraction data were acquired with a Princeton Instruments CCD detector approximately 15 cm beyond the sample. Frames were not corrected for spatial distortions within the detector optical taper. Using a sintered corundum standard, the software package *Datasqueeze*, and a JCPDS data card for corundum, we calibrated detector pixel positions to *Q*-values and subsequently re-refined the data using the hydroxyapatite (002) peak as an internal standard. A representative diffraction pattern from the impact region illustrating the (002) oriented hydroxyapatite crystallites is shown in Figure 2.3A. The plots in Figure 2.3B were generated by integrating around the azimuthal coordinate (0-360 degrees χ) to produce intensity vs. *Q* plots with *Q* ranging from 0 to 3 ($Å^{-1}$). Diffraction patterns were acquired from the dactyl club impact and periodic regions as well as a hydroxyapatite mineral standard, a dried bovine bone sample, and a

commercially available crustacean chitin standard from MP biomedical (Catalog Number 101334).

For the X-ray composition maps shown in Figure 2.3C, a 31x25 mesh of diffractograms was acquired from a dactyl club, with each spot separated by 100 □m in both directions for a total of 775 diffraction patterns. For mapping the hydroxyapatite and amorphous phase distributions shown in Figure 2.3C, we integrated the areas under the highlighted zones of the impact and periodic region diffraction patterns in Figure 2.3B, which predominately corresponded to the (211), (112), and (300) reflections of hydroxyapatite and a broad amorphous hump in the periodic region. These data were collected for each diffractogram and their relative concentrations were normalized to 100% intensity. The orientation of the hydroxyapatite crystallites was determined by approximating the preferred orientation in χ of the (002) reflection for each diffractogram (Figure 2.3A) and its relative angle was denoted as a sloping black line through each pixel of the hydroxyapatite distribution map. The resulting data sets were plotted independently and then combined in the lower left of Figure 2.3C so that a direct comparison could be made to the obtained X-ray transmission data.

The orientation of chitin fibers was measured using the techniques detailed in (24) and more generally (Dowling, 2006), by assuming that crystalline chitin grains exhibit fiber symmetry (a preferred c-axis but no preferred orientation within the plane normal to that axis), while the arrangement of the grains breaks this symmetry, with an angle □ between the fiber axis and a reference axis (the transmitted X-ray beam direction) that can vary from place to place within the sample. First, the (110) reflection of chitin was

identified, and intensity vs. Q plots as a function of detector azimuth χ were generated, integrated over a range of Q which bounded this reflection (Q = 1.3-1.4 $Å^{-1}$). As the fibers deviate from orthogonality with the beam, the location of their reflections on the detector do not remain separated by 180° in χ but have centroids displaced by an angle η. Diffracted peaks will obey:

$$\cos(\eta) = \tan(\theta)/\tan(\mu),$$

where θ is one-half the Bragg scattering angle. Representative data are shown in the 3 plots of Figure 2.4E, with the blue plot displaying peaks separated by 180 degrees χ, and the green and red plots displaying a varying distance between peaks due to the nonzero η values. Using the python programming language to automatically analyze a batch of plots, each plot was reduced to only consider points within the top 50 percent of intensity values. Using known approximate locations for peaks, the script found average peak positions weighted by intensity within the known regions. This produced two peak locations in χ for each diffractogram. The resulting measured η values were used to determine the fiber orientation angle μ for each diffraction pattern. Solving for μ provides one of the two angular coordinates needed to represent the average direction of the chitin fibers within the diffraction volume. The orthogonal coordinate which represents the angle around the beam is given by the midpoint between the two acquired peaks' positions.

Figure 2.4D depicts both angular coordinates calculated from each diffractogram as colored bars using the vpython graphics library. The result is a constant helical pitch (curved white lines), except where chitin fibers become parallel with the beam, where invalid assumptions in the rendering produce errors creating deviations in orientation.

3D Modeling of the Helicoidal Architecture

Using the vpython graphics library, rows of chitin fiber bundles in a helicoidal stack were visualized as close-packed cylinders. Each cylinder was colored half yellow and half blue to better visualize the constant rotational offset between each sequential layer. Curvature was then applied to the entire stack to represent the influence of the hemispherical dactyl club core and exterior. Finally, a plane was chosen to represent a polished cross section through the curved structure, and the points which defined each cylinder were collected from the intersecting plane, and visualized with their colors preserved (Fig. 2.8). The resulting visualization of the fibers precisely reproduces the fractures seen in the charge contrast scanning electron micrographs, providing strong evidence that fractures predominantly propagate between the chitin fibers within the helicoidal assembly.

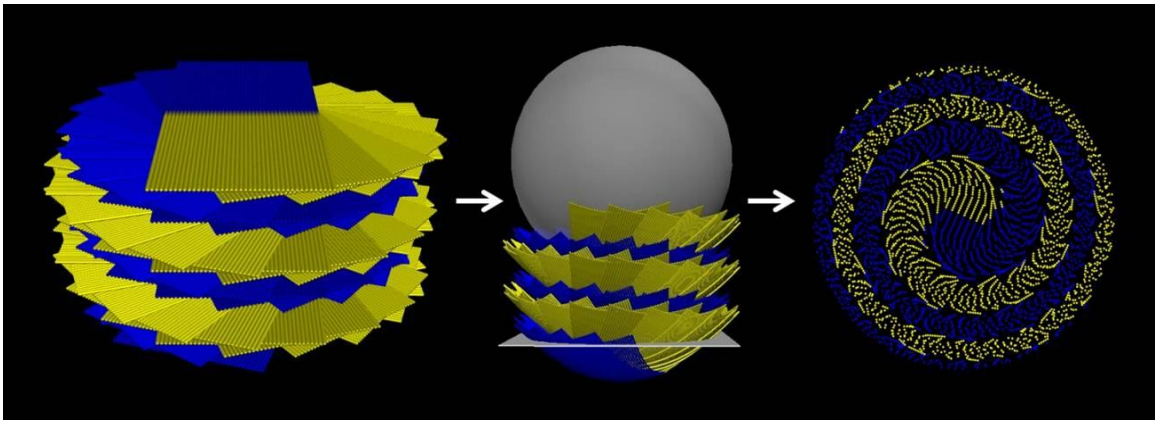

Figure 2.8: A helicoidal stack of cylinders representing chitin fiber bundles within the dactyl club (left). The same helicoidal stack with an applied curvature was achieved by wrapping the structure around a sphere and an intersecting plane (shown in gray) denotes the location of sectioning (middle). A collection of points representing the chitin fiber bundle locations accurately reproduces both the locations and curvature of the fractures seen in charge contrast scanning electron micrographs in Figure 2.4 (right).

Dynamic Finite Element Analysis

Dynamic Finite Element Analysis (DFEA) of an impact event between the dactyl club and a solid target was carried out using the finite element software Abaqus/Explicit (39). Our model considered the entire geometry of the dactyl, the propodus, and the target as depicted in Figure 2.5A. Because the terminal two segments of the raptorial appendages can be approximated as a solid of revolution, we carried out a 2D axysymmetric analysis. The dactyl club has an average total length of ca. 5 mm and a radius of ca. 2 mm. The entire distance from the top of the club (impact region) to the end of the propodus is ca.10 mm. These dimensions are representative of a typical adult sized specimen of *Odontodactylus scyllarus* (and similar to the one analyzed in this paper and used for other previous experimental work (Patek, 2005)). The complex macroscale

geometry of the dactyl club and propodus presented in Figures 1.1-1.4 was followed with high fidelity in our models. The mechanical response of the material was modeled as isotropic linear elastic with different mechanical properties and mass densities (matching our nanoindentation and compositional data) assigned to each of the sections indicated in Figure 2.5A. In addition, the water-filled cavities (containing the internal musculature) of the dactyl and propodus were simulated as an acoustic medium to properly account for the wave propagation in the fluid and its interaction with the rest of the club. The finite element mesh contains a total of 433,787 nodes and 429,987 elements. In these simulations, the target initially traveled at 20 m/s and impacts the dactyl club producing a compressive stress wave traveling through both the target and dactyl. Because we were interested in the impact event, we did not consider the effect of the water surrounding the dactyl club (although we do consider the water inside the central cavity, as it is very important for transmission of the stress waves). Due to the relative low impedance of water, the boundary of the dactyl and propodus were modeled as free surfaces.

The total impact force was calculated as the sum of the individual nodal forces in the direction of the impact along the lower surface of the target. The image in Figure 2.5C is a composite showing the maximum principal stress in green tones to indicate when the maximum principal stress lies in the computational plane, and in red tones when the maximum principal stress lies in the direction perpendicular to the computational plane. The blue regions are those where the three principal stresses are negative with similar values. Based on these observations, the compressive stress is regarded as hydrostatic.

Finally the effect of the propodus was examined by performing additional DFEM without the propodus present. As expected, and since the maximum stresses are achieved at 2 μs following impact (Fig. 2.5B), the propodus does not have any effect on the internal stress distribution at that time. However, the propodus does affect the strike force. It is noted that the difference in the recorded strike force begins at 3 - 4 μs after impact which is when the propagating stress wave from the propodus arrives to the target. The peak forces in both cases (with and without the propodus) take place at roughly the same time (with 0.1 μs delay in the case with the propodus). However, the main differences are in the peak force and, more remarkably, the impulse energy (area beneath the force vs. time curves). The peak force in the case without the propodus recorded in our simulations was 692 N, whereas the one with propodus was 717 N (representing an increase of 3.6% with respect to the case without the propodus) (Fig. 2.9). The impulse in the case without the propodus is $4.17 \cdot 10^{-3}$ $N \cdot s$ and with the propodus is $5.27 \cdot 10^{-3}$ $N \cdot s$, which implies that the propodus contributes 26.4% more impulse energy.

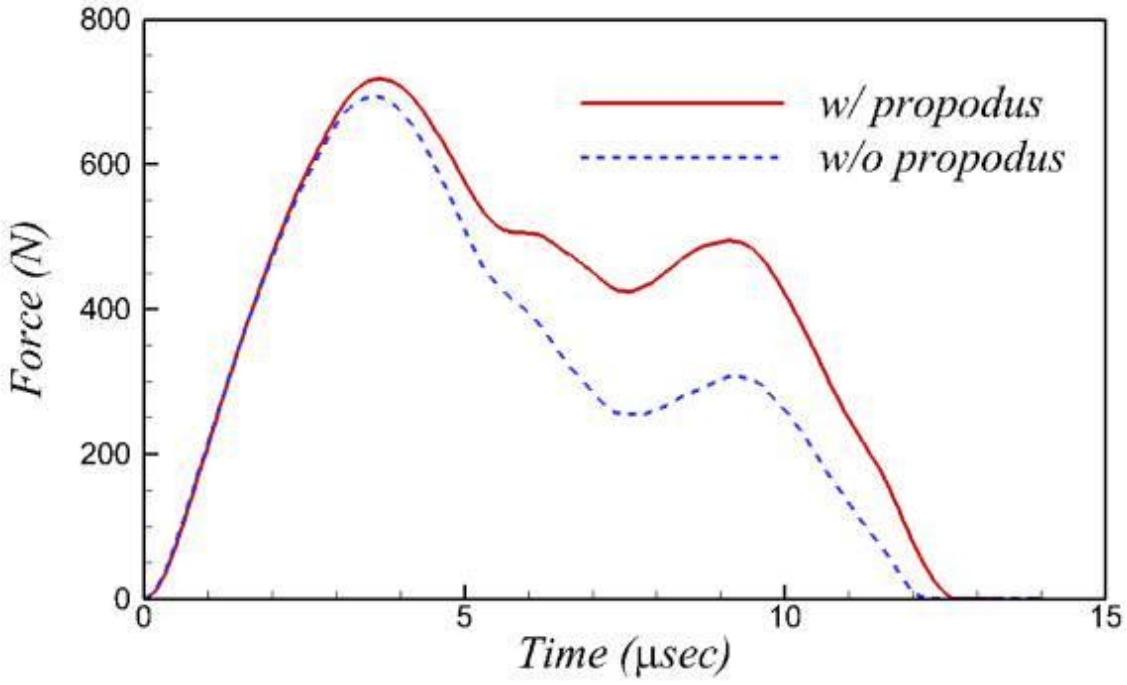

Figure 2.9: Graph illustrating evolution of the force recorded at the impacted target (or sensor) with and without the propodus present for a representative simulation.

Chapter 3: Helicoidal fractures in porous helicoidal composites: a branching failure regime for lightweight ultra-tough impact resistant materials.

Abstract:

There is a large disparity between the use of helicoidal composites by man and nature. Nature has independently evolved the structure many times, where humans have rarely taken advantage of it. Features of the helicoidal architecture in the stomatopod dactyl club are characterized, and mimetic structures were built and tested. Implications to how the material grows, mechanisms behind its toughness, and how its lessons may be applied are discussed.

Introduction

Aircraft, body armor, and a multitude of other application spaces have historically demanded advances in materials which must strike a balance between all that is desired of them. Desired properties such as toughness, weight, strength, stiffness, and impact tolerance are all coupled, with some couplings that are undesirable. Engineering new materials is an incremental process whereby small gains are made by altering structure and chemistry across the full spectrum of scale. The more time spent modifying the materials at each hierarchical scale, the more they become refined for their function. This tinkering process is analogous to the evolutionary processes that have been optimizing biological materials since the origin of life. In many cases a biomaterial may be optimized for the same constraints (lightweight, tough, etc.), and even the same function (armor, wings, etc.). Human engineering does not share many of the constraints which life has been evolving under; therefor, many engineering materials have surpassed the capabilities of biological materials. However, biological evolution has had a tremendous head start, and in many cases, makes better use of energetically cheap constituent materials by utilizing mechanisms that have, to date, eluded our species creative potential.

Bioinspired materials engineering seeks to understand the mechanisms demonstrated within the materials created by life, and attempt to combine these structure-function relationships with those on the frontier of materials science. Ultimately, a biomimetic engineer may modify an established engineering practice with a mechanistic hypothesis, which is supported by its analogous existence in a biomaterial. If the structure being mimicked is a convergent one, which has independently evolved multiple times

across different clades, then the magnitude of the support is multiplied. One such structure is the helicoidal architecture seen ubiquitously in biomaterials ranging from chordates and arthropods to plants (Gubb, 1975). This structure goes by many names such as bouligand (Gharagozlou-van Ginnekcn, 1975), rotated plywood (Weiner, 1997), twisted plywood (Giraud, 1978), and continually twisted structurally chiral medium (CTSCM). This thesis predominately refers to the composite structure as a helicoidal composite. In each of the phyla listed the organic material, which is assumed to cholesterically self-assemble, is a different biomolecule. In the case of chordates it is collogen, plants use cellulose, and arthropods use α-chitin (Kadler, 1996). Each of these biological fibers takes on a twisted conformation producing helical fiber bundles.

The helical nature of two adjacent bundles causes them to interlock with a translational mismatch equal to a fraction of the pitch depending on whether a double or triple helix is formed (Rey, 2010). This mismatch is continued as more fibers are placed adjacently to form a sheet of parallel fibers. The final sheet then has grooves which run diagonally with respect to the parallel fiber direction. The angle between the fibers and grooves monotonically decreases with increasing helical pitch of the molecular conformation. The grooves function as a template for the position of new fibers in successive sheets causing each sheet to form in the grooves of the one beneath. Therefor, each sheet takes an ever-increasing angle until a 180° rotation is complete and the liquid crystal unit cell is defined (after a 360° rotation, the distance between layers is referred to as a helicoidal pitch). This process of liquid crystalline self-assembly provides a convenient mechanism for building an organic matrix, but only if the structure is worth

assembling (Sellinger, 1998). In the case of insects and other non-crustacean arthropods this organic matrix is infiltrated with air post molt and subsequently sclerotized. This cross links the proteins surrounding the α-chitin fibers rigidifying an otherwise liquid architecture.

Crustaceans utilize the benefits of their strong oceanic presence by mineralizing their organic framework in conjunction with the protein cross linkages. After molting, a crustacean will inflate the organic matrix of their skeleton with a concentrated solution of ions. The organic matrix in many cases is thought to provide nucleation sites for amorphous or crystalline precipitation until all but a regular porous network is left producing a fiber reinforced biomineral (Digby, 1964; Endo, 2004).

Stomatopods are a group of marine crustaceans, which can produce highly specialized segments of their exoskeleton in order to impact and destroy the armor of their prey (Caldwell, 1975). They are an old group that has likely been coevolving with many other species to produce impact tolerant materials (Bibo, 1996; Caldwell, 1975; Schram, 2007).

The substructure of the stomatopod dactyl club contains an ensemble of morphological features unique to crustacean cuticle, but there are also very familiar features as well. The ubiquitous helicoidal architecture plays a central role in the club and dominates the volume of the structure. There are certain features of the helicoidal architecture within the dactyl club of *Odontodactylus scyllarus* which are unusual, but its presence suggests that stomatopods after millions of years have never adopted a new structure, better favored for impact tolerance. This implies that the helicoidal architecture

is an important component of a locally optimized impact resistance structure. The differences in loading behavior of impact vs. static loads has been shown to be substantial, so it is surprising to consider an architecture that could be robust and versatile enough to withstand both in different species (Cheng, Thomas, 2011).

One key separation between the stomatopod's periodic region, named in reference to the visible helicoidal pitch, and helicoidally fiber reinforced biominerals of other crustaceans is the presence of a large gradient in the pitch from the core to the impact region of the club. Other crustaceans will change their pitch but a graded pitch is rare, and for the gradient to extend across such a large range is exceptional (ranges have been observed from <5 microns to 200 microns.) One possible explanation for this feature is that the dactyl club is unique in that it requires a much thicker portion of cuticle in order to attain impact tolerance, but this segment must fit within the club prior to molting. This requires a percent change in size much larger than is typical. The expanded gradient may be a consequence of infiltrating a compact organic scaffold with an exceptional amount of mineral. It is therefore possible that understanding the expansion process during molting could aid in developing expandable designs, such as helmets and shelters.

It has long been suggested that there exists a toughening synergy between the pores, mineral, fibers, and proteins, but the exact mechanisms employed have remained elusive. Some mechanisms have been proposed (Chapter 2), and like nacre, the tough material in mollusk shell, these mechanisms are likely important pieces to the whole picture. The goal of this research is to propose and test additional and refined

mechanisms to bring our understanding of the system's mechanics and growth closer to completion.

Fiber and Mineral Characterization

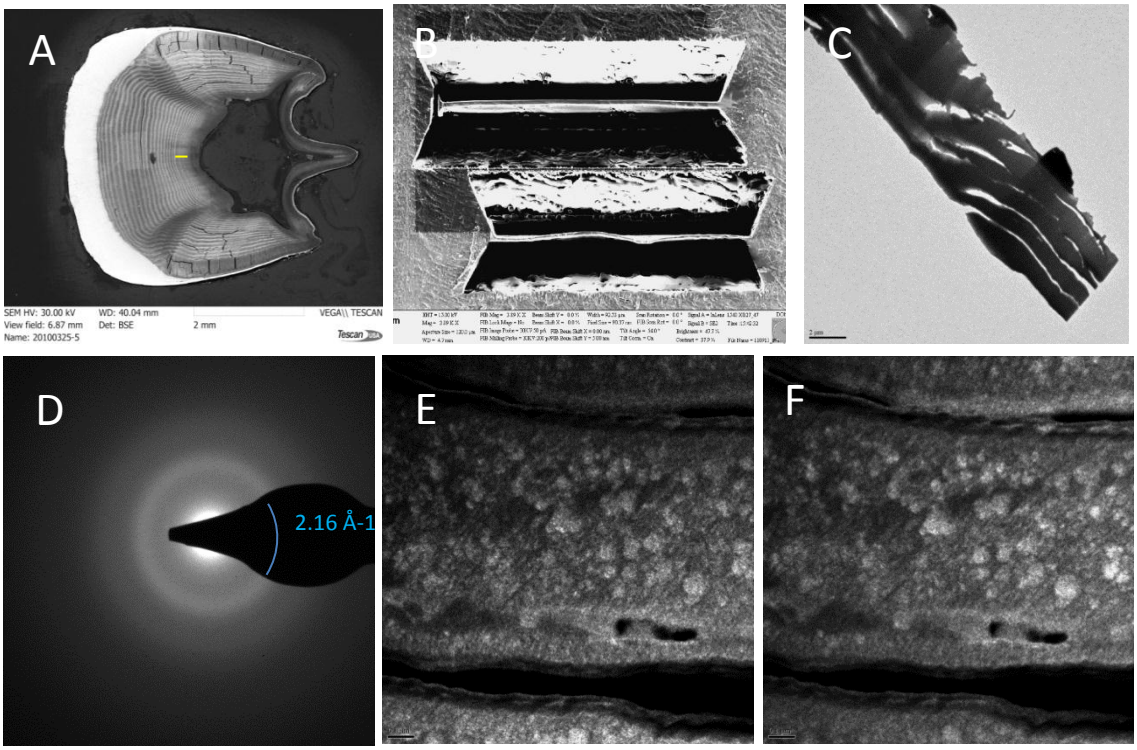

Figure 3.1: (A) a transverse club with a yellow line denoting the relative location of the foil in (B)(C). (D) A diffraction pattern highlighting the amorphous band produced by the spherical minerals in (E)(F). Note the white mineral spherules in the TEM dark field micrographs of (E) and (F) incur minimal change even though their selected areas of the diffuse ring were located 90 degrees apart.

One of the most challenging issues with studying a helicoidal composite is their ability to confound various measurement techniques. As of this writing the authors have yet to develop a reliable way of measuring the parameters which produce the helicoidal structure within the dactyl club. The pitch is trivial to measure with optical microscopy, but is unfortunately dependent on a collection of parameters which produce non unique values for a given pitch. Specifically, these values are the thickness of each layer, the thickness between layers, and the angle between layers. To make a truly biomimetic

composite these parameters would need to be measured. An attempt was made using a focused ion beam (FIB) to produce a thin foil which was examined with transmission electron microscopy (TEM); unfortunately, the crystalline chitin does not survive the process, so neither its presence nor orientation can be measured using electron diffraction. Dark field imaging (Fig.) from the amorphous ring centered at $Q=2.16$ ($Å^{-1}$), attributed to the amorphous mineral (Fig. 3.1) corroborated the crustacean cuticle model which describes amorphous mineral contained in spherules surrounded by a stabilizing organic (Cribb, 2009).

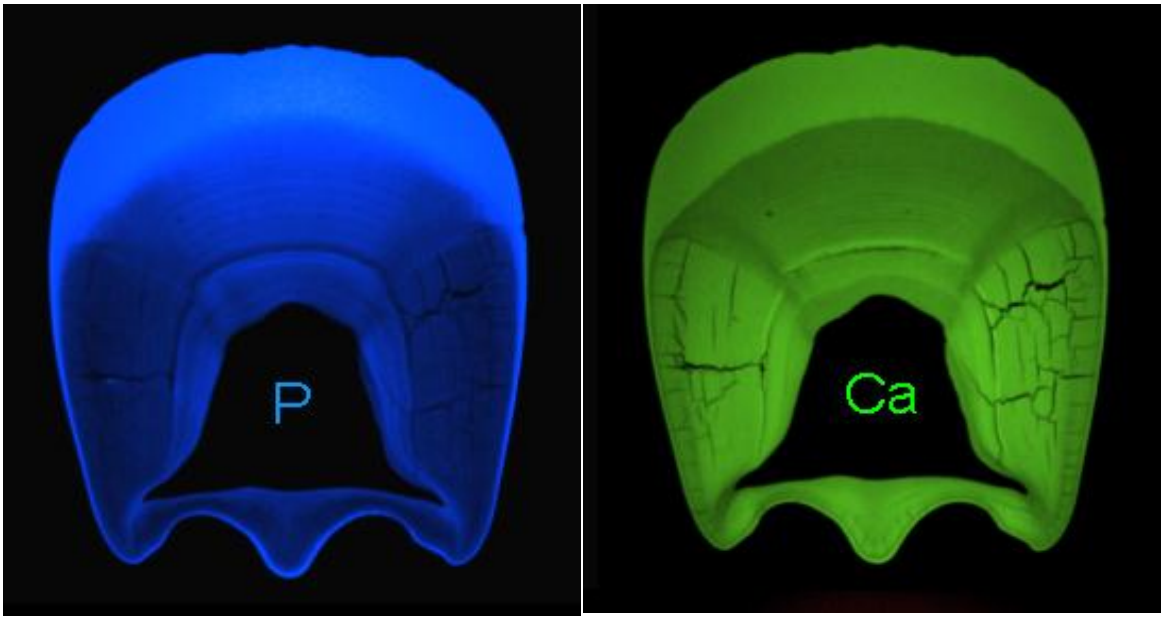

Figure 3.2: EDS maps from a transverse cross section of the dactyl club. (left) The phosphorus content is larger in the medial periodic than the lateral, but the opposite is true for the Calcium map (right).

In addition to confirming the presence of hydroxyapatite in the impact region vibrational spectroscopy such as RAMAN microscopy can help distinguish amorphous mineral phases where diffraction cannot. EDS hints at a phase difference between the medial and lateral periodic regions of the dactyl club, measuring a decreased phosphorus

concentration in the lateral periodic region (Fig. 3.2). This could be due to a decrease in mineral, but this disagrees with nano-indentation maps which report a greater stiffness and hardness in the lateral periodic region compared with the medial periodic region (Chapter 2). Additionally, the calcium concentration increases (Fig. 3.2), and X-ray

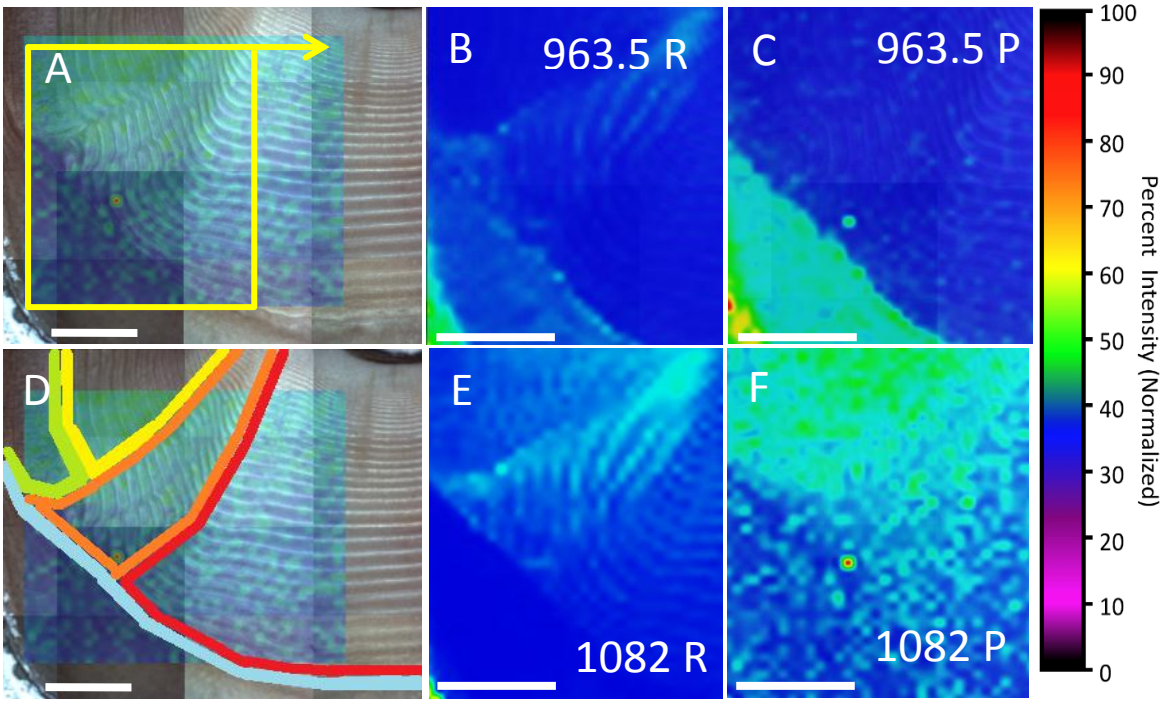

Figure 3.3e: (A) the yellow square denotes the area for the maps: (B)(C)(E)(F). (D) is a color map defining the rgion boundaries using the color code from Fig. 2.1E. (B) is a map from of the raw measured peak intensity for 963.5 cm^-1. (C) is the same map after baseline correction, renormalization, and data smoothing. (E) and (F) follow a similar trend for 1082 cm^-1. Note the lateral periodic phase difference in (F). All scale bars are 500 microns.

transmission intensity decreases (Fig. 2.3C), both suggestive of an increase in mineral concentration. It is likely that the elemental decrease in phosphorus is due to the decrease in calcium phosphate and an increase in calcium carbonate. This hypothesis cannot be supported with EDS alone because carbon concentration is coupled to the organic as well the carbonate molecule.

RAMAN maps extending into the medial and lateral periodic regions show minor intensity for the primary P-O stretch peak at 963.5 cm^-1 (Koutsopoulos, 2002; Penel, 1998) when compared to the impact region. However, the triply degenerated P-O stretch peak at 1082 cm^-1, known to increase in intensity for carbonated apatites (Koutsopoulos, 2002; Penel, 1998), is most intense in the lateral periodic region. This provides convincing evidence to confirm the hypothesis that the mineral in the lateral periodic has an increased concentration of calcium carbonate.

Characterization Obscurity

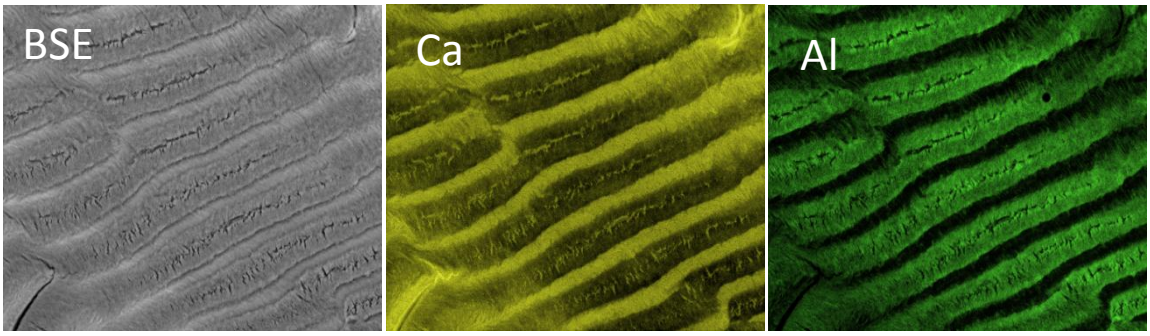

Figure 3.4: (left) a backscattered electron micrograph of the periodic region. Calcium (middle) and aluminum (right) concentration maps of the same region. Note the illusory concentration gradients.

Helicoidal architecture can be confounding not just in its difficulty to acquire specific structural parameters, but when applying standard characterization techniques. If characterizing a polished surface, backscattered electron microscopy can create contrast as a function of regional elemental and concentrational differences. Furthermore, EDS can estimate the concentrational differences for each individual element. In both cases these measurements produce results which suggest concentrational differences in phase

with the helicoidal pitch (Fig. 3.4). Nanoindentation would seem to corroborate the presence of mineral concentration gradients as this technique also measures in phase stiffness and hardness changes (Fig 2.2). A qualitative measure of the periodic stiffness is visible from an SEM micrograph of a nanoindentation line scan. Each triangular indent is produced by loading the sample to the same predefined force; the smallest triangle is located on the lines which produce the largest BSSEM intensity (Fig. 3.5). These lines denote a chitin sheet with fiber axes parallel to the polished surface.

The presence of Aluminum in Figure 3.4 was due to the alumina polishing media used, which provides even further support for concentrational gradients given that the alumina only impregnated the softer less calcified region, except it is also reasonable that the polishing media was able to impregnate the fibers more easily when they run orthogonal to the polished surface. Furthermore, the presence of concentration differences runs counter to the model for how the structure forms. Assume the pitch is the result of a cholesteric assembly, which is symmetric through a rotation and translation down the pitch axis. What could possibly distinguish one layer from the next such that a concentration could be changing in phase with the pitch? Due to the unlikelihood of this scenario, we conclude that the mechanical and elemental properties measured are likely a

result of the fiber orientation, and that no concentration differences occur.

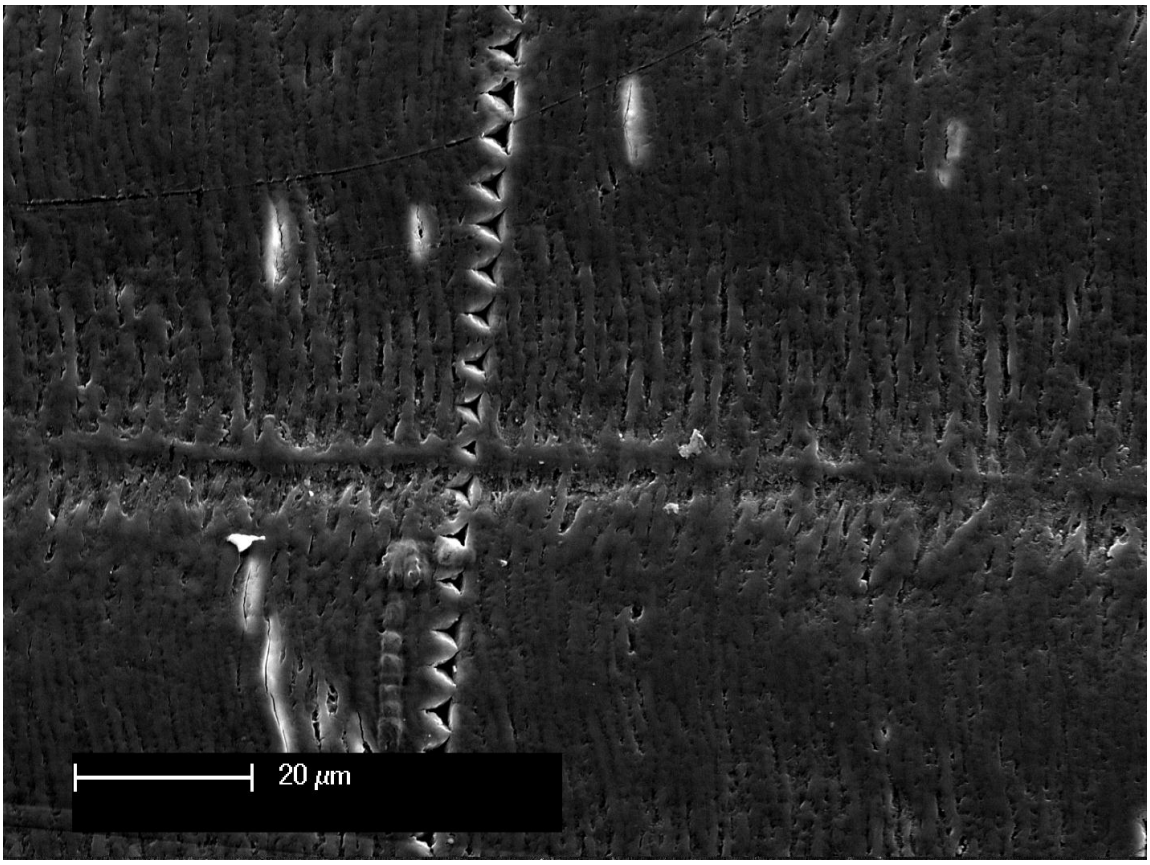

Figure 3.5: A SEM micrograph of indents taken at identical max load. The size of the indents is inversely proportional to the material hardness. Note the smallest triangle's location on the line denoting fibers parallel with polished surface.

To test the hypothesis of a fiber orientation resulting in the measurement of illusory concentration gradients, synchrotron x-ray transmission scans were acquired which showed no considerable changes in the transmission intensity along a single pitch (a flat line of data, not shown). Because synchrotron is a transmissive technique it is not subject to the same limitations of techniques which gather data from an interaction volume that extends only a few microns beneath a surface (this is the case for EDS and BSSEM).

Further evidence for the lack of pitch coupled concentration was provided by predicting the contrast pattern that would be observed from performing back scattered SEM on the corner bridging a sagittal and transverse cross-section of a stomatopod dactyl club. The edge between these two planes is where the visible periodicity displays a one quarter pitch offset. This is because a 90 degree corner is equivalent to observing a 90 degree jump in the layer's orientation. A single pitch is a 360 degree rotation, so a 90 degree shift is a quarter pitch shift. Any phenomenon which is a result of fiber orientation will also experience the ¼ pitch offset. However, if the presence of a concentration gradient was real then its corresponding contrast would be observable as wrapping around the corner, independent of fiber orientation. This is not the case. The contrast remains coupled to fiber orientation demonstrating that the interpretation of concentration differences is false (Fig. 3.6). A mechanism for the coupling between fiber orientation and contrast is not proposed here, but the observations made raise concerns regarding the robustness of techniques which rely on characterization from small interaction volumes

near a surface, especially when applied to complex materials.

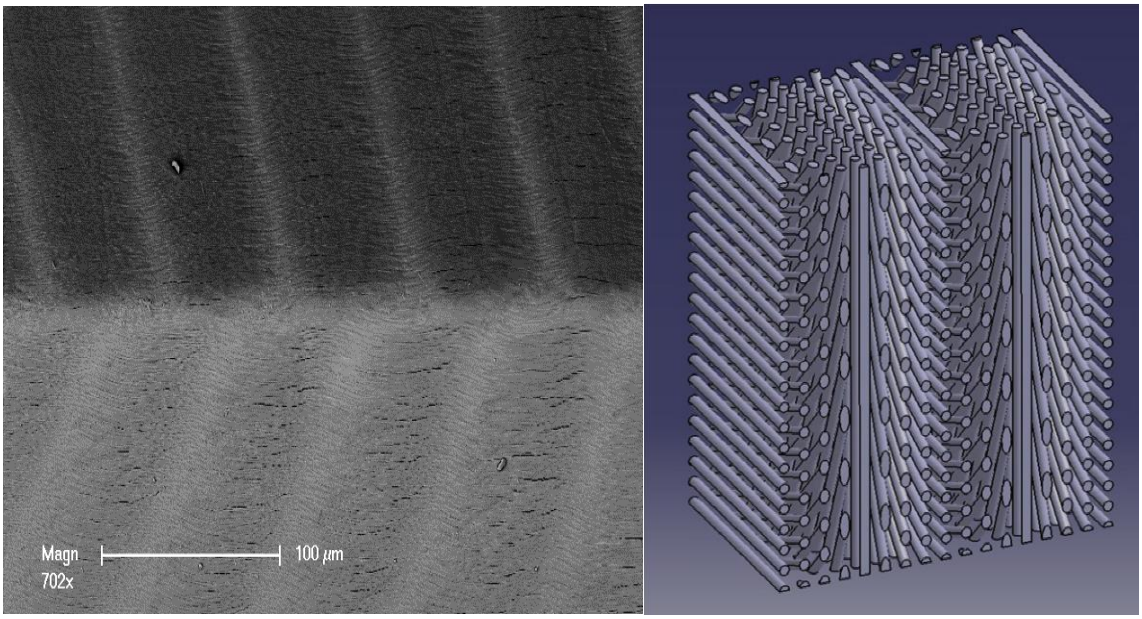

Figure 3.6: (left) A Backscattered electron micrograph from a transverse/sagittal corner of the periodic region of the dactyl club. Note the predicted ¼ pitch offset in the backscattered contrast, proving that it is an artifact of the rotation. (right) A model of helicoidal fibers is included with two sliced planes to aid in visualizing the phenomena on the left.

Ultra-toughening From Controlled Fracture

The presence of pores within an ultra-tough composite can seem unintuitive since pores are something to be avoided as a source of failure (Fernandez, 2012). In some cases pores have been known to provide arresting sites for fractures causing the crack tip stress to become delocalized (Dubensky, 1987). However, no references to pores operating as sites to nucleate energy dispersive fractures have been found. It requires energy to fracture a material because it requires energy to break bonds and create surfaces with higher energy. This is typically a very inefficient method of energy dispersion because a very small portion of the bonds within a material can break before a fracture is propagated to the material's edges, resulting in catastrophic failure.

The proposed energy dispersive mechanisms for nacre (the material inside the shells of some marine snails) are thought to maximize the amount of energy dispersed for a given fracture, by forcing the fractures to break additional bonds (nano-asperities, mineral bridges, sacrificially bonded proteins, etc.) in order to broaden the crack opening angle and continue propagating. If fractures could be initiated and subsequently arrested throughout a material, then the material would be capable of accepting large amounts of energy, resulting in a very high toughness. Depending on how the fractures form within the bulk volume the remaining material network could still retain a high percentage of its original stiffness after considerable fracturing.

Fractures within the medial periodic region of the stomatopod dactyl club have been proposed to favor a path which travels between fibers as opposed to severing them or travelling in such a way that the fibers bridge the fracture (Chapter 2). Only a few possible fracture paths can be taken which follow this constraint. Assuming a fracture

nucleates from a through thickness pore channel due to a uniform stress in all directions parallel to a fiber sheet then it must grow away from the long axis of the pore. However, to remain between fibers its initial propagation direction must continuously change down the length of the pore, forming a helicoidal fracture. Supporting this claim, is the shape of the pore channels in crustacean cuticle prior to nucleating fractures, which is also known to be helicoidal (Cheng, Liang, 2011). Additionally, Helicoidal fractures are also known to form in amorphous media around fibers (Gillham, 1968). The pore channels function as stress concentrators ready to begin splitting fibers, as can be seen from the surface of a delaminated fiber sheet from a demineralized club (Fig). As the fractures propagate radially from a pore channel their path becomes twisted, asymptotically rotating 90 degrees, resulting in a purely a delaminating regime. After a distance r from the nucleating pore channel the fracture must delaminate layers for a distance r*(layer offset angle)/layer. The proportionality with r causes increasing delamination, and a decreasing net component of the mode I force parallel to the sheets, thereby diminishing the crack's

driving force.

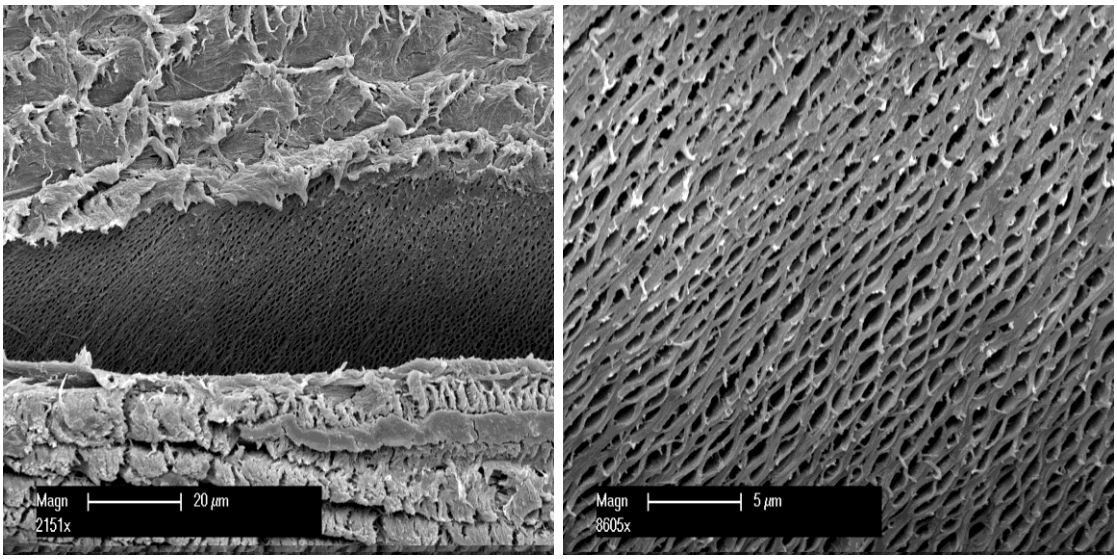

Figure 3.7: (left) a delamination of two sheets in the periodic region after demineralization for 8 hours in acetic 10% acetic acid. (right) a higher magnification of a sheet's surface revealing a wavy fiber motif reminiscent of expanded metal. These pores typically have a lot more mineral in them, but a channeled pore structure is always present.

If the fracture's vertical growth (through successive sheets) is considered, then it follows a helicoidal path, but catastrophic fractures in 3-dimensional materials must travel in at least 2 directions to create the required surfaces. Therefore, the effect of increasing the radius of the vertically propagating helicoidal fracture must be considered. With increasing radii the fracture must traverse larger distances of delamination in order to remain continuous. As before, the driving force decreases for a delaminating fracture, due to the primary forces applied parallel to the fiber sheets. It appears more likely that vertically propagating fractures branch into multiple helicoidal fractures with smaller radii and therefor higher driving forces. The presence of pore channels to seed the branching fractures facilitates this branching process.

Helicoids have the desirable property of having a high surface area while maintaining the ability to nest within each other. This means that with every branching 2 new fracture growth directions are created, and neither fracture runs the risk of arresting the other. This maximizes the amount of fracturable material, and lets the natural arresting mechanisms of the helicoidal architecture dictate the size that each fracture grows to, before its driving force is reduced to an arrestable magnitude. Without the pores to seed the branching process a single fracture could still propagate to catastrophe without having the stress responsible for its driving force relaxed from the initiation of new fractures. Concurrently without the helicoidal architecture the pores would seed a fracture, but its driving force would not diminish as it grows dropping below the threshold value where initiating a new fracture becomes favorable. It is the synergy between these two structural features that is responsible for the ultra-toughness of the

dactyl club.

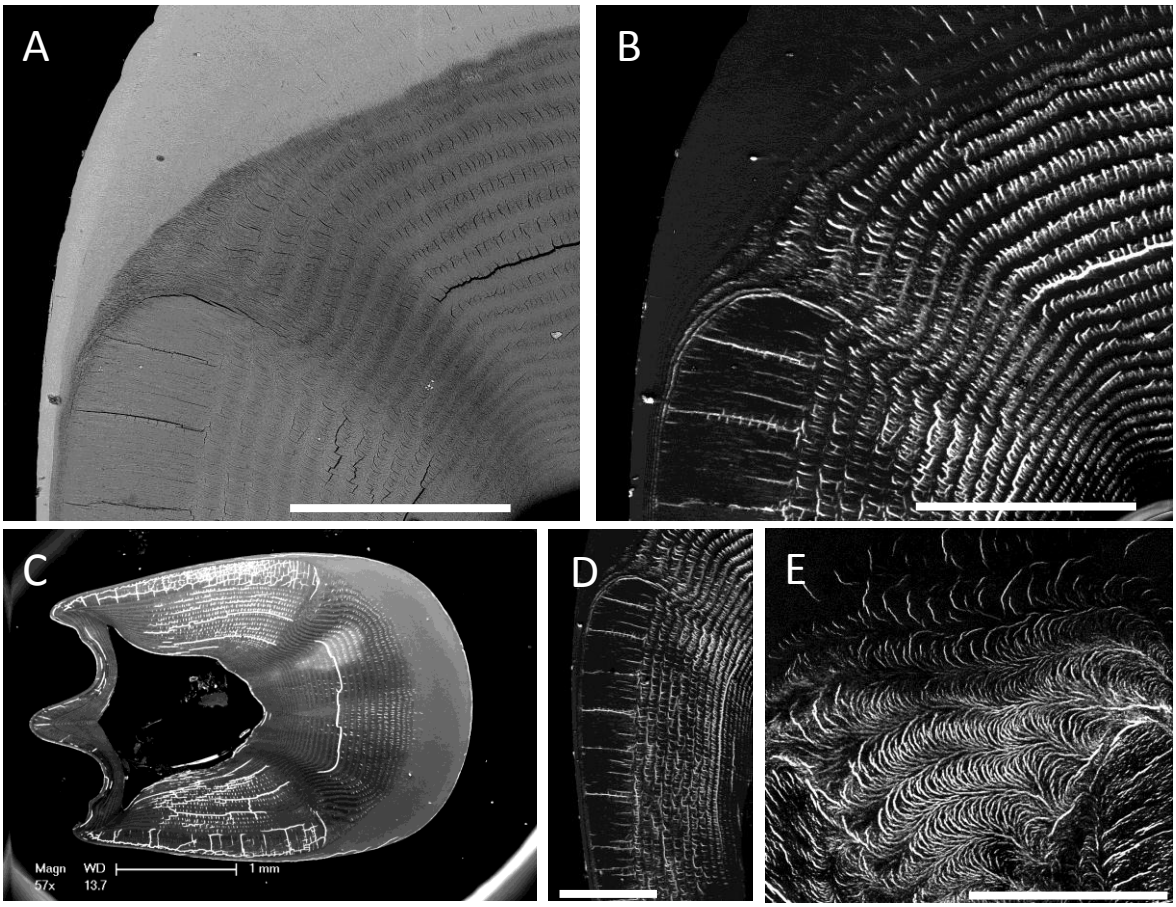

Figure 3.8: (A) a backscattered electron micrograph and its corresponding charge contrast image (B). (C)(D)(E) Assorted charge contrast images demonstrating the club's ability to nucleate and control extensive fracturing without compromising structural integrity (no fractures propagate to the edge.)

The result of the nested fracture toughening mechanism is best illustrated through charge contrast imaging (Fig. 3.8). In (Fig. 3.8E) the nested fractures (white) reveal the handedness of the chitin organization throughout the periodic region, and hint at the possibly that the lateral and medial periodic regions could assemble as three separate liquid crystal grains, which would also explain the large number of dislocations, and smaller radii of sheet curvature, in the interface between these regions.

After assembling, the liquid crystals must expand post molt in the directions perpendicular and parallel to the sheets. The perpendicular direction is proposed as the reason for heavily expanded pitch in the dactyl, but the parallel growth direction has implications as well. The growth mechanism proposed here is that each sheet expands at designated sites along the fibers where they separate from their adjacent fibers. The sheets remain periodically attached and result in an expansion in the direction orthogonal to the fibers, and a contraction parallel to the fibers. The Poison's ratio remains less than 1 throughout the extension of the sheet, so the expansion exceeds the contraction for each sheet. Because the sheets continuously rotate though the stack the net effect is an expansion in all directions parallel to the sheets.

Aside from allowing the exoskeleton to grow after molting, the expansion process proposed causes each fiber bundle to take on a wavy as opposed to strait conformation. This leaves lots of room for mineral, pores, and pore channel fibers which run through the pores stitching the sheets together, and provides a mechanism for turning a liquid crystal into a pore channeled composite.

Biomimetic Synthesis

The exact parameters and synthesis routes to recreate a dactyl club are unknown or nonexistent, but if a mechanism is proposed to explain its ultra-toughness, which utilizes the features of interest then a bioinspired material can be produced to capture the features essential for promoting the proposed mechanism without taking on optimized values. Then signatures for the mechanism can be predicted, and measured to provide confirmation of a working mechanism. This approach uses estimation, theory, and qualitative arguments to accommodate for lacking quantitative data, and once the mechanism has been translated to a synthetic system it will likely need to be quantitatively optimized due to the inevitable differences between the systems, and the limited control over experimental parameters.

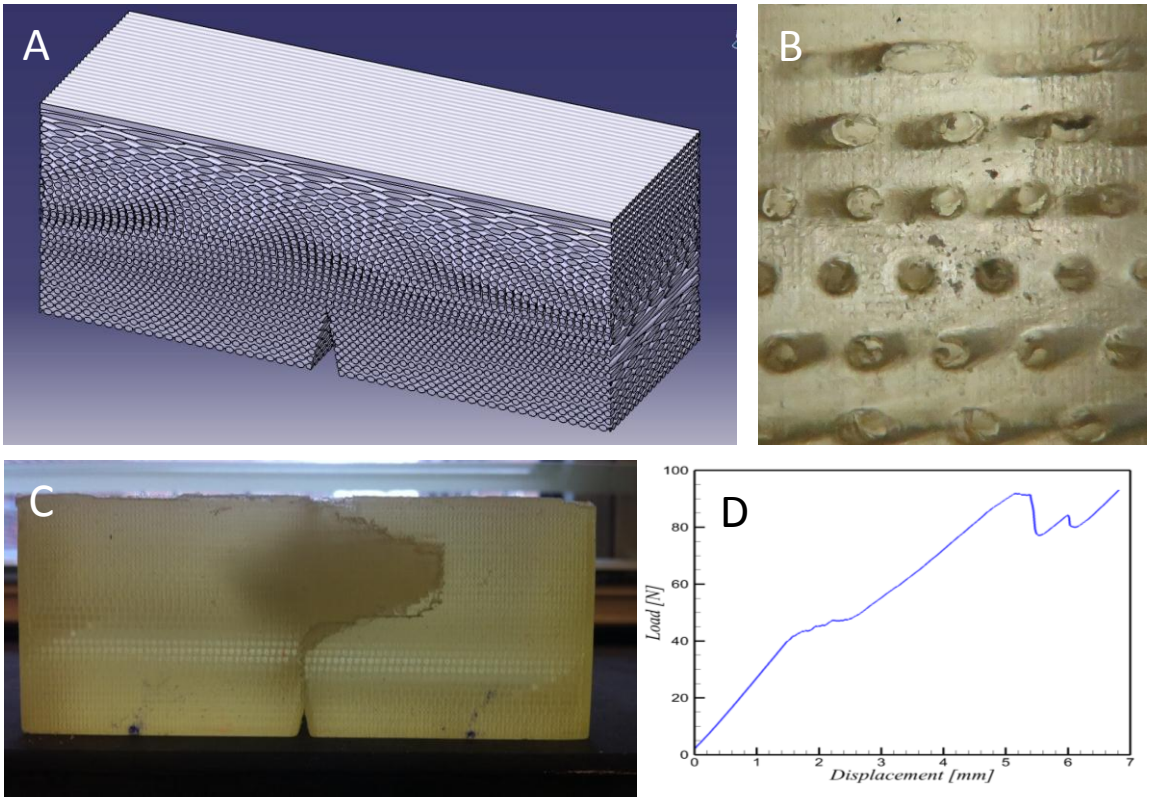

Figure 3.9: (A) a model used to print a helicoidal composite (B). (C) A helicoidal crack is evidenced after the part was loaded to failure, and a load-displacement curve was obtained (D).

To test the ability for a helicoidal composite to rotate a fracture, such that it remains between the fibers, a 3d model of a helicoidal composite was constructed and used to print a heavily simplified scaled up flexural beam. Only two materials were available on the printer used, so the stronger material was chosen to represent the fibers, and the soft support material represents the mineral matrix. A notch was built into the bottom of the model to initiate a fracture and observe its growth. The predicted fracture rotation was confirmed, and the fracture propagated as a helicoid between the fibers, solidifying the helicoidal architecture as a 3D problem that cannot simply be modeled as

a 2D graded composite.

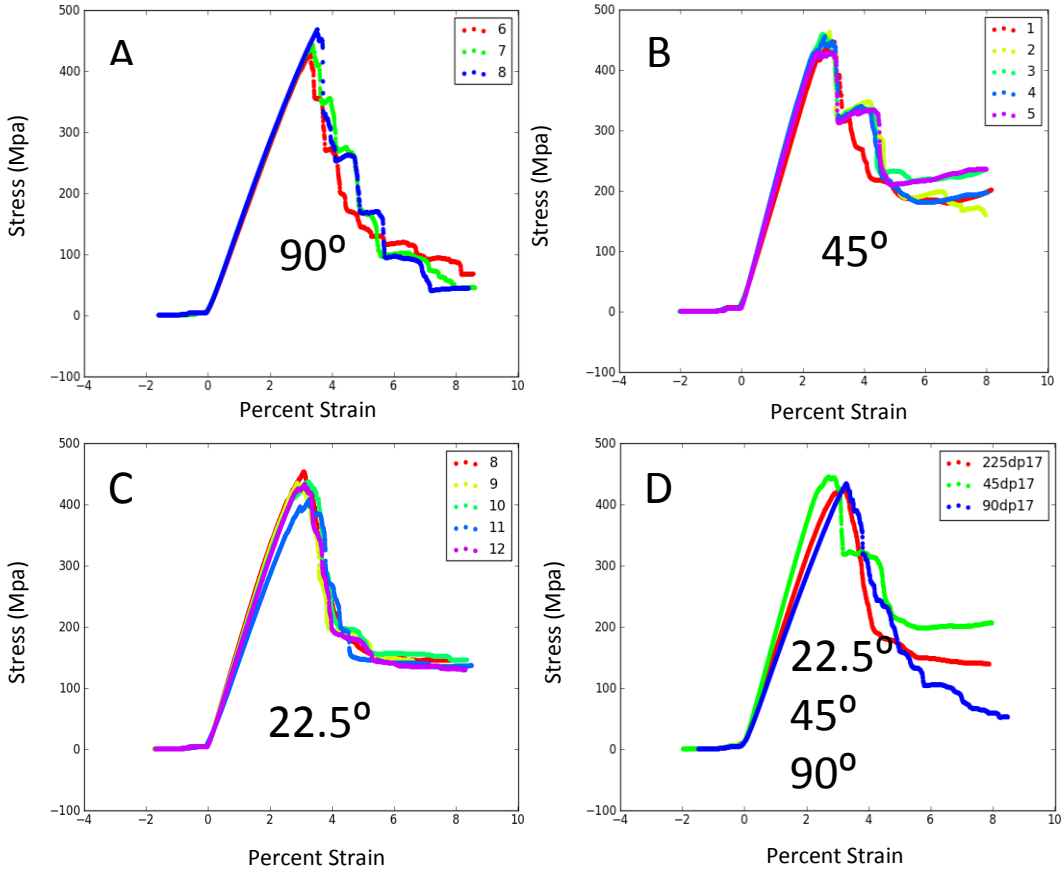

Figure 3.10: Stress strain curves generated by loading 17-ply samples in a 3-point bend configuration. The offset angles between plies were (A) 90^0, (B) 45^0, (C) 22.5^0, (D) composite of all 3 average curves.

In an effort to further validate the proposed mechanisms and put them to application, composites were synthesized which could incorporate the necessary design features. First, the helicoidal architecture was tested in 9, 17, and 25 ply composites with offset angles between plys of 11.25°, 22.5°, 45°, 78.75°, and 90°. Some composites were tested with through thickness stitching prior to infiltration. Threads of nylon and polyester were chosen to represent the pore channel fibers for their hydrophobicity which

would prevent their bonding to the hydrophilic epoxy. The lack of bonding between sewing thread and epoxy was intended to represent the pore channels and seed fractures.

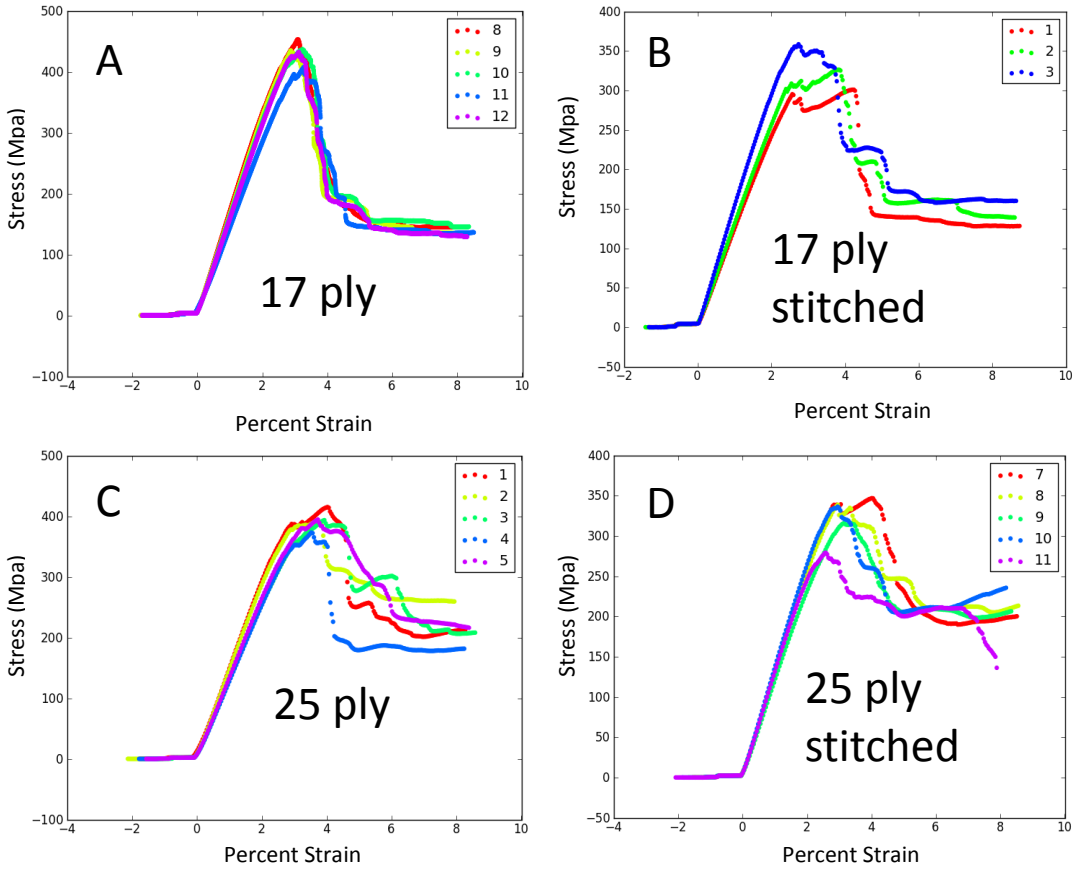

Figure 3.11: (A) Fig3.10C reproduced for comparison. (B) The same composite, but with polyester stitching. (C) Also a 22.5 degree offset sample, but with 25 layers instead of 17, and the same thing with stitching (D). Note the difference in the stress scale, and the promising post failure toughness of the thicker helicoidal composites.

All attempts to mimic the fracture nucleating pores have not succeeded in promoting branched fractures. It is likely that we have not yet approached the required scale and uniformity such that a pore channel is always a few microns from a propagating fracture, ready to relieve its driving force. In spite of this, the enhanced post failure toughness seen in the 25 ply composite appears promising. Thicker samples have more

periods, and therefore more opportunity to “catch” stray fractures in the fracture rotating regime.

Conclusion

Helicoidal composites are challenging materials to construct and characterize, but their ubiquity in nature across many functional systems including scales, bones, and hammers provides strong support for realizing their full potential as engineered materials. The ability for a helicoidal composite to rotate fractures has been demonstrated, and it has been proposed that a helicoidal composite with channeled porosity can achieve simultaneous weight reduction and enhanced toughness through synergistic mechanisms of promoting energy dispersive fractures. By considering how this structure must grow and expand it is suggested that designs could take advantage of the expandability for helmets and portable shelters.

Materials and Methods

Specimen Handling and Sample Preparation

Live specimens of *Odontodactylus scyllarus and Lysiosquillina maculata* from the tropical Indo-Pacific were obtained through commercial sources and maintained live in a recirculating seawater system until ready for use. The dactyls were dissected from these specimens and rinsed in fresh seawater to remove any loose organic debris. The samples were then rinsed briefly in deionized water to remove any residual salt and then air dried at 30 ºC. The resulting samples were either imaged in their entirety for whole-club scanning electron microscopy (SEM) or imbedded in Epofix resin for the preparation of cross-sections. The obtained resin blocks were manually trimmed down to the desired imaging plane with a diamond saw and polished to P1200 with progressively finer grades of silicon carbide paper and then with polycrystalline diamond suspensions down to 100 nm to obtain a smooth finish. In some cases samples were demineralized for 2-8 hours in 50ml of a 5% acetic acid and water solution on a shaker table. The resulting samples were imaged either by optical microscopy and/or scanning electron microscopy.

Raman spectroscopy

Raman spectroscopy was performed using a Thermo Fisher Scientific DXR Raman microscope (λ = 780 nm) with low laser power conditions (6 mW) to minimize heating.

Scanning Electron Microscopy (SEM) and Energy Dispersive Spectroscopy (EDS)

Polished or demineralized samples were platinum/palladium coated and examined with an FEI XL-40, or a Tescan VEGA TS-5130MM scanning electron microscope. A Tescan VEGA XMU scanning electron microscope equipped with an Oxford Instruments

(X-Max) energy dispersive spectrometer was used to acquire EDS line scans and compositional maps at a 20 kV accelerator voltage.

Synchrotron X-Ray Transmission Studies

Synchrotron X-ray data was collected at Beamline X13B at the National Synchrotron Light Source, Brookhaven National Laboratory, using 19 keV X-rays (λ = 0.65 Å) and a beam spot focused to ca. 5 μm × 5 μm. Specimens consisting of dactyl clubs embedded in Epofix resin were sliced with a diamond saw to create 0.5 mm thick slices which were then mounted onto the beamline sample holder in transmission geometry. Transmitted X-ray intensity was recorded using a photodiode detector fixed beyond the sample at the beam stop and normalized by incident intensity measured with an upstream ion chamber.

3D Printing and Mechanical Testing:

An 3D printer was used to print models with using the two materials to represent fibers and mineral matrix. A notch was incorporated into each model to initiale a crack and observe its behavior. Samples were loaded in an Instron mechanical loading apparatus in a 3 point bend configuration. Resulting force vs. displacement curves were recorded in real time.

Composite Layup Synthesis and Mechanical Testing:

A 4 sq. ft. polished steel plate was waxed with a car wax and the surface was lined with masking tape along the edges. A layer of polyvinyl alcohol was applied with a plastic spreading tool, and the quality of waxing was determined by observing a uniform

wetting between the PVA and the waxed metal. After the PVA was dry it was scored with a razorblade along the masking tape's edge. After removing the masking tape a layer of grey sealant tape was applied in its place to the PVA-free surface of the steel. 1 foot of spiral tubing was placed along the middle of the inside edge for three of the four sides. 1x1 sq. ft. Layers of unidirectional fiber glass were stacked on top of each other at predetermined angles to form a fiber layup. In some cases, fabric sheets had their edges taped to prevent fraying, or the whole layup was stacked, stitched with various threads and patterns, and then placed on the steel plate.

A layer of nylon peel ply was placed atop the fiber layup, followed by a layer of blue plastic, then breather cloth. Four 1 in. squares of breather were cut, 2 for each injection port. The breather was cut to extend on two sides of the layup, and 2 squares are placed under each injection port on either side of the layup such that the port has three layers of breather between it and the steel plate to prevent a seal forming between the injection ports and the steel during vacuum infiltration. The exit port is closest to the side with no spiral tubing, and the entry port is on the opposite side. The injection ports were sanded to prevent their molding seems from tearing holes in the vacuum bag. A 2.5X2.5 sq. ft. piece of flexible vacuum bagging material was cut from a roll and two holes were cut offset from the middle by the distance between the ports. Yellow sealant tape was applied to the base of the injection ports, and then they were placed into the holes to create a seal between the port and bag. The bagging material and ports were placed over the entire assembly, lining up the injection ports to their previous location, and sealing the bag to the grey sealant tape, making a pleat if necessary.

PVC sealant was applied to the tops of each port, and vacuum tubing was attached to both ports. A vacuum pump was attached to a sealed resin reservoir with a vacuum gauge. An air release valve was hand adjusted such that the vacuum gauge remained at a constant 15 +- 1 mmHg. The resin reservoir was then attached to the exit port tubing decreasing the pressure within the bagged assembly, allowing for leaks to be found and repaired with yellow sealant tape. System 2000 epoxy Resin and System 2020 epoxy hardener were mixed well at a ratio of 100:27 and the entry port tubing was placed into the mixing bucket to initiate infiltration. The vacuum release valve was adjusted if necessary and the assembly was left for 12+ hours to cure. After initial curing the infiltrated layup was carefully removed from the rest of the assembly, and allowed to finish curing between two polished steel plates. The resulting composite was considered ready for testing after 72 hours, or once the thin resin near the edge began to exhibit immediate brittle failure, instead of plastic deformation, upon stress.

A tile saw was used to slice the composite into beams suitable for flexural testing. The astm spec D790 was attempted to be adhered to whenever possible or appropriate. The spec dictated that samples be circa 3 mm thick, 12.7 mm, and 60mm long. The pieces were cut at predetermined angles with respect to the fiber layup, and their edges were sanded flat. A micrometer was used to measure the thickness 1 mm from each corner, and width at 3 places along the sides. These 7 measurements were tabulated for each sample and used to estimate the average thickness and width. Samples were loaded with a specified “up”, defined by their surface texture, onto an instron mechanical loader, using a 3 point bend configuration with a span of 3.2 mm. Max strain was not always set

at the ASTM specified value of 5%, but in some cases the data acquisition was allowed to continue through strains up to 10% to provide more data for the analysis of post-failure toughness. Note that the values obtained are not necessarily accurate beyond 5% strain, but still indicative of how the material behaves at high values of strain.

Data collected during loading was recorded, and analyzed using the previously measured average geometric parameters. Average stress-strain curves for a corresponding set of experimental parameters were generated by averaging the data from 5+ samples together.

Chapter 4: Retrodictions of stomatopod cuticle structures derived from impact mechanics, feeding behavior, and common decent.

Abstract

The regional substructural complexity of the stomatopod dactyl club from *Odontodactylus scyllarus* represents a challenging biomimetic system in the study of impact tolerant biominerals. This substantial complexity demands that each region be given its own thorough investigation. The striated region of the dactyl club is one such region, of which the investigation has revealed not only its function with respect to impact tolerance of the club ultrastructure, but also implications regarding its evolutionary history. Presented is the effect of the striated region in the prevention of catastrophic cracking within the energy dispersive regions of the club, and evidence for substuctural exactation within the stomatopod clades.

Introduction

Impact resistance is not a defined intrinsic property of material, but rather an aggregate of a material's properties and extrinsic form. By definition an impact is a dynamic event, making it very difficult to model because many assumptions used to understand static systems are not appropriate. In some cases the term impact resistance is interchanged with toughness because impact implies high speeds, and therefor energy. Kinetic energy is proportional to the square of an object's velocity, and toughness is a measure of a material's capacity for energy dissipation. However, this approach is easily confounded. Elastomers for instance have exceptional toughness, but with increasing speeds impact forces have less time to distribute, and can therefor exceed the strength of the rubber without utilizing the toughening mechanisms within the rubber. The glass transition in rubber is just one example of the imposed difficulty when designing impact resistant materials. To meet the demands of the defense and transportation industries an alternative approach to garner insights is by investigating biomaterials which have been

optimized for impact tolerance via millennia of natural selection.

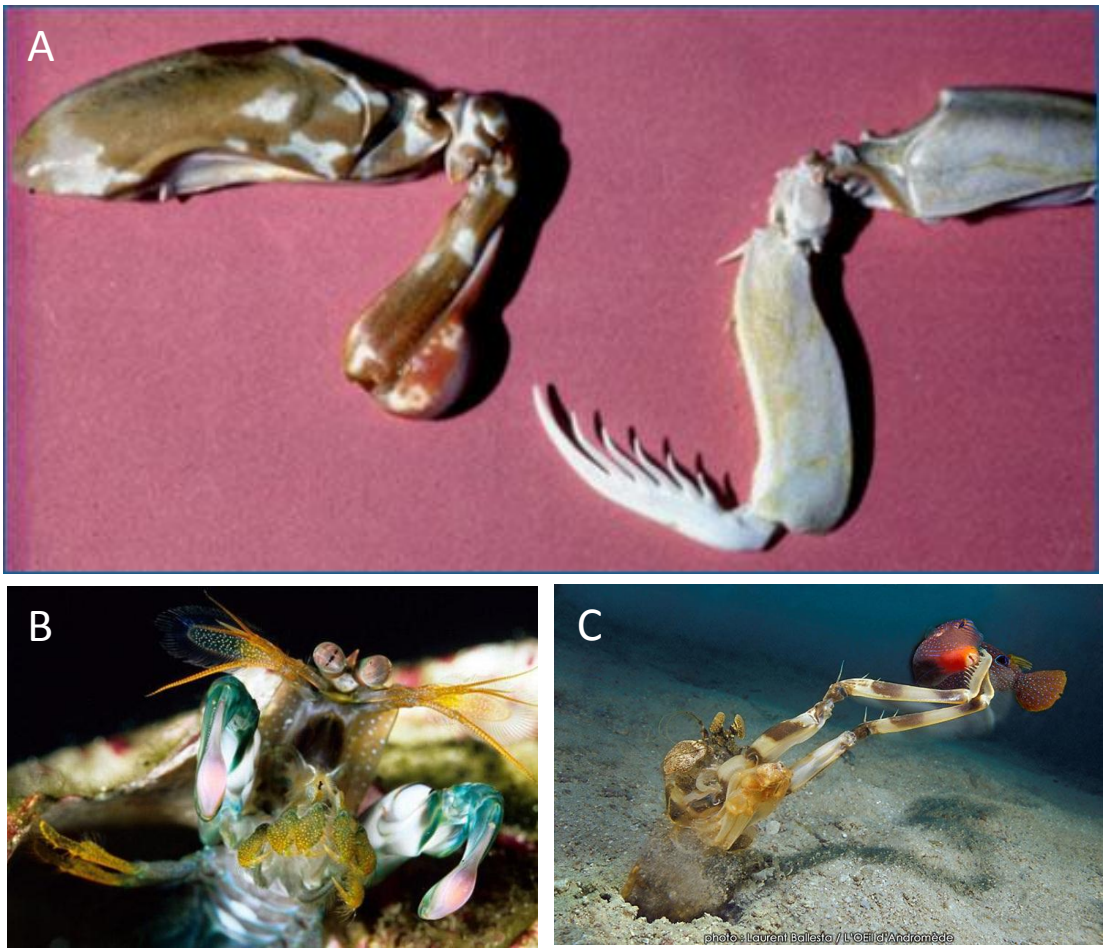

Figure 4.1: (A) The 2nd maxillipeds of stomatopods allow for easy distinction between (B) smashers and (C) spearers.

Biomimetics seeks to utilize the biological fields to learn insights applicable to engineering practices (Bhushan; 2009; Munch, 2008). However, sometimes this pursuit can give back to the biological field by enhancing our understanding of how the organisms of interest evolved. The ability to make predictions about the substructure of an organism based on conclusions drawn regarding an organism's evolution is an example of a retrodiction. The stomatopods are one group where such an activity is

possible due to the divergent evolution of their second thoracic appendages. Stomatopods can be broken into two distinct groups (Fig 4.1), the first of which attack their prey with a raptorial strike earning the stomatopods the name mantis shrimp. This group is called the "spearers" and includes *Lysiosquillina maculata*. The spearers are distinguished by the dactyl of their 2nd thoracic appendage (maxilliped), which is elongated and specialized for grasping prey. This group is older, and the newer group is the result of an exactation, or repurposing, of the 2nd maxilliped. The spearing stomatopods are burrowing ambush predators, which developed excellent vision and very fast feeding strikes in order to capture agile soft bodied prey, such as fish. The biomechanical structures to accomplish this feat supplied a foundation for exactation, as selection began favoring the bludgeoning force of impact that occurred when the target was "accidentally" hit near the joint of the dactyl. The second group of stomatopods, known colloquially as the "smashers," has been favoring the bludgeoning attack for so long that a prominent bulbous growth can be found on the dactyl of their 2nd maxilliped, which is powered by superficially identical machinery to that found primarily in the merus segment of the "spearers."

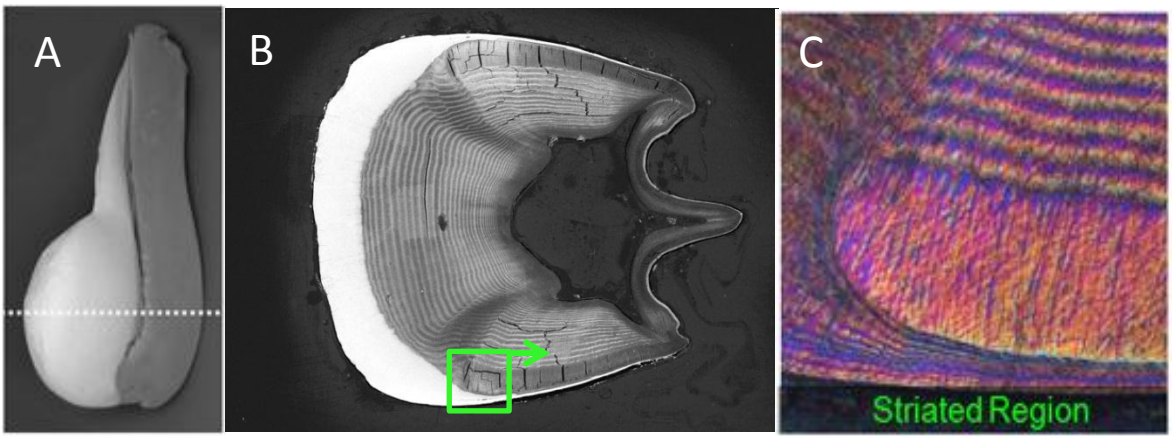

Figure 4.2: (C) a polarized light micrograph of the striated region from a (B) transverse cross-section of a (A) stomatopod dactyl club.

The substructure and impact tolerance of the dactyl club from the smashing stomatopod *Odondactylus scylarrus* has been previously investigated by Currey (Currey, 1982) and later Weaver et al (Chapter 2). Weaver et al showed that a transverse cross-section from the dactyl club reveals a regionally variant ultrastructure with distinct interfaces which can be used to define boundaries between regions. These regions include the impact region, periodic region, and the striated region. The impact and periodic regions can be further divided into subregions, and are likely homologous to the exocuticles and endocuticles which have been well described in all arthropods. The periodic region, for instance, is named due to the optically visible periodicity resulting from the helicoidally stacked α-chitin sheets embedded in a mineral matrix. This is the established morphology of arthropod endocuticles. Conversely, the striated region exhibits morphology unique to crustacean cuticle. To first approximation, it appears to be parallel bundles of amorphous mineral rods with α-chitin cores. This structural pattern may be unique to crustaceans, but is highly reminiscent of the structures found in the mineralized teeth of chitons (Towe, 1967; Weaver, 2010).

The obvious application of mineralized rods with fiber cores is for the resistance of tensile loads. In order to understand the regiospecific forces experienced by the dactyl club under impact, a simulation was employed using the finite element method by Weaver et al. This simulation is known to be incomplete considering that forces were generated in the impact region which far exceed the strengths of the materials present there, but it still provides an approximate representation of the forces felt in each region.

One shortcoming of the model is the input of values measured from nano-indentation. While nano-indentation provides the most relevant regiospecific mechanical information available, it is a compressive technique. This means the values input into the model may not be representative of the tensile mechanical properties, which can be quite different, for a fiber reinforced composite, than what can be measured from a compressive technique. The goal of this report is to update this model, and provide a deeper understanding of the purpose, evolution, and applicable insights of the striated region.

Structural Characterization

From optical or SEM micrographs of a transverse cross section through a dactyl club of *Odontodactylus scyllarus* the striated region is easily distinguished. The periodic region can divided into 2 subregions: the medial and lateral zones, with a 3rd subregion separating the two. The lateral periodic region, contained on the sides of the club, is harder, stiffer, and more mineralized. This is assumed to provide support for the softest region which absorbs the bulk of the impact forces: the medial zone of the periodic region. Each super-layer seen in an optical image from the periodic region is actually many sheets of chitin that have undergone a 180 degree rotation between the top and bottom of each super-layer. What at first may appear to be an exceptionally thick super-layer terminating the lateral periodic region near the club exterior surface, actually

exhibits a completely different structure. This is the striated region.

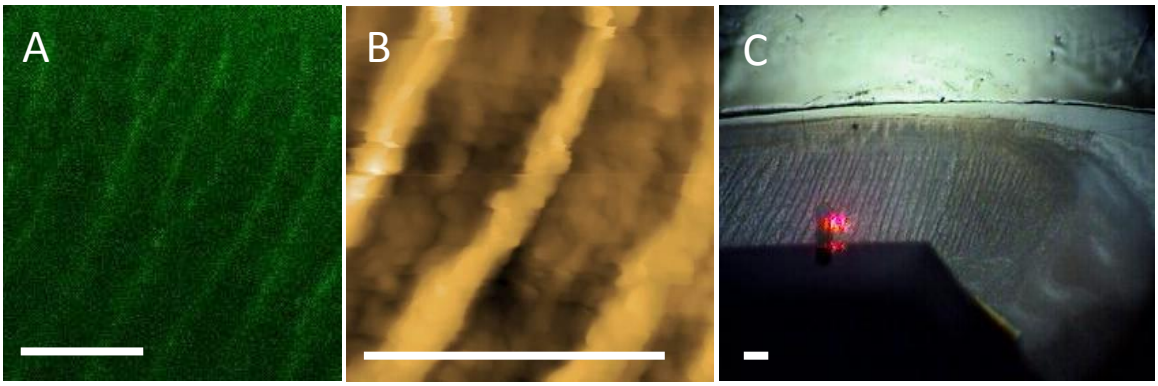

Figure 4.3: (A) an EDS phosphorus map revealing the phosphorus rich striations that define the striated regions namesake. (B) the same striation seen in an AFM topographic map, and corresponding optical image revealing mechanical differences in the striation from a polished surface. All scale bars are 20 µm.

The striated region is named due to the striations seen in this region from a transverse cross-section which run radially outward, from the core to the club exterior surface. These striations are observable in SEM and optical microscopy. EDS reveals that the striations are richer in phosphorous than their surrounding material (Fig. 4.3A). Phosphorous is present in the hydroxyapatite found in the impact region, as well in the amorphous calcium phosphate and calcium carbonate found within the period region. Synchrotron X-ray diffraction suggests that the mineral phases of the striated and periodic regions are comparable. AFM phase maps reveal that the striations have different mechanical properties than their surrounding material (Fig 4.3B). The striations are also present in fracture surfaces as sheets of material separating the mineralized rods that dominate the region (Fig 4.4C). The structure-function relationship of the striations themselves is a puzzling pursuit, but is beyond the scope of this report. The more

fundamental question is the purpose of the region as a whole, and the structure of the region can be first approximated without the striations, which will become apparent.

The structure of the organic material relative to the mineral is an important step in understanding the properties of this region. Synchrotron X-ray diffraction can distinguish between the crystalline α-chitin and the surrounding amorphous mineral. Evidence that the α-chitin within the striated region runs perpendicular to the transverse plane of the dactyl club is contained within the X-ray diffractograms taken from this region. The (110) α-chitin reflection is measured as a nonuniform ring (Fig 4.4F,G). This indicates that there are bundles of parallel fibers with a stochastically distributed orientation about their c-axis aligned roughly parallel with the beam. The beam was travelling perpendicular to a transverse cross-section so the fibers must also be running perpendicular to the transverse plane. Synchrotron X-ray diffraction has the advantage of nondestructively investigating a diffraction volume of interest, but the presence of parallel α-chitin bundles can be observed much less abstractly by demineralizing a transverse cross-section and noting the orientation of α-chitin bundles that remain in the

striated region (Fig 4.4D,E).

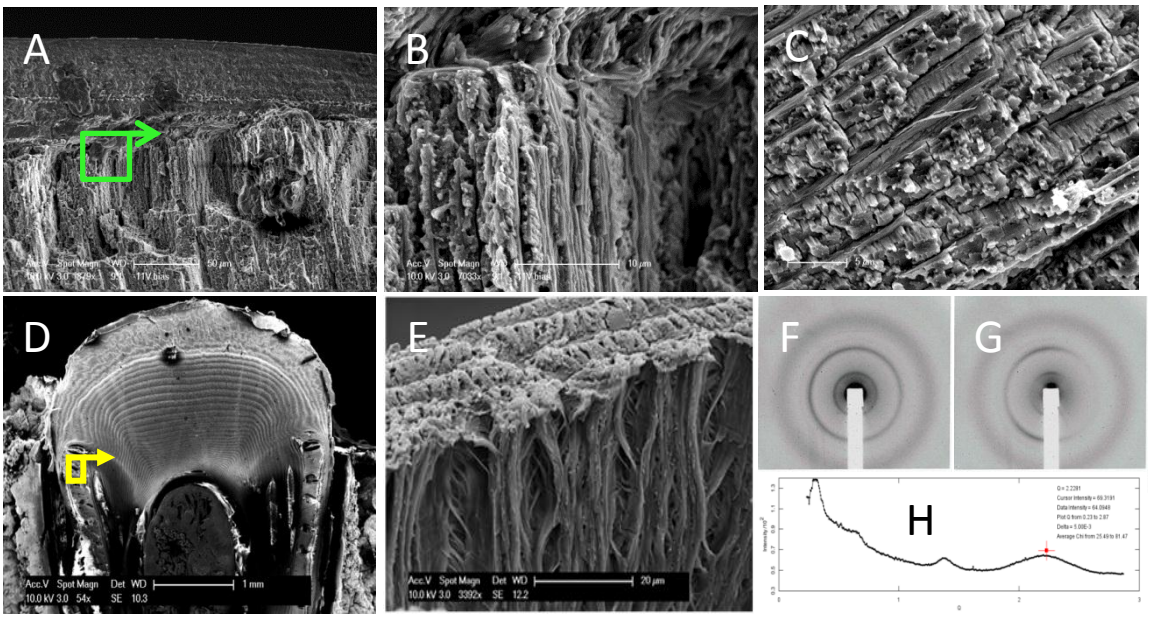

Figure 4.4: (A)(B)(C) Assorted fractograms from the striated region at varying levels of magnification. Note the presence of mineral rods, despite the negligible crystallinity. (D)(E) Micrographs from a demineralized transverse cross-section. Note the bundles of parallel chitin left behind. (F)(G) two representative diffractograms from the striated region with the beam approximately parallel to the chitin's c-axis. (H) a representative diffraction spectra from the striated region with only amorphous mineral and alpha-chitin distinguishable.

Mechanical Analysis and Discussion of Simulated Impact

In lieu of accurately measured values from the biomineral, estimations were made from the known anisotropic properties of chitin and the measured structure to modify the finite element model from Weaver et al. (Chapter 2). When the model was updated to better represent the striated region's capacity to resist out of plane tensile loads, the simulation reflects the presence of such loads during impact. This suggests that the striated region serves the purpose of providing additional support for the energy absorbing medial periodic region. During impact the medial periodic region's sheets are compressed against each other. Due to an assumed positive Poisson's ratio in this region, the result is the sheets experiencing tensile forces, which radiate in all directions parallel to the plane of each sheet. This, in turn, causes fractures to nucleate and grow within the medial periodic region. The nucleation, growth, and control of these fractures appears to be a dominate energy dispersion mechanism for the club ultrastructure, but if the mechanisms which control the fractures fail then a fracture could potentially continue to

propagate such that it results in the catastrophic failure of the ultrastructure.

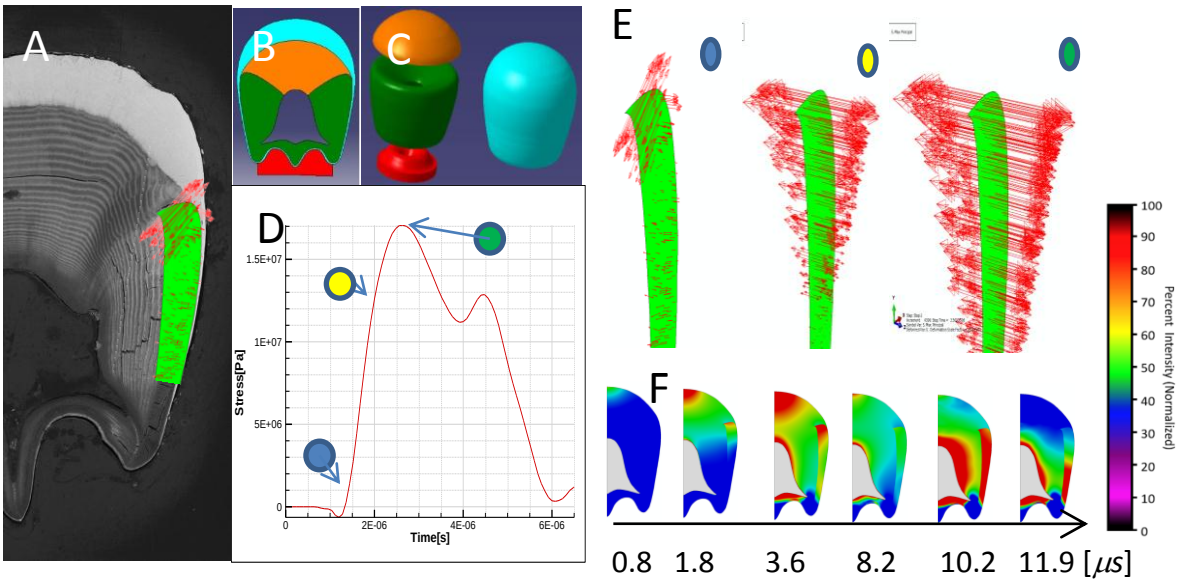

Figure 4.5: (A) a transverse cross-section of a dactyl club with the modeled data from (E) superimposed. (B) a cartoon of the representative regions modeled in the analysis, with a 3d expanded view (C) provided to illustrate the rotational symmetry assumed in the analysis. (D) The maximum stress follows a nonlinear path during impact. The out of plane forces (E) experienced during impact reached at 3 times during impact can be seen to reach a maximum value (F) after 10.2 µs from impact.

Due to the relative softness (lower elastic modulus) of the medial periodic region (Chapter 2) smaller relative forces are required to create large extension, displacement, or strain. As each sheet in the medial periodic region is strained outward, Mode I cracking is induced. The outward strain causes the fibers in the striated region to experience tensile loads which restricts the strain in the medial periodic region. A balance must be stricken such that the medial periodic region is not restricted to the point where failure occurs in the striated region, but the strain is still mitigated. Because the energy dispersive mechanisms are assumed to be contained in the helicoidal architecture of the periodic region, failure must be confined there, but the striated region serves the purpose of

helping control the failure. The driving force for a propagating fracture is proportional to the crack opening angle (Shih, 1981), and the crack opening angle is in turn proportional to the experienced strain (Shih, 1981). This is one reason why fractures in monolithic materials are frequently catastrophic: they become easier to propagate as their length increases. This mechanism must be counteracted if fractures are to be used as an energy dispersive mechanism because otherwise fractures would be unarrestable. By limiting the strain within the periodic region to a range that fractures can still nucleate and grow, but their maximal driving force is constrained, an optimal energy dispersive, and therefor impact resistant structure is formed. The finite element simulation supports this hypothesis, but if this function is correct there is one glaring question regarding the striated region. If its role is to resist strain of the medial periodic region during impact, why does it surround the entire club?

Investigation of Multifunctionality

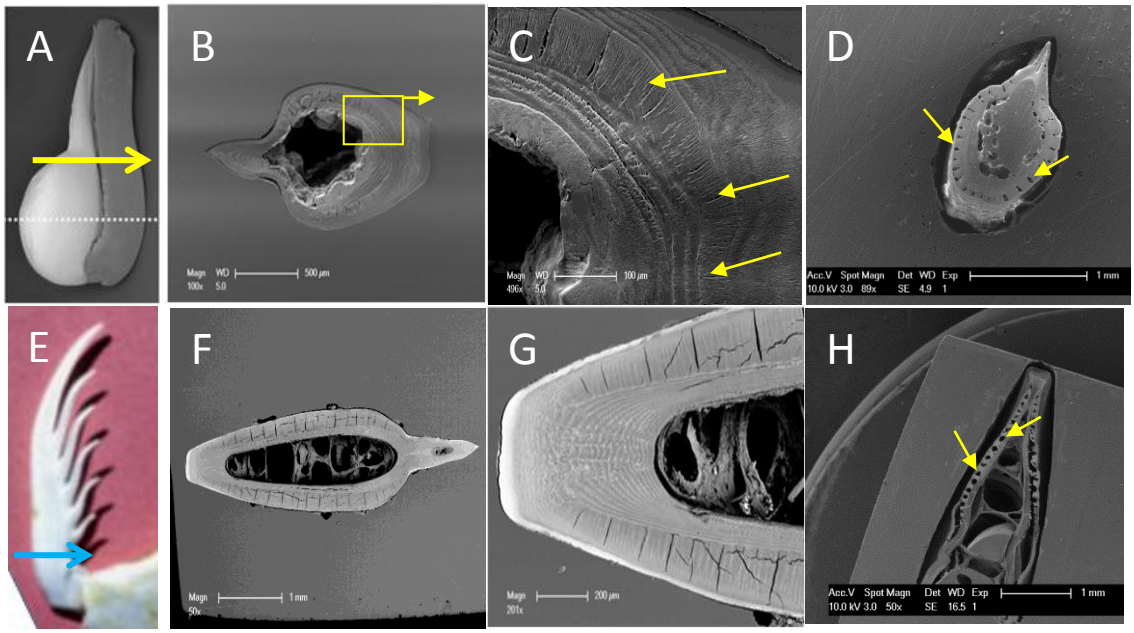

Figure 4.6: (A) a dactyl from a smashing stomatopod with a yellow arrow denoting the elevated cross-section taken to reveal a (B)(C) connected striated region near the spike. (D) The same section after demineralization demonstrating that the morphological structure of the striated region remains predominately parallel chitin bundles. (E) the dactyl of a slearing stomatopod sliced to reveal (F)(G) a striated region with predictable differences based on behavior. (H) demineralization also reveals a parallel bundled structure in the spearers as well.

The striated region is thickest where it would be expected to be if the impact tolerant hypothesis is at least partially correct, but the striated region extends all the way around the back of the club connecting both regions (Fig. 4.2B). The proposed hypothesis cannot account for this, but perhaps the striated region is multifunctional, in which case it has an additional structure-function relationship which could explain its presence in unexpected areas. The first clue is provided by the fact that the club itself is multifunctional. The dactyl and propodus of *Odontodactylus scyllarus* together have become a functional club, but the organism is still capable of separating these two segments, revealing a spike that protrudes from the dactyl. This spike is more than just a

vestigial remnant of a spearing dactyl. It functions as a piercing weapon, which can perforate soft bodies resistant to impact (a fact known “first hand” by those who have not been careful enough during sample collection). A spike structure with a large aspect ratio is susceptible to flexural loads which could break the spike from its basal support. Perhaps the striated region originally evolved to support the flexural loads of the spearing dactyl and was repurposed to enhance impact tolerance in the smashing stomatopods.

The first retrodiction to be made is the presence of the striated region within a transverse cross-section of the spike protruding from the dactyl. Furthermore, since the spike could experience loads in all directions it could be predicted that the striated region will connect across the analogous medial periodic region within the spike. Because the perimeter of an object will experience the largest loads when a beam is loaded, it is common practice in composite materials manufacture to reinforce a flexural member with longitudinal fibers in order to resist tensile loads which could result in failure. When a transverse cross-section from the spike is observed under SEM, a connected striated region is clearly present (Fig. 4.6B, C) and after demineralization the expected orientation of the fibers is confirmed (Fig. 4.6D) (the fiber axes run parallel to the long axis of the spike).

Evidence for Substructural Exactation

To further confirm that exactation of the striated region occurred, and that the structure-function relationship has been solved, a complete fossil record of the divergent evolution would be necessary, but the hypothesis could be strongly supported by making retrodictions about the substructural features of extant spearing stomatopods. The fossil record does show that extant spearing stomatopods are still utilizing similar raptorial appendages (Haug, 2010). Therefore, it is likely that they have maintained similar substructure, and the presence of a striated region to prevent flexural loads can be retrodicted. Moreover, features of a spearer's striated region can also be retrodicted. If there is a striated region present it will likely take up a larger percentage of the cross-sectional area than is seen in smashers since the flexural load is more important to resist than an impact load. Additionally, because the spearing stomatopods favor a more streamlined dactyl, to move quickly through the water, the striated region will likely be thickest along the sides. To understand this, the spearing dactyl's section modulus must be considered.

Section modulus is a geometric measure of beam's cross-sectional shape about a defined neutral axis. The section modulus, material properties, and the span (beam length) combine to define a beam's mechanical properties under a flexural load. The neutral axis defines the directional the beam is to be loaded. An I-beam has the highest section modulus of any shape, but only when loaded such that the flat sections at the top and bottom receive the maximal stress. A hollow cylinder has the highest section modulus/area of any isotropic shape (no dependence on loading direction or neutral axis). A solid cylinder has a section modulus of pi*(r^3)/4 while an ellipse has a section

modulus of pi*(a^2)b/4. This means that the ratio of the section modulus for the two principle axes of an ellipse is the ratio of a/b, where a and b are half the lengths of the long and short axes of the ellipse. The ratio of a/b then defines the ratio of yield moments (yield moment equals section modulus multiplied by yield strength, and is a measure of the forces required to cause failure in a beam).

To confirm the above retrodictions, dactyls from the extant spearing stomatopod *Lysiosquillina maculata* were sectioned transversely in the region comparable to the impact location of a smashing stomatopod. Its dactyl can be roughly approximated as an ellipse with a/b=3 (Fig 4.6). From the formula above this means that if the dactyl were a uniform ellipse its short axis would have a yield moment 3 times less than the long axis. This highly eccentric elliptical shape likely serves both to reduce the hydrodynamic water resistance, and strengthens the club in the direction which it will be loaded when grasping prey. However, due to the dynamic nature of prey capture the weakness of the orthogonal direction must be compensated for, and ideally in such a way that doesn't add to the fluid resistance during a feeding strike. The enhanced strength imparted by a striated region is a perfect substructural feature to accomplish this feat, the presence of which is clearly visible in (Fig. F,G). Furthermore, all of the predictions, based on its proposed function, regarding is location and size, are confirmed. In fact the striations themselves are even more prominent, and take on a clear dichotomous pattern of branching. To show that the striated region present in *Lysiosquillina maculata* does not just show superficial resemblance to that found in *Odontodactylus scyllarus*, dactyl cross section from

Lysiosquillina maculata were demineralized to reveal the characteristic bundled fiber architecture (Fig. 4.6H).

The fact that the striated region of *Lysiosquillina maculata* is not thickest near the homologous impact region, but is in *Odontodactylus scyllarus* provides strong evidence that the striated region's multifunctional structure-function relationship has been solved. Furthermore, the implications are that the striated region originally evolved to enhance the yield moment in the weaker direction of the dactyl, but ultimately provided a potentially crucial foundation for a structure which could be repurposed for impact tolerance.

Investigation of Convergent Evolution

To complete the evidence to support the hypothesis regarding the structure-function relationships of the striated region convergently evolved species were investigated to determine whether a striated region had also independently evolved in other organisms with raptorial feeding strikes, superficially similar to mantis shrimp. The obvious first choice is the mantis shrimp's namesake organism: the praying mantis. Preying mantids are also arthropods, which mean they also rely heavily on helicoidally assembled chitin architectures. However, as an insect the proteins that surround these structures are cross-linked to provide structural rigidity in lieu of the mineralization that occurs in crustaceans. In order to determine whether the praying mantis utilizes similar bundled chitin architectures akin to the striated region of mantis shrimp a tibia (the segment corresponding to the dactyl in mantis shrimp) was sectioned transversely near its base (Fig. 4.7).

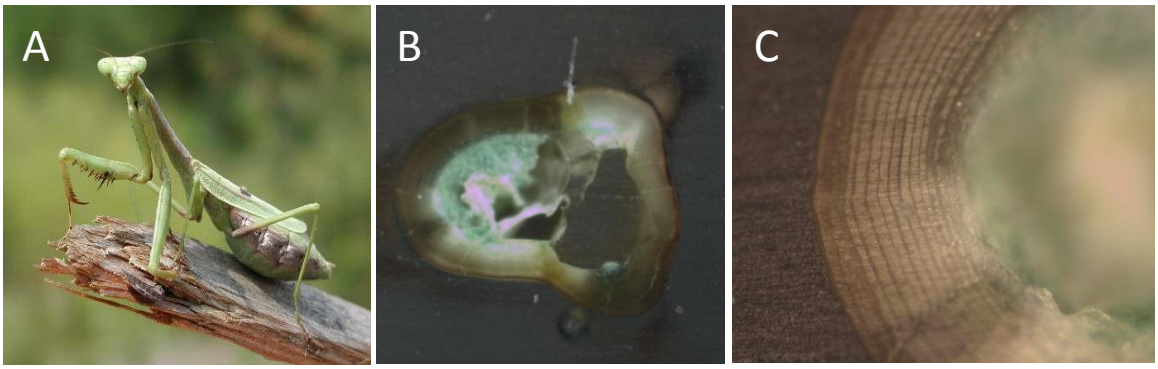

Figure 4.7: (A) a praying mantis, and a cross-section from its tibia at (B) low and (C) high magnifications revealing its periodic cuticle, absent of a convergent striated region.

The first observation was the lack of a striated region, but this can be explained by considering the environmental differences of these otherwise largely convergent structures. The praying mantis feeds in a medium 3 orders of magnitude less dense. This means that water resistance for a mantis shrimp is far more limiting on speeds than air resistance for a praying mantis. Because fluid resistance is proportional to the product of the density and the cross sectional area (coronal cross-section), the minimization of the cross-sectional area, of the mantis shrimp dactyl, is crucial to achieve decent acceleration. Conversely, the praying mantis can virtually disregard this constraint, so instead of modifying its substructure to account for the otherwise weaker section modulus in the direction orthogonal to grasping, it simply enhanced the section modulus in that direction, increasing its cross-sectional area (coronal). The (transverse) cross-sectional shape of a praying mantis tibia has a much more balanced section modulus without the high eccentricity seen in spearing mantis shrimp. This observation was additionally confirmed by inspecting another convergent structure from the independently evolved mantis fly. The mantis fly's tibia was comparable in cross section to a scaled down preying mantis tibia confirming that non aquatic arthropods with raptorial feeding limbs don't need substructural support in the form of an analogous striated region.

Biomimetics

From an engineering perspective the take-away insight with regards to flexural structures is nothing new, and simply reinforces known design cues, but regarding impact tolerant materials, there may be novel synthetic structures which could benefit from the mechanism employed by the striated region of the *Odontodactylus scyllarus* dactyl club. To confirm the utility of the striated region as a method for providing confinement of potentially catastrophic fractures propagating within a helicoidally structured composite, models of a helicoidal architecture, with and without annular rings (Fig. 4.8), were developed which could be printed and mechanically loaded. A soft material was printed to represent the amorphous mineral, and a stiffer material was used to represent the fibers. By comparing the load displacement curves with annular rings and a control without, the effect of the annular rings, which mimic the striated region, was isolated. While this is a preliminary result, it is clear the rings resulted in the redirection of a

propagating crack, and a vastly higher strength and toughness.

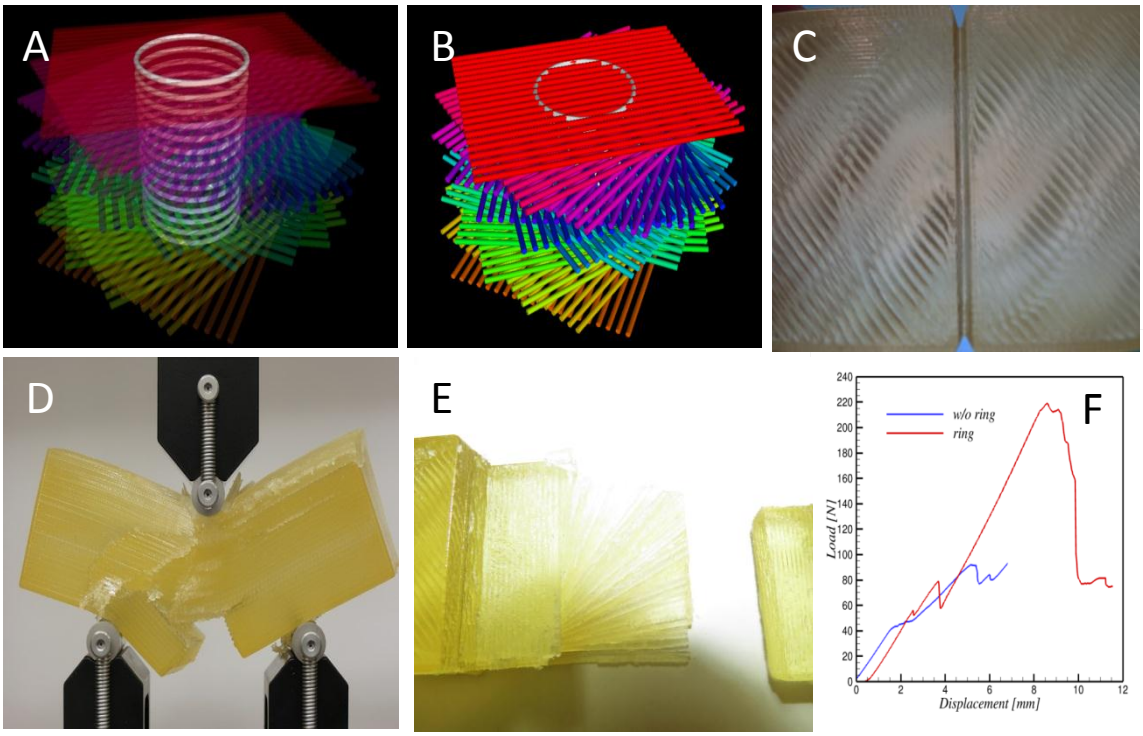

Figure 4.8: (A)(B) models used to aid in the visualization of the printed moded in (C-F). (D) shows the avoidance of the rings intended to mimic the striated region. (E) A rotated tortuous fracture path results in drastically improved mechanical properties compared to the model without the rings, as seen in their respective load vs. displacement curves (F).

The 3D printed models are many orders of magnitude larger scale than the structures being mimicked; therefor, scaling considerations must be made. It is likely that the benefit from the annular fiber support is highly scale dependent. As the annular fibers are placed further from a propagating fracture they will suffer a diminishing ability to reduce the strain and therefor crack opening angle and crack driving force. This is because the strain field surrounding a fracture is inversely proportional to the distance from the crack tip. The further the striated region is from a crack the less stress gets

transferred to the annular fibers, and their ability to limit strain in the helicoidal region is reduced. Thus incorporating the lessons learned from the striated region are difficult to incorporate into a fiber reinforced composite with macroscopic dimensions. This means the design must be modified into a repeating structure of mm scale diameter annular fibers throughout the composite. It will take some ingenuity to develop a synthesis process which can accomplish this feat.

Conclusion

The structure-function relationships of the striated region found in the impact tolerant biomineral from the dactyl club of *Odontodactylus scyllarus* have been proposed and a wealth of evidence to support these claim has been presented. The implications regarding the utility of such structures have been described in the context of flexural support and more notably: impact tolerance. If such structures could be incorporated into modern composite designs, along with the helicoidal architecture, then improvements in impact tolerance are expected. Furthermore, the insights presented resulted in unintentional implications regarding the convergent and divergent evolution of stomatopod dactyl substructure. This uncovered evidence for the history and development of substructural flexural support, and the repurposing of such structure to reduce the driving force for potentially catastrophic fractures during impact.

Materials and Methods

Specimen Handling and Sample Preparation

Live specimens of *Odontodactylus scyllarus and Lysiosquillina maculata* from the tropical Indo-Pacific were obtained through commercial sources and maintained live in a recirculating seawater system until ready for use. The dactyls were dissected from these specimens and rinsed in fresh seawater to remove any loose organic debris. The samples were then rinsed briefly in deionized water to remove any residual salt and then air dried at 30 ºC. The resulting samples were either imaged in their entirety for whole-club scanning electron microscopy (SEM) or imbedded in Epofix resin for the preparation of cross-sections. The obtained resin blocks were manually trimmed down to the desired imaging plane with a diamond saw and polished to P1200 with progressively finer grades of silicon carbide paper and then with polycrystalline diamond suspensions down to 100 nm to obtain a smooth finish. In some cases samples were demineralized for 2-8 hours in 50ml of a 5% acetic acid and water solution on a shaker table. The resulting samples were imaged either by optical microscopy, scanning electron microscopy.

Scanning Electron Microscopy (SEM) and Energy Dispersive Spectroscopy (EDS)

Polished or demineralized samples were platinum/palladium coated and examined with an FEI XL-40 scanning electron microscope.

Synchrotron X-Ray Diffraction Studies

Synchrotron X-ray data was collected at Beamline X13B at the National Synchrotron Light Source, Brookhaven National Laboratory, using 19 keV X-rays (λ = 0.65 Å) and a

beam spot focused to ca. 5 μm × 5 μm. Specimens consisting of dactyl clubs embedded in Epofix resin were sliced with a diamond saw to create 0.5 mm thick slices which were then mounted onto the beamline sample holder in transmission geometry. Transmitted X-ray intensity was recorded using a photodiode detector fixed beyond the sample at the beam stop and normalized by incident intensity measured with an upstream ion chamber. Diffraction data were acquired with a Princeton Instruments CCD detector approximately 15 cm beyond the sample. Frames were not corrected for spatial distortions within the detector optical taper. Using a sintered corundum standard, the software package *Datasqueeze*, and a JCPDS data card for corundum, we calibrated detector pixel positions to *Q*-values.

The orientation of chitin fibers was measured using the techniques detailed in (24) and more generally (Dowling, 2006), by assuming that crystalline chitin grains exhibit fiber symmetry (a preferred c-axis but no preferred orientation within the plane normal to that axis), while the arrangement of the grains breaks this symmetry, with an angle μ between the fiber axis and a reference axis (the transmitted X-ray beam direction) that can vary from place to place within the sample. First, the (110) reflection of chitin was identified, and intensity vs. *Q* plots as a function of detector azimuth χ were generated, integrated over a range of *Q* which bounded this reflection (Q = 1.3-1.4 $Å^{-1}$). As the fibers deviate from orthogonality with the beam, the location of their reflections on the detector do not remain separated by 180° in χ but have centroids displaced by an angle η. Diffracted peaks will obey:

$$\cos(\eta) = \tan(\theta)/\tan(\mu),$$

where θ is one-half the Bragg scattering angle. However, this equation can only useful for values of μ above a threshold. Because μ is nearly zero for the chitin in the striated region of our experimental setup, all that can be done is confirm that μ is indeed small by measuring the expected diffractograms seen in (Fig. 4.4).

Dynamic Finite Element Analysis

Dynamic Finite Element Analysis (DFEA) of an impact event between the dactyl club and a solid target was carried out using the finite element software Abaqus/Explicit (39). Our model considered the entire geometry of the dactyl, the propodus, and the target as depicted in Fig. 5A. Because the terminal two segments of the raptorial appendages can be approximated as a solid of revolution, we carried out a 2D axysymmetric analysis. The dactyl club has an average total length of ca. 5 mm and a radius of ca. 2 mm. The entire distance from the top of the club (impact region) to the end of the propodus is ca.10 mm. These dimensions are representative of a typical adult sized specimen of *Odontodactylus scyllarus* (and similar to the one analyzed in this paper and used for other previous experimental work (Patek, 2005)). The complex macroscale geometry of the dactyl club and propodus presented was followed with high fidelity in our models. The mechanical response of the material was modeled as isotropic linear elastic with different mechanical properties and mass densities (matching nanoindentation and compositional data from previous work (Chapter 2)) assigned to each of the sections indicated in Fig. 4.5 In addition, the water-filled cavities (containing the internal musculature) of the

dactyl and propodus were simulated as an acoustic medium to properly account for the wave propagation in the fluid and its interaction with the rest of the club. The finite element mesh contains a total of 433,787 nodes and 429,987 elements. In these simulations, the target initially traveled at 20 m/s and impacts the dactyl club producing a compressive stress wave traveling through both the target and dactyl. Because we were interested in the impact event, we did not consider the effect of the water surrounding the dactyl club (although we do consider the water inside the central cavity, as it is very important for transmission of the stress waves). Due to the relative low impedance of water, the boundary of the dactyl and propodus were modeled as free surfaces.

The total impact force was calculated as the sum of the individual nodal forces in the direction of the impact along the lower surface of the target. The compressive stress is regarded as hydrostatic.

3D Printing and Mechanical Testing:

An 3D printer was used to print models with using the two materials to represent fibers and mineral matrix. A notch was incorporated into each model to initiale a crack and observe its behavior. Samples were loaded in an Instron mechanical loading apparatus in a 3 point bend configuration. Resulting force vs. displacement curves were recorded in real time.

Chapter 5: Conclusion

There are many perspectives in which our world is framed. “The material world” is one of the most common and fundamental descriptions. Materials define the properties that dictate nearly every interaction we experience. The limitations of materials translate to the limitations within of all design and engineering. If we had better materials, we would have better products, tools, homes, and even bodies. However, a “better” product is a subjective description until a problem is well defined. A material can only be better suited for a given application, because one application may require a minimization, while another requires maximization and another application an optimization, all of the same material property. A primary task of materials science is to discover ways to tune or control material properties at a range of scales, diminishing their limitations. Mechanical properties are a fundamental set of properties which govern among other things how materials fail under mechanical forces. Almost every product will receive mechanical loads, while being used for its intended purpose, which it must resist in order to continue functioning. Depending on the application this consideration can range from negligible to primary.

Some applications endure such substantial and dynamic loads that there are no materials which can meet their demand for a failure-proof material, especially where weight is a concern. Instead engineers do their best to mitigate inevitable material failure by sequestering damage and dissipating as much energy as possible. In the case of cars, the bumpers can only withstand a collision at far lower speeds than what the car can provide. Weight is such large concern for personal aircraft that they do not always protect

against atmospheric debris; the planes are often built to barely survive the loads during flight. Pilots must also take great care when choosing their flight path to minimize the load of flight; one wrong move can tear the wings from certain planes. Board sport enthusiasts are always willing to pay for the lightest board, but it must also withstand the rider's weight and abuse. Finally, body armor would save more lives if it was lighter and more flexible, because then more people whose lives it could save would wear it. For this reason body armor comes in different classes based on the scale of the impact it can protect against. However, even the most cumbersome body armor has limitations in how many and the type of impacts it can receive before failure. Furthermore, even if a trajectory is not allowed to penetrate into the person's body the shock or acoustic wave generated upon impact is still enough to cause fatal injuries a large percentage of the time.

If materials could be designed which have increased toughness, strength, stiffness, and lower density then all of these applications and more would reap the benefits, and new applications could even open up. To accomplish this, the first step is to investigate what the best materials are capable of and how. The best materials are not necessarily available for use, but they can still be investigated. The best materials may not even have the best properties, but may demonstrate mechanisms which produce the most improvement in the impact tolerant properties desired with the materials they are made of. The materials sought may be a combination of structures which produce the synergistic mechanisms missing in the materials of modern man. However, understanding what is available is an unsurmountable task. Once biological materials are recognized as

containing possible solutions, the number and diversity of materials to be studied is overwhelmingly large. To approach the problem reasonably, organisms must be prioritized based on the likelihood of finding mechanisms worth mimicry.

The peacock mantis shrimp *Odontodactylus scyllarus* was chosen for a number of reasons based on its behavior, ancestry, and environment. Mantis shrimp are a living fossil, so they have had plenty of time to refine their materials for their function. This is evidenced by their eyes, which are some of the most complex known. A great deal of specialization is also seen in their second pair of thoracic appendages, which are capable of one of the fastest animal movements known, certainly the fastest in water. The stomatopod dactyl club is accelerated via an elastic battery to speeds of 23 m/s in order to strike and promote failure in the coevolved mineralized structures of their prey, structures similarly studied for their impact tolerance. The prey is subjected to forces of 700 N from direct impact, and an additional shock from the collapse of cavitation bubbles created by the shearing of the sea water, as the club rapidly decelerates upon impact. Forces are equal and opposite, so the club must repeatedly endure every force it delivers between molting events. Understanding how the club is able to survive such large impacts and retain a functional club by the end of its molting cycle was the initial goal of this thesis. Demonstrating the lessons learned by modifying existing composite materials synthesis techniques was the ultimate goal of this thesis. Auxiliary insights, models, synthesis routes, and more have added to the impact of this work to serve the primary thesis goals. Unfortunately, at the time of writing much of the impactful progress made on these projects is undisclosable, do to intellectual property considerations.

Characterization and Modeling of Dactyl Club Ultrastructure

Biomaterials are often complex, hierarchical, multifunctional, and contain structure which can be either vestigial or serve a purpose that doesn't concern the investigation. When faced with this situation, scientists begin simplifying, modeling, estimating, and assuming. Inevitably, this is an incomplete approach, but it provides a foundation which can be continuously refined and updated. The dactyl club of the peackock mantis shrimp contains a spike protruding from the top, and is attached to the propodus via a joint at the bottom. The dactyl and propodus together form the functional club, which is arced through the water from the joint between propodus and merus. The impact point is contained on a curved surface which could be approximated as a half sphere. Taking a transverse cross section through this point reveals a regionally segregated substructure. The key structural features are assumed to be represented from this cross-section, allowing a revolution of this cross-section about the centerline to represent an approximate club. This allows the disregard of the complexity imparted to the 3-dimensional ultrastructure from the spike above and the joint below this cross-section.

Nanoindentation reveals a thin exterior surrounding the club, which is harder and stiffer than anywhere else. This is likely the first line of defense against impact and causes the ultrastructure to remain relatively stiff. This is important for delivering the largest impact forces to its prey for a given speed and fixed weight. Upon impacting two materials of different stiffness, the less stiff material experiences more strain, so its exterior must remain stiff relative to its prey. The next region beneath the hard exterior epicuticle is the impact region. This is a thicker region with the next highest mineral

content. The mineral phase is hydroxyapatite (HAP) with the c-axis of the crystal grains oriented perpendicular to the impact surface as they curve around the club (Fig. 2.3c). HAP is the mineral in our bones, and known to be anisotropically stiffest in the basal direction (Viswanath, 2007). These HAP crystals are reinforced by interstitial organic structured to form a network which produces a macroscopic "herring bone" pattern under polarized light microscopy. We have hypothesized that the organic could be an organization of α-chitin similar to the helicoidal architecture seen ubiquitously in crustaceans. Preliminary evidence suggests that the impact region could exhibit a micro buckled conformation of the cholesteric ordering (Fig). This process is likely guided by the vertically aligned through thickness fibers which template the mineralization of the oriented HAP.

Failure in impact resistant materials often occurs on the opposite side from impact where tensile forces nucleate fractures. This is likely why the region after the impact region is the thickest in the whole club. The periodic region contains amorphous mineral likely because fractures are easier to control in amorphous material. Without crystallographic planes the fractures have fewer constraints on their direction of propagation, making them easier to redirect. At this level of approximation the dactyl club could be described as equivalent to abalone with a hard crystalline exterior, and a tough fracture resistant interior, but the club is more complex than that. The periodic region can be further classified into three sub regions based on their location around the core of the club, and another region beneath the exterior, on the sides of the club (the striated region) appears relevant to the impact tolerance.

Each region and subregion has specific chemistry and structure suited to its function, and understanding how they all synergize to form a complete ultrastructure is a long term goal of this project's continuation. FEM simulations constructed from nanoindentation and strike force data provide a first pass approximation of the time dependent force fields contained in the club during impact. However, this model also proves its own incompletion by generating forces far exceeding the strengths of the club's materials. The model needs to be improved before it can be verified, but it still provides our best estimation of how each region responds to an impact event.

Just as each kingdom of life contains a wealth of biomimetic systems, the club itself contains a wealth of regions worthy of focused study. While the impact region is an obvious choice of priority for its unique and complex structure, and its ability to withstand and deliver direct impact, it was deprioritized. Understanding the structure function-relationships to create hard exteriors is a worthy thesis project, but the focus taken here was in understanding how to accept the impact energy. We sought structure-function relationships which support hard exteriors imparting toughness to an ultrastructure. The hypothesis that pores play a large role in the toughening mechanism provides the added benefit of decreased density, which is a high priority in our target applications. For this thesis the interest in tougher components exceeded that of harder components. Controlling fractures in a brittle composite and utilizing them as an energy dispersive mechanism is something that fiber-reinforced composites could great greatly benefit from, whereas plenty of engineered materials have exceptional hardness.

The transition between the impact region and the periodic region is analogous to the dentine enamel junction or many other modulus mismatch architectures. The hypothesis proposed is that fractures which travel into the impact region from the periodic region encounter the mismatch which provides a crack arresting or redirecting front preventing “exit” at the surface. The medial periodic region is the central energy absorber of the club, and is supported by the stiffer lateral periodic regions. The striated region limits the radial expansion of the medial periodic via confinement provided by tensed fiber bundles. This confinement provides an additional support by preventing crack opening angles from becoming too large and undermining the synergy between the helicoidal architecture and the pore channels.

Testing the hypotheses regarding the striated regions function was done by utilizing knowledge of common decent, which allowed for the structures in related species to be retrodicted. Insights into the evolution of raptorial appendages from the perspective of beams were gained for both terrestrial and marine fauna. In addition the FEM models were updated to include estimations that better reflect the tensile stiffness of α-chitin bundles. The result was out of plane tension experienced in the striated region suggesting confinement does occur.

Mimetics and Future Work

Printing 3D models which test specific property distributions and producing fiber layups which test specific architectures, has provided physical evidence for sought mechanisms. Synthesis is still in its early stages, and testing the composites under dynamic impact has only been performed qualitatively with a few tests at a firing range, but we are continuing to test new prototype materials which incorporate the synergistic structures we seek. Enhances in toughness, especially after the ultimate strength has been exceeded have been obtained, but many parameters could still be investigated to optimize the structures.

The layers could benefit from having their thickness reduced resulting in a smaller pitch for a given offset angle. The fibers could be switched from fiberglass to carbon, basalt, or aramid. A lot of work could be done in testing blends of fibers, which could make use of a periodic modulus within a unidirectional fiber sheet (e.g., ripstop fabric). Furthermore, the process of using a layup or prepreg could be replaced by utilizing a cholesteric self-assembly process. If tubular molecules, such as organic or inorganic fullerenes, could be functionalized to form a helical conformation, which was tunable, then high tension cholesterics could be engineered. Ferro fluids under magnetic fields allow for liquid molding, which can impart porous channeling at the microscale. This or another mechanism could be utilized to create density reducing fracture seeds.

Large amounts of work could be done just realizing the potential of the lessons uncovered by inventing and modifying synthesis methods and putting them to use in new materials, but every step of the biomimetic funnel will also continue to provide a wealth of stomatopod-based research opportunities. At the characterization level the impact

region, hard outermost exterior, and the region separating the medial and lateral periodic regions still have many questions regarding their precise structures and function, but these are in just one species: *Odontodactylus scyllarus.* If behavioral information could be collected about the differences in average strike force, frequency, etc. for different species and genders, then correlations between behavior and structure could be investigated across gender, and species. As an example, comparing the hardest hitting structures to the most frequently hit structures could provide evidence for how each region can be modified to suit a modified purpose.

Finally, there is good reason to trust that large improvements will be made in the area of modeling. As computation time becomes cheaper, simulations with more nodes become reasonable to run. A heavily simplified model of a complex 3-dimensional material, such as a helicoidal composite, can only be created at a very low resolution before the number of nodes becomes unreasonable. This situation only improves with better algorithms and cheaper computation time. A fully parameterized helicoidal composite with pore channels and pore channel fibers, has a large number of parameters including, pore diameter, pore channel fiber diameter, pore channel fiber mechanical properties, helicoidal fiber mechanical properties, fiber waviness, sheet offset angle, space between sheets, mechanical properties of the mineral matrix, etc. With such a large parameter space, optimization of the design parameters can be difficult. Eventually, an iterative process could be developed which simulates and mutates the model in order to find optimums within the parameter space by utilizing feedback from the simulation (i.e., a genetic optimization routine).

An Objet Connex500 is 3D printer capable of printing single parts with more than 2 types of materials across a range of material properties. With this machine select parameters could be printed to test regions of the parameter space. Initially, the softest material would be used to represent the pore channels, and the stiffest material would represent the fibers, and a medium stiffness material representing the mineral matrix. This would extend the current tests which have only been capable of printing fibers and matrix without a pore mimic.

Every stage in the biomimetic funnel has been explored, and the foundation for more work at each stage in the funnel has been laid. The evolution, behavior, structures, and properties of the stomatopod dactyl club have been investigated, and its substructural functions have been theorized, modeled, and simulated. Insights have been gleaned which were unexpected and unintuitive. These insights have been demonstrated with printed and synthesized composites, which are nearing readiness for application. The stomatopod dactyl club has proved an excellent muse for understanding the problem of lightweight impact-resistant materials, and the insights acquired will likely find their way into future products.

References

1. S. T. Ahyong, C. Harling, *Aust. J. Zool.* 48, 607-642 (2000).
2. B. J. Aizenberg, G. Lambert, L. Addadi, S. Weiner, *Advanced Materials* 8, 222-226 (1996).
3. Al-Sawalmih *et al*., *Adv. Funct. Mater.* 18, 3307-3314 (2008).
4. T. Apichattrabrut, K. Ravi-Chandar, *Mech. Adv. Mater. Struct.* 13, 61-76 (2006).
5. M. F. Ashby, L. J. Gibson, U. G. K. Wegst, R. Olive, T. R. Society, P. Sciences, *Proc. R. Soc. Lond. A* 450, 123-140 (1995).
6. E. Arzt, P. Fratzl, H. Gao, B. Ji, I. L. Ja, *Most* 100, 5597-5600 (2003).
7. F. Barthelat, H. Tang, P. Zavattieri, C. Li, H. Espinosa, *Journal of the Mechanics and Physics of Solids* 55, 306-337 (2007).
8. G. A. Bibo, P. J. Hogg, *J. Mater. Sci.* 31, 1115–1137 (1996).
9. F. Bosia, T. Abdalrahman, n. M. Pugno, *Nanoscale* 4, 1200-1207 (2012).
10. B. Bhushan, *Philosophical transactions. Series A, Mathematical, physical, and engineering sciences* 367, 1445-1486 (2009).
11. W. K. Brooks, *Report on the Scientific Results of the Exploring Voyage of the H.M.S. Challenger*, vol. 45., Stomatopoda. (Neill and Co., Edinburgh, 1886)
12. B. J. B. Bruet, J. Song, M. C. Boyce, C. Ortiz, *Nat. Mater.* 7, 748-756 (2008).
13. R. L. Caldwell, *Naturwiss.* 62, 214-222 (1975).
14. J. Castanet, M. M. Giraud, J. Castanet, F. J. Meunier, Y. Bouligand, *Tissue and Cell* 10, 671-686 (1978).
15. K. S. Chan, M. Y. He, J. W. Hutchinson, *Mater. Sci. Eng., A* 167, 57-64 (1993).

16. S. Chandrasekhar, *Contemp. Phys.* 29, 527-558 (1988).

17. B. Chen, X. Peng, C. Cai, H. Niu, X. Wu, *Materials Science and Engineering: A* 423, 237-242 (2006).

18. L. Cheng, A. Thomas, J. L. Glancey, A. M. Karlsson, *Composites Part A: Applied Science and Manufacturing* 42, 211-220 (2011).

19. L. Cheng, L. Wang, A. M. Karlsson, *J. Mater. Res.* 23, 2854-2872 (2011).

20. T. Claverie, E. Chan, S. N. Patek, *Evol.; Int. J. Org, Evol.* 65, 443-461 (2011).

21. B. W. Cribb et al., *Arthropod structure & development* 38, 173-178 (2009).

22. T. W. Cronin, N. J. Marshall, *Nature* 339, 137-140 (1989).

23. J. D. Currey, A. Nash, *J. Mater.* 17, 1939-1944 (1982).

24. S. Deville, E. Saiz, R. K. Nalla, A. P. Tomsia, *Science* 311, 515-518 (2006).

25. P. S. B. Digby, *J. Physiol. Lond.* 173, 29-30 (1964).

26. N. E. Dowling, *Mechanical Behavior of Matererials* (Prentice Hall, New Jersey, ed. 3, 2006)

27. E. M. Dubensky, D. A. Koss, *Metallurgical Transactions A* 18, 1887-1895 (1987).

28. J. W. C. Dunlop, P. Fratzl, *Annu. Rev. Mater. Res.* 40, 1-24 (2010).

29. H. Endo, Y. Takagi, N. Ozaki, T. Kogure, T. Watanabe, *Biochem. J.* 384, 159-167 (2004).

30. G. E. Fantner, T. Hassenkam, J. H. Kindt, J. C. Weaver, H. Birkedal, L. Pechenik, J. A. Cutroni et al, *Nature materials* 4, 612-616 (2005).

31. J. G. Fernandez, D. E. Ingber, *Advanced materials* 24, 480-484 (2012).

32. P. Fratzl, H. S. Gupta, F. D. Fisher, O. Kolednik, *Adv. Mater.* 19, 2657-2661 (2007).

33. P. Fratzl, R. Weinkamer, Nature's hierarchical materials, *Progress in Materials Science* 52, 1263-1334 (2007).

34. I. D. Gharagozlou-van Ginnekcn, Y. Bouligand, *Cell Tiss. Res.* 159, 399-412 (1975).

35. J. K. Gillham, P. N. Reitz, *Polymer Engineering and Science* 8, 227-234 (1968).

36. M. M. Giraud-Guille, *Tissue and Cell* 16, 75-92 (1984).

37. M. M. Giraud-Guille, *Current Opinion in Solid State & Material Science*, 221-227. (1998)

38. M. M. Giraud-Guille, E. Belamie, G. Mosser, *Comptes Rendus Palevol* 3, 503-513 (2004).

39. W. Gronenberg, *The Journal of experimental biology* 199, 2021-2033 (1996).

40. D. Gubb, *Tissue and Cell* 7, 19-32 (1975).

41. S. Habelitz, G. W. Marshall, M. Balooch, S. J. Marshall, *J. Biomech.* 35, 995-998 (2002).

42. J. T. Haug, C. Haug, A. Maas, V. Kutschera, D. Waloszek, *BMC evolutionary biology* 10, 290 (2010).

43. M. Y. He, J. W. Hutchinson, *Int. J. Solids Struct.* 25, 1053-1067 (1989).

44. A. H. Heuer *et al*., *Science* 255, 1098-105 (1992).

45. V. Imbeni *et* al., Nature *Mater.* 4, 229-232 (2005).

46. K. E. Kadler, D. F. Holmes, J. A. Trotter, J. A. Chapman, *The Biochemical journal* 316, 1-11 (1996).

47. M. Komfeld, L. Suvorov, *Journal of Applied Physics*, 15, 495-506 (1944).

48. S. Koutsopoulos, *Journal of biomedical materials research* 62, 600-612 (2002).

49. E. Loste, *J. Cryst. Growth* 254, 206-218 (2003).

50. H. Lichtenegger, M. Müller, O. Paris, C. Riekel, P. Fratzl, *J. Appl. Crystallogr.* 32, 1127-1133 (1999).

51. H. A. Lowenstam, S. Weiner, On Biomineralization (Oxford Univ. Press, New York, 1989)

52. F.C. Lukis, *Mag. Nat. Hist. J. Zool., Bot., Minera., Geol., and Meteorol.* 8, 459-464 (1835).

53. G. Luquet, F. Marin, *Comptes Rendus Palevol* 3, 515-534 (2004).

54. M. A. Meyers, A. Y. M. Lin, P. Y. Chen, J. Muyco, *Journal of the mechanical behavior of biomedical materials* 1, 76-85 (2008).

55. R. Minke, J. Blackwell, *J. Mol. Biol.* 120, 167-181 (1978).

56. E. Munch, M. E. Launey, D. H. Alsem, E. Saiz, A. P. Tomsia, R. O. Ritchie, *Science* 322, 1516-1520 (2008).

57. C. Ooi, M. Hamdi, S. Ramesh, *Ceram. Int.* 33, 1171-1177 (2007).

58. O. Paris, M. Muller, *Nucl. Instrum. Methods Phys. Res.* B 200, 390-396 (2003).

59. S. N. Patek, R. L. Caldwell, *J. Exp. Biol.* 208, 3655-3664 (2005).

60. G. Penel, G. Leroy, C. Rey, E. Bres, *Calcified tissue international* 63, 475-481 (1998).

61. Y. Politi *et al*., *J. of Mater*. 22, 161-166 (2010).

62. D. Raabe, C. Sachs, P. Romano, *Acta Materialia* 53, 4281-4292 (2005).

63. M. L. Reaka, *J. Morphol.* 146, 55-80 (1975).

64. A. D. Rey, *Soft Matter* 6, 3402-3429 (2010).

65. R. Roer, R. Dillaman, *Am. Zool.* 24, 893-909 (1984).

66. K. Rugg, B. Cox, K. Ward, G. Sherrick, *Composites Part A: Applied Science and Manufacturing* 29, 1603-1613 (1998).

67. A. Sellinger, P. M. Weiss, A. Nguyen, Y. Lu, R. A. Assink, W. Gong, C. J. Brinker, *Nature* 394, 256-260 (1998).

68. F. R. Schram, *J. Paleontol.* 81, 895-916 (2007).

69. Z. W. Shan, G. Adesso, A. Cabot, M. P. Sherburne, S. A. S. Asif, O. L. Warren, D. C. Chrzan et al, *Nature materials* 7, 947-952 (2008).

70. C. F. Shih, *J. Mech. Phys. Solids* 29, 305-326 (1981).

71. C. Y. Tan, K. L. Aw, W. H. Yeo, S. Ramesh, M. Hamdi, I. Sopyan, *Ceramics*, 326-329 (2008).

72. Z. Tang, N. A. Kotov, S. Magonov, B. Ozturk, *Nature materials* 2, 413-418 (2003).

73. J. R. A. Taylor, S. N. Patek, *J. Exp. Biol.* 213, 3496-3504 (2010).

74. L. Tombolato, E. E. Novitskaya, P. Y. Chen, F. a Sheppard, J. McKittrick, *Acta biomaterialia* 6, 319-330 (2010).

75. K. M. Towe, H. A. Lowenstam, *Journal of ultrastructure research* 17, 1-13 (1967).

76. M. Viani, T. E. Scha, J. B. Thompson, N. A. Frederick, J. Kindt, G. D. Stuckyk, F. K. Hansma, *Nature* 399, 761-763 (1999).

77. B. Viswanath, R. Raghavan, U. Ramamurty, N. Ravishankar, *Scr. Mater.* 57, 361-364 (2007).

78. J. C. Weaver et al, *Mater. Today* 13, 42-52 (2010).

79. S. Weiner, T. Arad, I. Sabanay, W. Traub, *Bone* 20, 509-514 (1997).